Quantum Information Processing in Multi-Spin Systems

by

Paola Cappellaro

Submitted to the Department of Nuclear Science and Engineering
in partial fulfillment of the requirements for the degree of

Doctor of Philosophy in Nuclear Science and Engineering

at the

MASSACHUSETTS INSTITUTE OF TECHNOLOGY

June 2006

Author .....
Department of Nuclear Science and Engineering
May 5, 2006

Certified by .....
David G. Cory
Professor
Thesis Supervisor

Read by .....
Sow-Hsin Chen
Professor

Accepted by .....
Jeffrey A. Coderre
Chairman, Department Committee on Graduate Students

Quantum Information Processing

in Multi-Spin Systems

by

Paola Cappellaro

Submitted to the Department of Nuclear Science and Engineering
on May 5, 2006, in partial fulfillment of the
requirements for the degree of
Doctor of Philosophy in Nuclear Science and Engineering

Abstract

Coherence and entanglement in multi-spin systems are valuable resources for quantum information processing. In this thesis, I explore the manipulation of quantum information in complex multi-spin systems, with particular reference to Nuclear Magnetic Resonance implementations.

In systems with a few spins, such as molecules in the liquid phase, the use of multi-spin coherent states provides a hedge against the noise, via the encoding of information in logical degrees of freedom distributed over several spins. Manipulating multi-spin coherent states also increases the complexity of quantum operations required in a quantum processor. Here I present schemes to mitigate this problem, both in the state initialization, with particular attention to bulk ensemble quantum information processing, and in the coherent control and gate implementations.

In the many-body limit provided by nuclear spins in single crystals, the limitations in the available control increase the complexity of manipulating the system; also, the equations of motion are no longer exactly solvable even in the closed-system limit. Entanglement and multi-spin coherences are essential for extending the control and the accessible information on the system. I employ entanglement in a large ensemble of spins in order to obtain an amplification of the small perturbation created by a single spin on the spin ensemble, in a scheme for the measurement of a single nuclear spin state. I furthermore use multiple quantum coherences in mixed multi-spin states as a tool to explore many-body behavior of linear chain of spins, showing their ability to perform quantum information processing tasks such as simulations and transport of information.

The theoretical and experimental results of this thesis suggest that although coherent multi-spin states are particularly fragile and complex to control they could make possible the execution of quantum information processing tasks that have no classical counterparts.

Thesis Supervisor: David G. Cory
Title: Professor

Acknowledgments

This thesis would have not been possible without all the persons that have offered their advice and support during my Ph.D. research and my life in Cambridge. I have been very privileged to have so many wonderful friends and collaborators.

First, I am grateful to my advisor David Cory for teaching me so much about science and for always pushing me to challenge myself. Talking to him is always a source of inspiration, not only to find new ideas and angles to approach a problem, but also to gain new motivations in the struggle that is sometime the Ph.D. research.

I would also like to thank all the Cory group members -past and present- with whom I have worked. In particular Nicolas Boulant, for all the classes attended together and the discussions about the meaning of physics; Jonathan Hodges, with whom I shared the office and the rumbles about graduate student life; and Sekhar Ramanathan for teaching me so much about NMR and spin dynamics. Many thanks also to all the other group members that have been not only lab-mates but also very close friends: Anatoly Dementyev, Benjamin Levi, Cecilia Lopez, Dan Greenbaum, Debra Chen, Dimtri Pouchine, Jamie Yang, Joon Cho, Joseph Emerson, Karen Lee, Michael Henry, Suddha Sinha and Troy Borneman. I am also thankful to Lorenza Viola, for insightful conversations about science and my future career path.

All the friends that I have met here have been invaluable to make my experience at MIT so enriching (and also to convince me to stay for two more years in Cambridge): Joanna Yu and all the girls from volleyball, the Euro-Asia team, Christian Grippo, Antonio Damato and especially James Seo, who has accompanied me during my last and most stressful year.

Finally, my family in Italy has always been my biggest support, to them is dedicated this thesis.

Contents

List of Figures

List of Tables

Foreword

Quantum information science is an exciting, emerging field that holds the promise to dramatically improve the acquisition, transmission and processing of information. This field has attracted much interest among scientists from different backgrounds and the general public, not only for the possible practical implications that a quantum computer and quantum communication devices could have, but also for the variety of fundamental physical questions that it could help answer. New theoretical ideas and important technical advances are paving the road toward a scalable quantum computer. The greatest challenge in building quantum information processing devices is to develop techniques for the coherent control of complex quantum systems. This implies not only the improvement of experimental techniques and the theory of coherent control, but also a deeper knowledge of the candidate physical systems for quantum information processing applications.

There are many aspects to quantum information science, from computer-science questions, like devising algorithms, which exploit the advantages of quantum superposition and interference, and error correction schemes, which enable a correct processing of information in the presence of noise, to physical implementations and control issues. Nuclear Magnetic Resonance (NMR) provides an ideal environment to explore many of these issues. Correspondingly, my dissertation work has spanned different subjects, touching various aspects of Quantum Information Processing (QIP) as well as exploring two different, although related, experimental techniques. Nuclear magnetic resonance of small molecules in a liquid solution has been used in experiments described in the first part of the thesis, while the second part investigates ideas of QIP related to a solid state experimental implementation, using as a tool nuclear resonance of single crystals.

From the very beginnings of QIP, liquid state NMR was recognized as an important test-bed to explore issues of relevance in any possible scalable implementation of a quantum

information processor. These issues have been codified in a very concise and clear way by D. DiVincenzo in five simple criteria for a scalable quantum computer [43]:

1. A scalable physical system with well characterized qubits.
2. The ability to initialize the state of the qubits to a simple fiducial state.
3. A *universal* set of quantum gates.
4. Long relevant decoherence times, much longer than the gate operation time.
5. A qubit-specific measurement capability.

In the first part of the thesis I address some of these requirements, proposing new strategies toward their fulfillment. In particular, after describing the embodiment of qubits in liquid state NMR, I discuss qubit initialization and control. Since it has been recognized that one promising road toward fault tolerant computation is to encode information in logical qubits, immune to particular classes of noise, I will focus on logical qubits. In chapter 2 I present a new initialization procedure, that reduces the signal loss associated with the purification of mixed states. In the following chapter, I discuss the added complexity associated with the control of logical qubits, introducing schemes aimed at reducing the deleterious effects of noise when the logical qubits leave the protection of the encoding for short periods of time.

The fifth DiVincenzo criterion is discussed in the second part of the thesis, where I present a novel approach to the long-standing problem of single nuclear spin measurement. This scheme introduces and exploits the properties of many-body spin systems in the solid state, in particular the entanglement among the spins in the system. The device presented is an example of quantum-mechanical devices, such as clocks, communication systems, information storages, etc., that take advantage of phenomena unique to the quantum domain, such as superposition and entanglement, concepts that have known a renewed interest thanks to quantum information science. Fully developed quantum computers will likely be out of reach for many years, despite great technological and theoretical advances. However, quantum sensors and actuators are less technologically demanding and may find application more quickly. I conclude this thesis by studying a particular system that can be used as a task-specific quantum information device, for example as a quantum simulator.

Part I

Liquid State NMR

Per correr miglior acque alza le vele
omai la navicella del mio ingegno,
che lascia dietro a sé mar sì crudele;

Dante Alighieri - Purgatorio I, 1-3

Chapter 1

Introduction

The fundamental unit of quantum information is the quantum bit, or qubit. A qubit is a system in a 2-dimensional Hilbert space. Ideally it is represented by an isolated 2-level physical system that can be used to store quantum information. Many implementations of qubits have been proposed, based on a wide range of experimental techniques, from photons to macroscopic solid systems. One of the first proposals for quantum information processing was based on liquid state NMR [40, 60]. In liquid state NMR the qubits are defined as magnetically distinct spins-$\frac{1}{2}$ of a given molecule, immersed in a solvent. Because of easy identification of qubits, good knowledge of their Hamiltonians, high level of control already developed by the NMR community and long decoherence times, liquid state NMR is recognized as one of the most flexible test-beds for QIP. One of its limitations is the exponential decrease in signal for each qubit added to the system, which is associated with the use of mixed states in ensemble QIP. Although not a scalable approach to quantum computation, liquid state NMR has made it possible over the years to test experimentally quantum algorithms and to study issues of control and fault tolerant quantum computation. In particular, in recent years the focus has been on studying the control of logical qubits, that is, qubits protected against errors by a logical encoding. Controlling the future quantum processors with high precision, so as to avoid errors, while keeping them isolated from the environment is the biggest challenge in QIP.

The interaction of a quantum system with its environment leads to the loss of quantum phase information and interference and, eventually, to the characteristics of the classical world. Quantum decoherence [156, 63, 20], in particular, describes a wholly quantum-

mechanical process, in which the system becomes entangled with the many degrees of freedom of the environment that are later disregarded: In this process, the system loses its coherent behavior. The application of quantum physics to information processing has transformed the nature of interest in decoherence. Quantum information manipulation is possible only if quantum devices can maintain coherence for an extended time. Therefore, the active study of decoherence attempts not only to understand the natural loss of information of a quantum state, but also to counteract it, using different strategies.

The discovery in the '90s of the possibilities of quantum error correction (QEC) by Shor[121] and Steane [128] has open the possibility to a practical implementation of quantum computation, lowering the requirements on control to a challenging but achievable level. As in classical computers, QEC aims at correcting errors naturally occurring during the normal operation of a quantum processor. Unlike classical error correction, however, QEC cannot rely on a simple repetition code in which many copies of the same object are created and a majority vote determines the correct answer. This approach is forbidden by the quantum no-cloning theorem [146]. It has been found, however, that by delocalizing the information, the environment responsible of errors and decoherence cannot acquire enough information about the system to destroy its coherence, and therefore the correct information can still be retrieved after correction.

The theory of QEC [82] provides codes that allow one to preserve the information encoded in orthogonal subspaces by detecting and correcting the errors introduced by decoherence. QEC allows one to perform a correct computation as long as the error rate is kept below a given threshold (this is the so-called *fault-tolerant* quantum computation [122, 5]).

A different strategy toward meeting the threshold for fault tolerant quantum computation is passive protection. When the noise operator presents distinct symmetries, it is possible to take advantage of the conserved quantities that are generally associated to symmetry properties. The information is thus encoded into subspaces or subsystems unaffected by the noise operator, called Decoherence Free Subsystem (DFS) [153, 46, 81, 137, 97, 8]. Likewise, dynamical decoupling techniques [138] symmetrize noise operators with an external modulation, to create the appropriate encoded subspace.

The common feature of these techniques is the encoding of the information on abstract degrees of freedom of the system, thus identifying logical qubits; this in turn will require special techniques for the initialization and control of these logical qubits, giving rise to new

challenges but also new opportunities.

A first challenge (see chapter 2) arises because these encodings, while promising to achieve fault tolerant QIP, come at the expenses of resource overheads. Up to now, QIP test-beds have not had sufficient resources to analyze encodings beyond the simplest ones. The most relevant resources are the number of available qubits and the cost to initialize them. It is therefore important to devise methods to reduce the initialization requirements. In this thesis we demonstrate an encoding of logical information that permits the control over multiple logical qubits without full initialization. The method of *subsystem pseudo-pure* states will allow the study of decoherence control schemes on up to 6 logical qubits, thus extending the contribution of ensemble QIP to the field of coherent quantum control and quantum computation.

A second challenge originates from additional experimental constraints emerging in most practical cases from the restriction to a subsystem, given realistic Hamiltonians. Although in principle DFSs allow universal quantum computation, preserving universal control can require leaving the protected subsystem. In this thesis we study the conditions under which quantum information can be manipulated and yet protected by a DFS encoding into logical qubits, even if the system leaves the DFS for short periods of time. We will address these issues in chapter 3 and furthermore show the importance of analyzing the noise spectral density, to devise efficient modulating schemes that can reduce decoherence below a desired threshold.

Before presenting these results, in the rest of this chapter we will present the model of NMR QIP that will be used in the rest of the first part of this thesis as a paradigm for describing issues and findings that are of general interest for quantum information processing. In particular, we will define the notations and conventions followed in the next chapters and the physical systems used in experiments.

1.1 The liquid state NMR system

Nuclear magnetic resonance (NMR), first observed by Bloch [12] and Purcell [113] in 1946, studies the quantum-mechanical properties and behavior of nuclear spin angular momenta. The most common nuclei observed in NMR spectroscopy have spin-$\frac{1}{2}$ (higher spins are also used, but the electric quadrupole moment adds complexity to the dynamics). These nuclei, in the presence of a magnetic field $\vec{B}$ have energy $-\vec{\mu}\cdot\vec{B}$ (the Zeeman energy), where the magnetic moment $\vec{\mu} = -\gamma\,\vec{I}$ is proportional to the spin operator $\vec{I}$ via the gyromagnetic ratio γ. The Zeeman energy scale is set by the gyromagnetic ratio and the field strength (see table 1.1) and for the superconducting magnets normally used it is on the order of MHz. For a strong magnetic field in the z direction, the Zeeman energy is much stronger than any other interaction and provides an axis of quantization for the spin operator.

Nucleus	**Natural abundance**	γ (Hz/G)	ω_0 **at 9.4 T** (MHz)	ω_0 **at 7 T** (MHz)
^{1}H	99.99	4,870	402	300
^{13}C	1.1	1,078	101	75.5
^{19}F	100	4,035	379	282.4

Table 1.1: **Table of spin-$\frac{1}{2}$ nuclei** used in the experiments reported in this thesis

Since the nuclear spins (for spins-$\frac{1}{2}$) are quantized in two energy states, they are convenient physical qubits, providing a straightforward mapping of qubits onto individual, distinguishable spins. Thus, the instrumentation and methods of NMR spectroscopy can be applied to the processing of quantum information (or, more generally, to the study coherent control of quantum systems).

In liquid state NMR, the spin-carrying nuclei are part of molecules dissolved in a solvent. As the couplings among molecules are weak and averaged to zero to first order by random motion, the molecules can be considered independent, so that the NMR sample is an ensemble of a large number ($N_m \approx 10^{18}$) independent molecules, or, in QIP terms, an ensemble of N_m independent quantum processors.

Internal Hamiltonian The N spins in each molecule are magnetically distinct: Not only different chemical species have different gyromagnetic ratios, but also the resonances of homonuclear spins depend on the local chemical environment. These differences in frequen-

cies are called *chemical shifts* and are usually on the order of 10-100ppm of the resonance frequency.

The spins interact with each other indirectly, the coupling being mediated by the electrons forming the molecular orbital between nuclei. The interaction strength is given by the *scalar coupling* constants $J_{k,h}$, which can range from a few Hz to hundreds of Hz.

The internal Hamiltonian of a molecule's nuclear spins in a large external magnetic field along the z-axis is then:

$$\mathcal{H}_{int} = \frac{1}{2}\sum_{k=1}^{N}\omega_k\sigma_z^k + \frac{\pi}{2}\sum_{k\neq h}J_{k,h}\vec{\sigma}^k\cdot\vec{\sigma}^h \tag{1.1}$$

where σ_α^k are Pauli matrices for the k^{th} spin.

It is usual in NMR to work in the so-called *rotating* frame, an interaction frame defined by the receiver frequency ω_0 and the total spin in the z-direction, $Z = \sum_k \sigma_z^k$. Thus the frequencies ω_k in Eq. (1.1) are to be interpreted as: $\omega_k = \Omega_k + \delta\omega_k - \omega_0$, where Ω_k is the Larmor frequency of the nucleus, $\delta\omega_k$ its chemical shift.

The values of the chemical shifts and J-coupling of a molecule's nuclear spins can be derived directly from their spectrum. We present here the constants of the internal Hamiltonian of the two molecules used in the experiments presented in this thesis, Crotonic acid ($C_4H_6O_2$) and Alanine ($C_3H_7NO_2$).

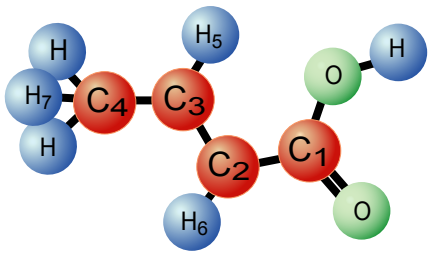

Figure 1-1: **Crotonic Acid** molecule.

Spin	**C_1**	**C_2**	**C_3**	**C_4**	**H_5**	**H_6**	**H_7**
ω_i (Hz)	6878.89	1882.63	4410.10	-8604.96	776.13	402.24	-778.60

Table 1.2: **Chemical Shift of the ^{13}C-labeled Crotonic acid** molecule in chloroform, in a 400MHz spectrometer. The spins are labeled 1-7 as in Fig. (1-1)

Spin	C_1	C_2	C_3	C_4	H_5	H_6
C_2	72.4					
C_3	1.4	69.6				
C_4	7.2	1.7	41.5			
H_5	6.5	-1.8	156.0	3.8		
H_6	3.3	162.9	-.7	6.2	15.5	
H_7	-.9	6.6	-7.1	127.5	6.9	-1.7

Table 1.3: **J-coupling** values (Hz) of the ^{13}C-labeled Crotonic Acid molecule in acetone. The spins are labeled 1-7 as in Fig. (1-1)

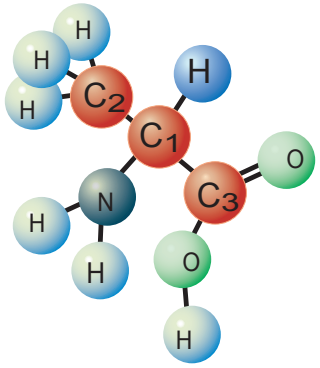

Figure 1-2: **Alanine** molecule.

Control The system is controlled by RF pulses and magnetic gradients. The Hamiltonian describing the interaction of the spins with the RF field is given by:

$$\mathcal{H}_{ext} \;=\; e^{-i\phi(t)\sum_k \sigma_z^k}\left(\tfrac{1}{2}\,\omega_{\mathsf{rf}}(t)\,\textstyle\sum_h \sigma_x^h\right) e^{\,i\phi(t)\sum_k \sigma_z^k} \tag{1.2}$$

where $\phi(t) = \omega_0 t + \varphi(t)$ is a time-dependent phase and $\omega_{\mathsf{rf}}(t)$ is a time-dependent amplitude. The phase and amplitude are independently controllable, allowing a high level of controllability. Several methods like shaped pulses [25], composite pulses [93], time-optimal control [79] have been used in NMR. In this thesis, we have used strongly-modulating pulses

Spin	C_1	C_2	C_3	H_T	H_3
ω_i (Hz)	7167.7	0	-2595.1	319.3	-371.9

Table 1.4: **Chemical Shift of the ^{13}C-labeled Alanine** molecule in acetone, in a 300MHz spectrometer. The spins are labeled as in Fig. (1-2)

Spin	C_1	C_2	C_3	H_T
C_2	54.1			
C_3	1.3	35.0		
H_T	4.6	145.2	4.5	
H_3	4.3	4.4	129.3	7.3

Table 1.5: **J-coupling** values (Hz) of the ^{13}C-labeled Alanine molecule in acetone. The spins are labeled as in Fig. (1-2)

(SMP) [56, 111] to drive the dynamics of the system. SMP are time-dependent RF fields designed by a numerical search, which perform precise rotations of one or more spins while refocusing the evolution of all other spins in a molecule [55, 16].

Magnetic field gradients $G_z = \frac{\partial B_z(t)}{\partial z}$ produced by a special coil run by a controllable current provide another control mechanism. The Hamiltonian associated with this interaction is given by:

$$\mathcal{H}_G = z\, G_z \frac{1}{2} \sum_k \gamma_k \sigma_z^k \tag{1.3}$$

Because the spectrometer records the total magnetization in the sample, averaging over the spatial coordinate, gradients can be used either as a non-unitary operation, which preserves only the terms in the density matrix that commute with the total angular momentum along z, or for simulating decoherence [54], relying on molecular diffusion to produce a stochastic, time-dependent field [125]. This decoherence mechanism is also present (although much weaker) in the absence of externally applied magnetic gradients, due to inhomogeneities in the external magnetic field or paramagnetic impurities in the sample. Other sources of errors are residual dipolar couplings among molecules [1], chemical shift anisotropies or inhomogeneities in the RF field.

Equilibrium State. Liquid phase NMR experiments are usually conducted at room temperature and in a large magnetic field, so that the spin system is in a highly mixed state. At equilibrium, the system is described by the Boltzmann distribution:

$$\rho_{th} = \frac{e^{-\beta\mathcal{H}}}{Z} \approx \frac{\mathbb{1} - \beta\mathcal{H}}{Z} \tag{1.4}$$

where Z is the partition function $Z = \mathrm{Tr}\left[e^{-\beta\mathcal{H}}\right]$, $\beta = 1/k_B T$ and $\mathcal{H}$ the system Hamiltonian. In the high temperature limit, where $\beta||\mathcal{H}|| \ll 1$, the density matrix can be approximated to first order by $\rho_{th} \approx \frac{\mathbb{1}-\beta\mathcal{H}}{Z}$. The partition function is given to first order by $\mathrm{Tr}\left[\mathbb{1}\right] = 2^N$ and assuming that the Zeeman energy is the only relevant part of the Hamiltonian, we can eventually write:

$$\rho_{th} \approxeq \frac{\mathbb{1}}{2^N} - \epsilon\rho_{eq} = \frac{\mathbb{1}}{2^N} - \frac{\epsilon}{2^N}\sum_{i=1}^{N}\sigma_z^i \tag{1.5}$$

where the last term ($\epsilon\rho_{eq}$) is a small, traceless deviation from the identity, which gives rise to the observable signal. Since the constant ϵ is on the order of 10^{-6} and the difference between the Zeeman energy is small, the signal generated by one spin is not enough to be detected and one needs a macroscopic sample to measure an observable signal.

Measurement The NMR signal is measured via the currents induced by the rotating bulk magnetization in a transverse coil tuned to the resonance frequency. Only the terms of the density matrix that have the same dipolar symmetry and orientation as the field generated by the RF coil will couple to it and be directly observables. The measured signal can be given as a trace: $\mathrm{Tr}\left[\rho(t)\sum_k \sigma_+^k\right]$, where $\sigma_+ = (\sigma_x + i\sigma_y)/2$[1].

NMR measurement are weak (as opposed to strong projective measurements), therefore the detection coil introduces only small distortions [14] in the system. The signal can then be acquired during an extended period of time, during which the system evolves under the internal Hamiltonian. Extra terms in the density matrix are therefore observable (those terms that evolve to a directly observable operator). This, and the ability to rotate the system, permits state tomography and therefore a precise measure of the control level reached in a QIP NMR experiment.

[1]The electronic apparatus allows us to simultaneously measure the real and imaginary part of the transverse magnetization through a phase shift of the signal

Chapter 2

Encoded Qubit Initialization

Liquid state NMR is playing an important role as test-bed for the new ideas of quantum information processing. Recently, much focus has been put on control of encoded information, that will allow the quantum computers of the future to avoid decoherence. The advantages brought by encoding the information come however at the expenses of physical resources, as encoding requires additional qubits to use as ancillas. For liquid state NMR to continue its role as QIP test-bed, the size of the systems used must therefore increase. This is a critical issue, because of the signal loss accompanying each added qubit in bulk quantum information processing schemes. We propose a new method to mitigate this signal decrease, that will allow the study of 3-6 logical qubits with the current experimental techniques. This scheme is based on the important insight that, because of the information encoding, only subsystems of the total Hilbert space are effectively used and need to be in a pure state. While the common experimental procedure consists in performing an encoding operation on the initial fiducial state of physical qubits, the direct preparation of logical fiducial states brings experimental advantages.

In this chapter we will first review the sources of signal loss tied to the creation of effectively pure state in NMR and introduce a new kind of logical pure states for which this signal loss is much reduced. For sake of concreteness, we present an example drawn from a particular encoding, before quantifying the gain in signal for a general encoding. We then also show an experimental realization on a four-qubit NMR system of the encoding used as example. Finally, we discuss the experimental results with particular attention to the metrics of control that the new kind of logical pure states allows us to measure and their

aptitude to quantify the actual control reached in experimental tests.

2.1 Subsystem Pseudo-Pure States

The equilibrium state of a spin system of liquid phase NMR is the highly mixed state:

$$\rho_{th} \approxeq \frac{\mathbb{1}}{2^N} - \epsilon\rho_{eq} = \frac{\mathbb{1}}{2^N} - \frac{\epsilon}{2^N}\sum_{i=1}^{N}\sigma_z^i \tag{2.1}$$

where the last term ($\epsilon\rho_{eq}$) is a small, traceless deviation from the identity, which gives rise to the observable signal (see Section (1.1)). The ability to use this system as a quantum information test-bed relies on effectively purifying the mixed equilibrium state. QIP can be performed on *pseudo-pure* states [37], states for which the dynamics of the observable operators are equivalent to the observables of a pure state. Among the methods used to create pseudo-pure states we can mention spatial averaging [37], temporal averaging [80] and logical labeling [60]. Unfortunately, the creation of pseudo-pure states comes at the expense of exponential consumption in experimental resources: time in the case of temporal averaging, signal in the case of spatial averaging, or usable Hilbert space in the case logical labeling.

Since the eigenvalues of a pseudo-pure state are in general different than those of the mixed state, a non-unitary completely positive operation, $\mathbb{T}$, must be used to create it:

$$\rho_P = \mathbb{T}(\rho_{th}) = \tfrac{\mathbb{1}}{2^N} - \epsilon\alpha(\rho_{pp} - \tfrac{\mathbb{1}}{2^N}) \tag{2.2}$$

where ρ_{pp} is a density matrix describing a pure state and the scaling factor α determines the signal loss. Since $\|\rho_{eq}\| \geq \|\mathbb{T}(\rho_{eq})\|$, α is bounded by the spectral norm ratio :

$$\alpha \leq \frac{\|\rho_{eq}\|}{\|\rho_{pp} - \mathbb{1}/2^N\|} \tag{2.3}$$

with $\|\rho_{eq}\| = \frac{N}{2^N}$. The SNR loss in the case of a full pseudo-pure state is thus $\frac{N}{2^N-1}$. This exponential loss of signal disqualifies[1] liquid state NMR as a scalable approach to QIP. Considering we have the ability to coherently control 10-12 qubits and possess spin systems responsive to such control, this loss of signal is also a serious limitation for benchmarking

[1]Other issues like frequency selectivity are also important

these systems.

To avoid this SNR loss when studying encoded operations, it is important to realize that only the subsystems encoding the information need to be pseudo-pure, while all other subsystems can be left in a mixed state, thus reducing the state preparation complexity.

To present the general structure that encoding imposes to the Hilbert space, we adopt the subsystem approach [140], that provides a unified description for Quantum Error Correction (QEC) and Decoherence Free Subsystems (DFS). A Hilbert space $\mathcal{H}$ of dimension $d = 2^N$ is used to encode $k \leq N$ qubits of information, protected against some noise $J = \{J_i\}$. With a change of basis to a direct sum[2] $\mathcal{H} \sim \bigoplus_i \mathcal{L}_i \otimes \mathcal{S}_i$, the noise acts only on the subsystems $\mathcal{S}_i$ (the syndrome) while the subsystems $\mathcal{L}_i$ are noiseless (for simplicity, we will often refer to a decomposition: $\mathcal{H} = \mathcal{L} \otimes \mathcal{S} \oplus \mathcal{R}$, with $\mathcal{R}$ an unprotected subspace).

To perform computations on logical qubits, they need to be prepared in a (pseudo-) pure state. The remaining subsystems $\mathcal{S}_i$ can however remain in a mixed state. We require only that the state evolves as a pure state in the logical subsystem, under the action of logical operations and we call these states *subsystem pseudo-pure* states.

If we are evolving the system with logical operators, the fact that they act only on the encoded subspace $\mathcal{L}$ ensures that information within this subspace will not leak out or mix with the orthogonal spaces during logical unitary transformations, thus preserving the purity of the encoded subspace under the noise model.

An important requirement for the subsystem pseudo-pure states is the ability to decode: the use of a mixed state should not introduce a mixing of the information contained in the logical qubits and in the unprotected subsystems, even when the information is transfered back to physical qubits by decoding. In general, setting the unprotected subsystem to the identity state will satisfy this requirement, even if other mixed states are possible for particular encodings. For a DFS, not being able to decode is inconvenient, as logical observables are in general difficult to measure experimentally. In the case of QEC the decoding step is fundamental to correct the errors occurred.

Let assume that we want to encode k qubits of information in a subsystem of dimension 2^k, with a corresponding syndrome subsystem, $\mathcal{S}$ of dimension d_s. Leaving this last subsystem in a mixed state, we can create a state that is pure on the logical degrees of freedom with a unitary operation that rearrange the eigenvalues, as long as there are at least as

[2]Further action of an appropriate operator A is required in the case of QEC codes [139]

many zero eigenvalues in the thermal state as in the k qubits pure state: $2^k - 1 < \frac{n!}{(n/2!)^2 d_s}$[3]. However, the eigenvalue spectrum of the equilibrium state of an N spin density matrix ($\lambda(\rho_{eq}) = \{N, N-2, ..., -N\}$) will most generally not generate the necessary eigenvalue spectrum required for decoding the k-qubits of information into k physical qubits without error. So a combination of unitary and not unitary operations must be used.

Before presenting a general model that allows us to quantify the SNR gain obtained by the subsystem pseudo-pure states, we will clarify the concept with an example.

2.1.1 Example - Subsystem Pseudo-Pure States in a Decoherence Free Subspace

Decoherence free subspaces (a subclass of DFS) are the most intuitive type of encodings, in which information is protected inside subspaces of the total Hilbert space that are invariant under the action of the noise. Here we consider the collective σ_z noise, which describes a dephasing caused by completely correlated fluctuations of the local magnetic field $B(t)$:

$$\mathcal{H}_{\mathsf{st}} = \omega(t)\, Z, \tag{2.4}$$

with $Z = \sum_k \sigma_z^k$, the total spin angular momentum along the quantization axis z and $\omega(t) = \gamma B(t)$ the noise strength. For 2 spins, the eigenspace of the noise operator Z with eigenvalue 0 is a 2-dimensional decoherence free subspace [54] and can be used to encode one qubit of information. The DFS is spanned by the basis vectors $|01\rangle$ and $|10\rangle$. A natural encoding of a logical qubit $|\psi\rangle_L$ is given by:

$$\alpha|0\rangle_L + \beta|1\rangle_L \Longleftrightarrow \alpha|01\rangle + \beta|10\rangle \tag{2.5}$$

[3]The state preparation procedure that bears the most resemblance to the method we propose is logical labeling [60], which uses a unitary transformation to change the equilibrium distribution of spin states into one where a subsystem of the Hilbert space is pseudo-pure conditional on a physical spin having some preferred orientation. The parts of Hilbert space that remain mixed are of no use to the computation whatsoever. It can be shown that a $m-$qubit effective pure state can be stored among the Hilbert space of $N-$qubits provided the inequality $2^m - 1 < \frac{n!}{(n/2!)^2}$ is satisfied. A key insight is that in the study of encoded qubits, one need not take this $m-$qubit effective pure state and perform an encoding of $k-$logical qubits under the hierarchy $k < m < N$. Instead, a k-qubit encoded state can be prepared directly from the equilibrium state of N qubits.

The encoded pure state for a DFS logical qubit is given by:

$$|01\rangle\langle 01| = \frac{\mathbb{1}_L + \sigma_{z,L}}{2} = \frac{\mathbb{1} + \sigma_z^1 - \sigma_z^2 - \sigma_z^1\sigma_z^2}{4} \tag{2.6}$$

In the case of the DFS considered, the Hilbert space can be written as a direct sum of the logical subspace $\mathcal{L}$ (spanned by the basis $|01\rangle$ and $|10\rangle$) and its complementary subspace $\mathcal{R}$ (spanned by the basis $|00\rangle$ and $|11\rangle$), $\mathcal{H} = \mathcal{L} \oplus \mathcal{R}$. If we add the identity on the $\mathcal{R}$ subspace to the logical pure state, we obtain a mixed state that is equivalent in terms of its behavior on the logical degrees of freedom:

$$\rho = \frac{1}{2}|0\rangle\langle 0|_L + \frac{\mathbb{1}_R}{4} = \frac{1}{4}(\mathbb{1} + \sigma_{z,L}) = \frac{1}{4}(\mathbb{1} + \frac{\sigma_z^1 - \sigma_z^2}{2}) \tag{2.7}$$

The traceless part of this state is simply $\propto \sigma_z^1 - \sigma_z^2$: From the thermal equilibrium, a unitary operation is enough to obtain this state, so no signal is lost. In general, the subsystem pseudo-pure state that one obtains with this method would require less demanding averaging procedure, resulting in a higher signal and less complex state preparation procedures.

As an example, consider the pure state of two logical qubits encoded into a 4 physical qubit DFS:

$$|00\rangle\langle 00|_L = \tfrac{1}{4}(\mathbb{1}_L^1 + \sigma_{z,L}^1) \otimes (\mathbb{1}_L^2 + \sigma_{z,L}^2) \tag{2.8}$$

If we add $\mathbb{1}_R$ to the unprotected subspace of each logical qubit, we obtain a state which is pseudo-pure within the subspace of the logical encoding:

$$\begin{aligned} \rho_{ep} &= \tfrac{1}{16}(\mathbb{1}_L^1 + \mathbb{1}_R^1 + \sigma_{z,L}^1) \otimes (\mathbb{1}_L^2 + \mathbb{1}_R^2 + \sigma_{z,L}^2) \\ &= \tfrac{12}{16}(\mathbb{1}^{12} + \tfrac{\sigma_z^1 - \sigma_z^2}{2}) \otimes (\mathbb{1}^{34} + \tfrac{\sigma_z^3 - \sigma_z^4}{2}) \end{aligned} \tag{2.9}$$

We still need a non-unitary operation to obtain this state, but the SNR loss is only 1/3 instead of 4/15 as for creating the full pseudo-pure state (or the even lower 2/13 we obtained in practice due to experimental constraint, see section 2.4). The preparation procedure is also less complex, since it only requires to prepare up to 2−body terms ($\sigma_z^i\sigma_z^j$) instead of 4−body terms ($\sigma_z^1\sigma_z^2\sigma_z^3\sigma_z^4$).

2.2 Bounds in Signal Gain

To illustrate the advantages the subsystem pseudo-pure states bring, we present now the scheme in more general terms, looking for a quantitative bound on the increase in sensitivity with respect to the full pseudo-pure state. When under a particular encoding the Hilbert space is transformed to $\mathcal{H} \sim \bigoplus_i \mathcal{L}_i \otimes \mathcal{S}_i$, in the encoded representation, the state we want to prepare will have the form:

$$\rho_{ep} = \bigoplus_i a_i \left(|\psi\rangle_L^i \langle\psi|_L^i \otimes \frac{\mathbb{1}_S^i}{d_{s_i}} \right) \tag{2.10}$$

The dimension of the i-th syndrome is d_{s_i}; a_i are subspace weighting coefficients, such that $\sum_i a_i = 1$, ensuring a unit trace of ρ_{ep}. We would like to analyze the conditions for the optimal signal, given that some freedom in the construction of the subsystem pseudo-pure states is available. In the previous example, the subsystem pseudo-pure and the mixed states were given the same subspace weighting coefficient: $a_1 = a_2 = \frac{1}{2}$. In general, different weightings could provide higher signal.

In particular, since we are interested in the information that we can manipulate, a good measure of sensitivity gain is the SNR of the qubits storing the information after the decoding. Instead of the total magnetization, which is the observable in NMR, we are therefore interested in:

$$SNR = \langle |\vec{M}| \rangle \propto S(\rho) = \frac{}{\sqrt{\mathrm{Tr}\left[\sum \sigma_z^i \rho\right]^2 + \mathrm{Tr}\left[\sum \sigma_x^i \rho\right]^2 + \mathrm{Tr}\left[\sum \sigma_y^i \rho\right]^2}} \tag{2.11}$$

where the sum only extends over the k information carrying qubits. Other metrics are of course conceivable, for example the total magnetization of the N spins or the spectral norm of the density matrix deviation, but they are not directly related to the signal arising from the information carrying qubits[4].

We consider to encode k logical qubits among N physical qubits, with a syndrome subsystem $\mathcal{S}$ of dimensions 2^s (the Hilbert space can be written as $\mathcal{H} = \mathcal{L} \otimes \mathcal{S} \oplus \mathcal{R}$)[5]. The

[4]Notice that even the chosen metric can be misleading, since in the case $k > 1$ some states give no signal (e.g. a non-observable coherence). However, any of these states can be characterized by especially designed read-out operations that transform it to an observable state, while preserving its information content. More specifically, we will consider only the ground state $|00\ldots\rangle$ signal, since any other state is isomorphic to it, via a unitary operation.

[5]We consider only the case where we can map qubits on the subsystem S, even if in general the subsystem

encoding operation is in general defined by its action on the initial state $|\psi\rangle_k|00\ldots\rangle_{N-k}$, giving the encoded state: $|\psi\rangle_L|0\rangle_S$. Hence, there is some arbitrariness in the choice of encoding operation (since it is defined only for ancillas initially in the ground state) but we can specify it with the assumption that the state in the encoded subsystem $\mathcal{S}$ is determined by the first s ancillas state:

$$U_{enc}|\psi\rangle_k|\phi\rangle_s|00...\rangle_{N-k-s} = |\psi\rangle_L|\phi\rangle_S \tag{2.12}$$

The subsystem pseudo-pure state is:

$$\rho_{ep} = a\left(|\psi\rangle\langle\psi|_L \otimes \frac{\mathbb{1}_S}{2^s}\right) + \frac{1-a}{2^N - 2^{s+k}}\mathbb{1}_R, \tag{2.13}$$

which after decoding following (2.12) becomes:

$$\rho_{ep} = \left(a|\psi\rangle\langle\psi| - \tfrac{1-a}{2^N-2^{s+k}}\mathbb{1}_k\right)\tfrac{\mathbb{1}_s}{2^s}|00\ldots\rangle\langle 00\ldots|_{N-k-s} + \tfrac{1-a}{2^N-2^{s+k}}\mathbb{1}, \tag{2.14}$$

so that the signal is given by: $S(\rho) = a\epsilon\alpha S(|\psi\rangle\langle\psi|_k) \propto a\alpha k$, where $\alpha \leq \frac{\|\rho_{eq}\|}{\|\rho_{pp} - \mathbb{1}/2^N\|}$. To obtain the spectral norm of the subsystem pseudo-pure state traceless part, we calculate its eigenvalues:

$$\{\frac{a}{2^s} - 2^{-N},\ -2^{-N},\ \frac{1-a}{2^N - 2^{s+k}} - 2^{-N}\} \tag{2.15}$$

The upper bound for the signal is obtained for $a = 2^{s+1-N}$ and we have: $SNR \propto N2^{s+1-N}$.

When one wants to use more than one logical qubit, each being protected against some noise, or if one wants to concatenate different encodings, a tensor structure of encoded qubits arises naturally. We analyze also this second type of construction, that can bring a further enhancement of the signal. We assume here to encode 1 logical qubit in n physical ones -each being a subsystem pseudo-pure state- and we build a logical $k-$qubit state with the tensor product of these encoded qubits.

The Hilbert space can be written as tensor product of direct sums as: $\mathcal{H} = \bigotimes_{i=1}^{k}(\mathcal{L}_i \otimes \mathcal{S}_i \oplus \mathcal{R}_i)$.

The corresponding partially mixed states differ with respect to the previous ones, in that subspaces that are not actually used to store protected information are not maximally

need not be of dimension 2^s. The results would be however the same, with slightly different notations.

mixed:

$$\begin{aligned}\rho_{ep} &= (a_1|\psi\rangle\langle\psi|_{L1} \otimes \tfrac{\mathbb{1}_{S1}}{2^s} \oplus \tfrac{1-a_1}{2^n-2^{s+1}}\mathbb{1}_{R1}) \\ &\otimes(a_2|\psi\rangle\langle\psi|_{L2} \otimes \tfrac{\mathbb{1}_{S2}}{2^s} \oplus \tfrac{1-a_2}{2^n-2^{s+1}}\mathbb{1}_{R2}) \otimes \dots\end{aligned} \tag{2.16}$$

Notice that we consider here that all the qubits have the same encoding and to make the problem more tractable we also choose $a_i = a, \forall i$. Other choices of course exist, and may lead to a better SNR, but they should be studied on a case by case basis, for every particular encoding and noise model. Upon decoding, this state is transformed to:

$$\begin{aligned}\rho'_{ep} = U^\dagger_{enc}\rho_{ep}U_{enc} \quad &= \bigotimes_{i=1}^{k}[(a|\psi\rangle\langle\psi|_1 - \tfrac{1-a}{2^n-2}\mathbb{1}_1) \\ &\otimes\tfrac{\mathbb{1}_s}{2^s} \otimes |00\dots\rangle\langle 00\dots| + \tfrac{1-a}{2^n-2}\mathbb{1}_n]_i\end{aligned} \tag{2.17}$$

To calculate the signal of this state, we should calculate terms like

$$S_\alpha = \left(\sum_k \mathrm{Tr}\left[\sigma^k_\alpha \rho'_{ep}\right]\right)^2 = \left(\sum_k (\mathrm{Tr}\left[\sigma^k_\alpha \rho^k_{ep}\right] \prod_{j\neq k} \mathrm{Tr}\left[\rho^j_{ep}\right])\right)^2, \tag{2.18}$$

where

$$\rho^j_{ep} = (a|\psi\rangle\langle\psi|_1 - \tfrac{1-a}{2^n-2}\mathbb{1}_1) \otimes \tfrac{\mathbb{1}_s}{2^s} \otimes |00\dots\rangle\langle 00\dots| + \tfrac{1-a}{2^n-2}\mathbb{1}_n]_j, \tag{2.19}$$

which has trace one. We obtain therefore $S_\alpha = \left(\sum_k \mathrm{Tr}\left[\sigma^k_\alpha \rho^k_{ep}\right]\right)^2$ and it is easy to show that the signal is again simply proportional to $a\alpha k$: Varying a we can find the optimal state. The eigenvalues for the traceless part of the subsystem pseudo-pure state are:

$$\begin{aligned}&\prod_{i=1}^{k}(\{\frac{a}{2^s}, 0, \frac{1-a}{2^n-2^{s+1}}\}_i) - 2^{-N} \\ &= \{(\frac{a}{2^s})^{k-p}\left(\frac{1-a}{2^n-2^{s+1}}\right)^p\Big|_{p=0}^{k} - 2^{-N}, -2^{-N}\}\end{aligned} \tag{2.20}$$

The maximum SNR depends on the relative dimension of the logical subspace and the syndrome and on the number of encoded qubits. To find the norm of the density matrix as a function of a, we must again find the maximum eigenvalue. Of the $\binom{k}{2}+1$ eigenvalues in (2.20), we can just consider the following three,

$$\{(\tfrac{a}{2^s})^k - 2^{-N}, -2^{-N}, \left(\tfrac{1-a}{2^n-2^{s+1}}\right)^k - 2^{-N}\} \tag{2.21}$$

since for $\frac{a}{2^s} - \frac{1-a}{2^n-2^{s+1}} > 0$ (< 0) the product $(\frac{a}{2^s})^{k-p}\left(\frac{1-a}{2^n-2^{s+1}}\right)^p$ is maximum for $p = 0$

$(p = k)$, giving the first (third) eigenvalue in (2.21). To determine which one is the maximum eigenvalue for any value of a, we consider the point at which the absolute values of the eigenvalues e_1 and e_3 are equal, $a = a_{13}$. If at this point $|e_1| > |e_2|$, then the maximum eigenvalue is given by e_1 for $a < a_{13}$ and by e_3 otherwise (see Fig. (2-1) right), and the maximum of $a\alpha$ is obtained for $a^* = a_{13}$. If instead $|e_1| < |e_2|$ at a_{13}, there is a region in a, where the maximum eigenvalue is just $|e_2|$, and to maximize $a\,\alpha$ we choose a such that $|e_1| = |e_2|$, $a^* = a_{12}$ (see Fig. (2-1)).

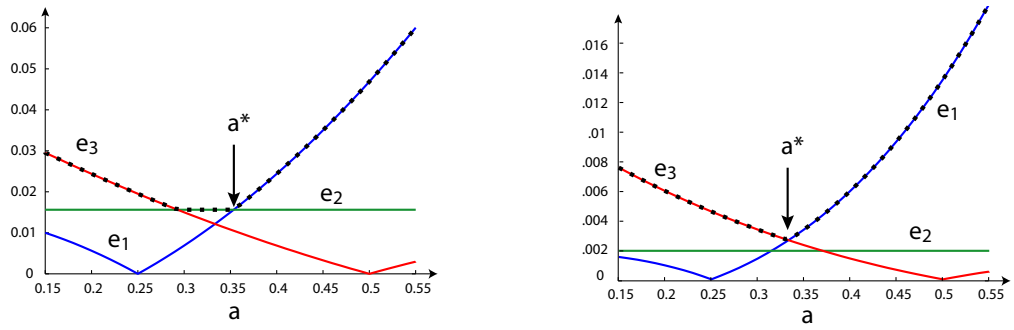

Figure 2-1: **Eigenvalues of the subsystem pseudo-pure density matrix** (its deviation from the identity), for $s = 1$, $n = 3$ and $k = 2$ (left) and $k = 3$ (right). The dotted line marks the maximum eigenvalue, that is, the norm of the density matrix. Notice that in the first case the maximum SNR is obtained for $|e_1| = |e_2|$, while in the second case for $|e_1| = |e_3|$

In particular:

When $k < \frac{-1}{\log_2(1-2^{s-n})}$ the $SNR \propto N2^{s+1/k-n}$ (The norm reaches the minimum value 2^{-N} for $a^* = a_{12} \equiv 2^{s+1/k-n}$).

When $k > \frac{-1}{\log_2(1-2^{s-n})}$, we obtain $SNR \propto \dfrac{N2^s(2^n - 2^s)^k}{2^N - (2^n - 2^s)^k}$: The minimum value for the norm $(2^n - 2^s)^{-1} - 2^N$ is obtained for $\dfrac{a}{2^s} = \dfrac{1-a}{2^n - 2^{s+1}}$, i.e. for $a^* = a_{13} \equiv \dfrac{2^s}{2^n - 2^s}$.

In both cases, the SNR obtained with a tensor product structure is higher than for the first construction presented.

The improvement brought by the subsystem pseudo-pure states can be generalized to many types of encoding. We now present three examples, applying our scheme to the case of the 4-qubit DFS already presented, a 3-qubit NS and a 3-qubit QEC, to illustrate some possible applications of the scheme proposed.

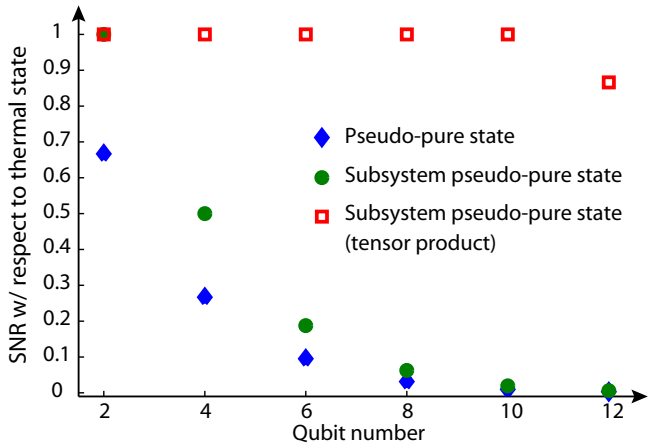

Figure 2-2: **Signal to Noise ratio** (normalized to the SNR for thermal state) for subsystem pseudo-pure states, as a function of the total physical qubit number. The encoding is a DFS protecting the system against collective dephasing noise. The DFS encodes 1 logical qubit on two physical qubits as in Section (2.1.1).

2.2.1 Application to various encodings

Decoherence Free Subspace The DFS encoding of two logical qubits has already been presented in Section (2.1.1) for the particular case $a = \frac{1}{2}$. Here we want to calculate the maximum SNR obtainable and compare it to what was found previously. In particular, we will see that the state giving the maximum SNR is more complex to prepare with the control available in NMR, and thus the state presented above is to be preferred. This compromise between SNR and initialization complexity is expected to be a general concern common to other encodings. If we adopt the first scheme presented, the state that we want to prepare is given by:

$$\rho_{ep} = a|0101\rangle\langle 0101| + \frac{(1-a)}{12}\mathbb{1}_R, \tag{2.22}$$

with

$$\mathbb{1}_R = \mathbb{1} - |0101\rangle\langle 0101| - |1001\rangle\langle 1001| - |0110\rangle\langle 0110| - |1010\rangle\langle 1010| \tag{2.23}$$

and $a = \frac{1}{8}$ for the maximum SNR$= 1/2$. The state is $\rho_{LPP} \propto \sigma_z^1\sigma_z^2 + \sigma_z^3\sigma_z^4 - \sigma_z^1\sigma_z^2\sigma_z^3\sigma_z^4$ and thus, even if the theoretical achievable SNR is higher than what obtained in Section (2.1.1), in practice this state will be more challenging to prepare. This state contains 4-body terms, which are more difficult to create in NMR, since they comport an interaction among non-neighboring spins which are only very weakly coupled (see for example the J-coupling

strength for crotonic acid in Section (1.1)).

With the tensor product scheme, we should prepare the state

$$\rho_{ep} = \left(a|01\rangle\langle 01| + \frac{(1-a)}{2}\mathbb{1}_R^1\right) \otimes \left(a|01\rangle\langle 01| + \frac{(1-a)}{2}\mathbb{1}_R^2\right) \tag{2.24}$$

where $a = \sqrt{2}/4$ to maximize the signal up to a theoretical SNR= 1. Again, practical considerations suggest that this state is more complex to prepare and in practice will lead to a lower SNR than the theoretical one.

Noiseless Subsystems. It has been observed that the smallest code that protects a system against an arbitrary collective noise can be realized with a 3 physical qubit DFS [57] (also called Noiseless subsystem to distinguish them from decoherence free subspaces). The collective noise conserves the total angular momentum J of the system. In the case of 3 spin-$\frac{1}{2}$ system, the Hilbert space can immediately be written as: $\mathcal{H} = \mathcal{H}_{3/2} \oplus \mathcal{H}_{1/2}$. Noting furthermore, that the second subspace ($\mathcal{H}_{1/2}$) is doubly degenerate, we can identify in it a protected subsystem, reflecting a logical degree of freedom: $\mathcal{H}_{1/2} = \mathcal{L} \otimes \mathcal{S}$, where the second subsystem is associated with the j_z quantum number.

Since the information is all encoded in the subsystem $\mathcal{L}$, we can safely leave the subsystem $\mathcal{S}$ in a mixed state, since we are no longer interested in its evolution. The state we want to create has thus the form: $|0\rangle\langle 0|_L \otimes \mathbb{1}_S/2$. In terms of physical operators, using the decoding operator in ref. [57], this corresponds to:

$$\rho_{ep} = (\mathbb{1} + \sigma_z^1 + \sigma_z^2 + \sigma_z^1\sigma_z^2)/8 \tag{2.25}$$

Only 1/3 of the signal must be lost to create this state.

Notice that we can also set the subspace corresponding to $j = 3/2$ to the identity state, with $a = \frac{1}{2}$ for the optimal SNR. With the encoding given in [57], the identity on the unprotected subspace $\mathcal{H}_{3/2}$ is $(\mathbb{1} - \sigma_z^1/2)/8$. The subsystem pseudo-pure state is then: $\rho_{ep} = (2 \cdot \mathbb{1} + \sigma_z^1/2 + \sigma_z^2 + \sigma_z^1\sigma_z^2)/16$ and 1/2 of the SNR is retained in obtaining this state instead of 3/7 for a full pseudo-pure state.

Quantum Error Correction Codes. When the noise does not present any useful symmetry, information can still be preserved by using QEC codes. These codes require a two

step operation for protecting against the noise: first one needs to encode the information in an appropriate subspace and then, after some eventual error has occurred, the qubit must be corrected based upon the state of the syndrome. It would seem therefore that the scheme proposed cannot be applied here, since when ancillas are not in the ground state but in a mixed one, they indicate that errors had already acted on the system, and QEC codes can protect only for a finite number of errors. However, if we initially populate the orthogonal syndrome subspaces with identity, recovery of the information is still possible and we obtain a subsystem pseudo-pure state with a higher SNR and the same observable dynamics as a full pseudo-pure state.

Consider for example the encoding for the 3 qubit QEC, protecting against a single bit-flip error (σ_x^i). The code subspace is spanned by the basis set:

$$|0\rangle_L = |000\rangle; \qquad |1\rangle_L = |111\rangle \tag{2.26}$$

The Hilbert space has an irreducible representation as the direct sum of 4 orthogonal subspaces: $\mathcal{H} = \mathcal{L} \oplus \mathcal{R}_1 \oplus \mathcal{R}_2 \oplus \mathcal{R}_3$, each $\mathcal{R}_i$ spanned by the basis: $\sigma_x^i\{|0\rangle_L, |1\rangle_L\}$, $i = 1, 2, 3$.

An error causes a swapping of the code subspace with one of the orthogonal subspaces, which is then corrected by the decoding operation. Starting from the pure state: $|\psi\rangle|00\rangle$, which we encode following (2.26), the final state after an error and decoding is $|\psi\rangle|xy\rangle$ ($x, y \in \{0, 1\}$) and the ancillas need to be reinitialized for the code to be effective against a second error. Since logical operations act only on the first subspace, we can set the other subspaces to the maximally mixed state. The state we want to prepare is thus given by:

$$\begin{aligned} &a|\psi\rangle\langle\psi|_L + (1-a)(\mathbb{1}_{R1} + \mathbb{1}_{R2} + \mathbb{1}_{R3})/6 \\ &= a|\psi\rangle\langle\psi|_L + (1-a)(\mathbb{1} - \mathbb{1}_L)/6 \end{aligned} \tag{2.27}$$

When we decode after an eventual error, we obtain the state: $(a|\psi\rangle\langle\psi|_1 - (1-a)\mathbb{1}_1/6)$ $|xy\rangle\langle xy| + (1-a)\mathbb{1}/6$. Since the identity $\mathbb{1}_1$ is not observable in NMR, this state carries the same information content as the full pseudo-pure state. With $a = 1/4$ we find that the SNR is reduced only to $\frac{3}{4}$ of the initial SNR for this mixed state, while it would be 3/7 for the full pseudo-pure state.

Generalizing to other QEC codes, one can always find an encoding operation that transform the Hilbert space to $\mathcal{H} \sim \mathcal{L} \bigoplus_i \mathcal{R}_i = \mathcal{L} \oplus \mathcal{R}$ and prepare a subsystem pseudo-pure

state following the constructions for the DFS, setting the subspace $\mathcal{R}$ to identity. However, this encoding only allows one to correct for a finite number of errors, a recovery operation is needed to reinitialize the ancillas. The recovering operation could in general be accomplished by a strong measurement, however this is not feasible in NMR; one must have fresh ancillas available. To correct for two errors in the previous example, a partially mixed state with 4 ancillas should be prepared, so that two new fresh ancillas can be used for correcting the second error. In general, in addition to the 3 qubit system that encode the state, a separated reservoir (not affected by the noise) of $2n$ ancillas is needed for correcting n errors. Even if ancillas must be all prepared simultaneously, the creation of subsystem pseudo-pure states increases the SNR, so that the number of ancillas, and therefore of errors that can be corrected, can be increased in actual experiments.

2.3 Experimental Validation of Subsystem Pseudo-Pure States on a Decoherence-Free Subspace

To illustrate the advantages provided by the subsystem pseudo-pure states, we have created an encoded Bell State on a liquid state NMR quantum information processor, repeating the experiment with a full and a logical pseudo-pure state. The encoding, protecting information against a collective σ_z noise, consisted in the 4 qubit DFS presented in Section (2.1.1). We have chosen the four 13-C labeled carbon spins ($I = \frac{1}{2}$) of crotonic acid (see tables 1.2,1.3) as our qubit system.

The pseudo-pure state was prepared using spatial averaging techniques [37]. Comparing Figures 2-3 and 2-4, the preparation of the logical state is much simpler, providing a more accurate initial state, in a shorter time ($0.0568s$ instead of $0.1194s$). Furthermore, we observed a further SNR drop to about 2/13 instead of the theoretical 4/15, due to experimental constraints in the preparation of the pseudo-pure state via spatial averaging.

The entangled state was prepared by implementing the logical gates via a combination of strongly modulated pulses [56, 111] and delays of free evolution. From Fig. (2-5) we see that the required operations are $\sigma_{z,L}$, $\sigma_{x,L}$ and $\sigma^1_{z,L}\sigma^2_{z,L}$. The first rotation $\sigma_{z,L} = (\sigma^1_z - \sigma^2_z$ is obtained from the evolution under the chemical shift term in the internal Hamiltonians. The two logical body interaction can be obtained by the operator: $\sigma^1_z\sigma^3_z$, which is much

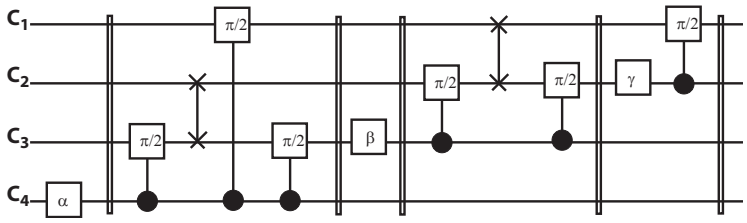

Figure 2-3: **Circuit for the preparation of the pseudo-pure state**. We represent single qubit rotations by square boxes, controlled rotations by closed circles on the controlling qubit linked to the applied rotation on the controlled qubit; swaps gate by two crosses on the swapped qubits, connected by a vertical line; non unitary operations (gradients) by double vertical bars. Notice the number of controlled operations, each requiring a time of the order of the coupling strength inverse, and Swap gates, each requiring three times more time.

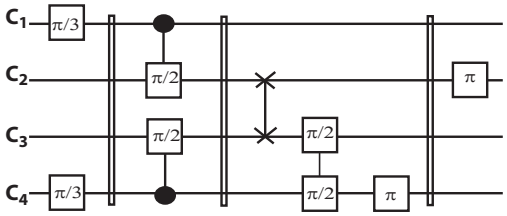

Figure 2-4: **Circuit for the preparation of the subsystem pseudo-pure state.** We use the same convention as in Fig. (2-3), with the square root of a swap gate indicated by two $\pi/2$-rotations linked by a vertical line. Compare the number of operations required for the subsystem pseudo-pure state with those required for the full pseudo-pure state: This preparation appears to be much simpler.

easier to implement then the full logical operator, given that the internal Hamiltonian of the 4-spin system under investigation has all pairwise $\sigma_z^i\sigma_z^j$ interactions.To produce a rotation about the logical x axis we can simply apply the operator $e^{-i\theta\sigma_y^1\sigma_y^2}$ instead of using the full logical $\sigma_{x,L} = (\sigma_x^1\sigma_x^2 + \sigma_y^1\sigma_y^2)/2$.

Since the molecule falls into the weak-coupling regime[6] the naturally occurring $\sigma_x^i\sigma_x^j$ of the scalar coupling cannot be used. The technique of re-introducing the strong coupling to a pair of spins via a Hartman-Hahn irradiation [70] as used in [54] also proves to be ineffective, as individual pairs of couplings cannot be selectively chosen with high fidelity. Instead, we have used a pulse sequence in the Carr-Purcell vein [28], which rotates the internal Hamiltonian to the transverse plane and then selects the desired operators out of the total Hamiltonian, by refocusing any unwanted evolution with a strong modulation, typically spin selective π-pulses.

[6]In the weak coupling regime, the large differences in chemical shift among spins, average to zero the part of the J-coupling interaction that is not along the z-axis, leaving only the interaction $\sigma_z\sigma_z$

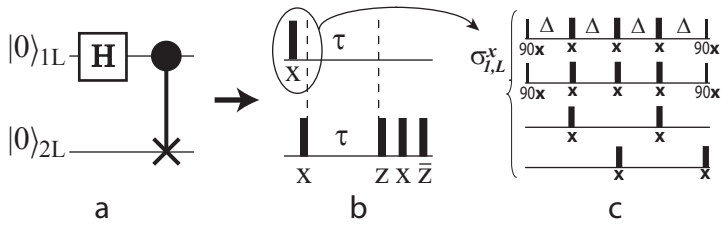

Figure 2-5: **Entangling circuit** on logical qubits (a) and corresponding logical pulses (b). Pulse sequence implementing the $\sigma^x_{1,L}$ logical rotation with physical qubits (c); similar pulse sequences are used for the other logical operations.

This sequence (Fig. (2-5.c)) thus generates a first order effective Hamiltonian [68] comprised solely of the operator of interest: $\sigma^1_y\sigma^2_y$. Logical rotations of an arbitrary angle, θ, can be executed by varying the delay times (Δ) between the π-pulses.

We have used robust, strongly-modulating RF pulses [56, 111] for each single qubit rotation in the sequence. The delay periods were further optimized using the simplex algorithm to maximize the correlation between the wanted and simulated final states. To avoid coherent errors due to the coupling between the Carbon and Proton spin systems, we have applied a WALTZ-16 decoupling sequence [120] to the protons during the length of the experiment. It is believed that Nuclear Overhauser Enhancement [107, 127] due to decoupling has a minimal effect on the populations of the carbon spin-states.

Notice that apart from the initialization sequence, the control sequence applied to the logical and full pseudo-pure states were the same. State tomography [124] of the final encoded state shows the creation of the logical Bell state, while identity is maintained on the non-logical degrees of freedom, with no noticeable mixing of the different subspaces. Comparing the results obtained with the full and the subsystem pseudo-pure states, we observe an improvement in the initial state preparation for the latter one, while the final Bell State presents similar errors (in particular, a drop of the off diagonal components with respect to the expected ones).

2.4 Metrics of Control for Subsystem Pseudo-Pure States

In order to quantitatively assess the extent of control of a quantum operation, we adopt a widely used metric, the correlation of the experimental density matrix with the expected one [56]. In particular, to take into account attenuation due to decoherent or incoherent

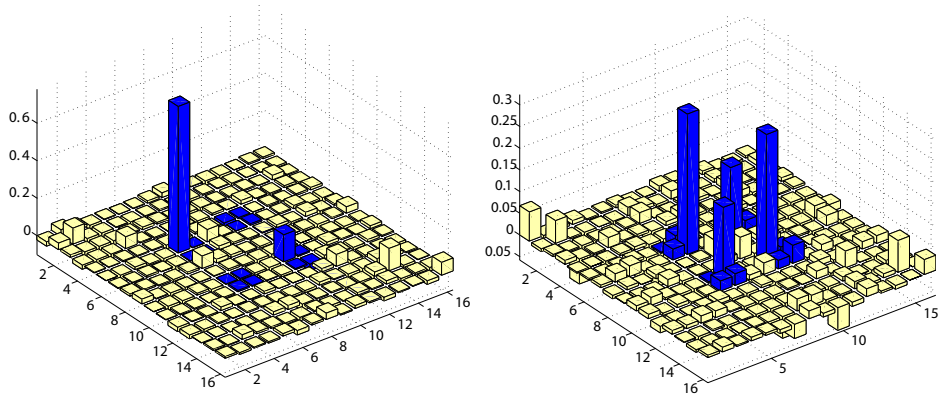

(a) Pseudo-Pure State (b) Logical Bell State

Figure 2-6: **Density matrices** for the initial pseudo-pure state over the entire Hilbert space(a) and the logical Bell State (b). The darker part indicates the states in the logical subspace.

Quantum state	$\mathcal{C}_{Sim}$	$\mathcal{C}_{Exp}$	$\mathcal{C}_{L}$
Full pseudo-pure	0.95	0.88	0.98
Full Bell state	0.75	0.53	0.59
Subsystem pseudo-pure	0.98	0.97	0.99
Encoded Bell state	0.92	0.73	0.61

Table 2.1: **Experimental and Simulated data for the implementation of Encoded Bell State Propagator**. The last column reports the correlation of the state considering the protected subspace only. Experimental errors of $\approx 4\%$ can be attributed to systematic errors in the fitting algorithm used to reconstruct the density matrix from NMR spectral data.

processes, we consider the attenuated correlation of two quantum states, defined as:

$$C = \frac{\mathrm{Tr}\left[\rho_{th}\rho_{exp}\right]}{\sqrt{\mathrm{Tr}\left[\rho_{th}^2\right]\mathrm{Tr}\left[\rho_{in}^2\right]}}. \tag{2.28}$$

Here $\rho_{th} = U\rho_{in}U^\dagger$, $\rho_{exp} = \mathcal{E}(\rho_{in})$, and ρ_{in} define the theoretical, experimental and input states respectively. Table (2.1) shows the attenuated correlations for both logical and full pseudo-pure and both initial and final states.

The relative drop in correlation between the initial state and the final state is comparable for both pseudo-pure state. It should be emphasized that apart from the advantages of SNR of the subsystem pseudo-pure state, the preparation of this state requires shorter, less

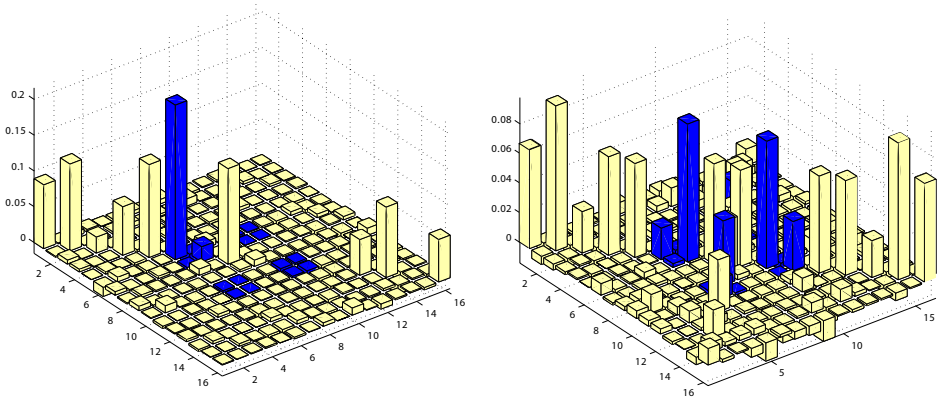

(a) Subsystem Pseudo-Pure State (b) Subsystem Logical Bell State

Figure 2-7: **Density matrices** for the initial pseudo-pure state over only the logical subspace (a) and the Bell-State (b) obtained from this initial subsystem pseudo-pure state. The darker part indicates the states in the logical subspace. Notice how in the case of the subsystem pseudo-pure states, areas of Hilbert space not in the logical subspace are in a mixed state.

complex pulse sequences, thus marginalizing coherent and incoherent errors. This is evident as the correlation of the subsystem pseudo-pure state is significantly larger than that of the full pseudo-pure state.

When we compare theoretical and experimental encoded states, their overlap has contributions that mirror the logical subsystem structure of the Hilbert space. Consider for simplicity a Hilbert space that can be written in terms of a logical and non-logical subspaces, $\mathcal{H} \sim \mathcal{L} \oplus \mathcal{R}$. Rewriting the experimental quantum process in terms of Kraus operators A_μ [84], ($\mathcal{E}(\rho) = \sum_\mu A_\mu \rho A_\mu^\dagger$) we can separate them into three groups: $\{A_{\mu,LL}, A_{\mu,RR}, A_{\mu,LR}\}$, which respectively describe the maps on the $\mathcal{L}$ subspace, $\mathcal{R}$ subspace, and the mixing of these two subspaces. The correlation will reflect these three contributions to the dynamics, $C = \alpha_{LL}C_{LL} + (\alpha_{LR}C_{LR} + \alpha_{RL}C_{RL}) + \alpha_{RR}C_{RR}$, where:

$$C_{KH} = \frac{\mathrm{Tr}\left[P_K \rho_{th} \sum_\mu A_{\mu,KH}(P_H \rho_{in} P_H) A_{\mu,KH}^\dagger\right]}{\sqrt{\mathrm{Tr}\left[(P_H\rho_{in})^2\right]\mathrm{Tr}\left[\rho_{th}^2\right]}}, \qquad \alpha_{KH} = \sqrt{\frac{\mathrm{Tr}[(P_H\rho_{in})^2]}{\mathrm{Tr}[\rho_{in}^2]}} \tag{2.29}$$

Here we define P_L (P_R) as the projector onto the encoded (non-logical) subspace. Notice that if the ideal state is inside the logical subspace, $P_R\rho_{th} = 0$ and the last term $C_R = 0$.

Instead of performing state tomography over the full Hilbert space, we can focus our attention on the logical subspace only. The ability to preserve and manipulate the informa-

tion inside the logical subspace can be better quantified by the correlation on this subspace, C_L, comparing the experimental logical state with the theoretical state inside the subspace only. If the input state of this process, ρ_{in}, is a full pseudo-pure state and inside the logical subspace, the correlation C_{LL} with the logical ideal state is the only contribution to the total correlation C. The density operator of the logical subspace could be reconstructed by measuring the logical observables of the subspace, or equivalently by decoding the k-logical qubits to k-physical qubits and measuring the reduced state density operator (These two methods result in the same correlation, as long as we assume a perfect decoding). Therefore, a reduced number of readouts is enough to characterize the correlation.

If a pseudo-pure state over logical degrees of freedom is used instead, $C_{LR} \neq 0$, since the output state in the protected subspace may contain contributions arising from the action of the map $\mathcal{E}$ on the identity in the non-logical subspace. Given an input state $\rho_{in} = a|\psi\rangle\langle\psi|_L + (1-a)\frac{\mathbb{1}_R}{d_R}$, from the experimental output state we can only measure the quantity (by observing only the k-logical qubits or their physical equivalents):

$$C'_{LL} = aC_{LL} + (1-a)C_{LR} = aC_{LL} + (1-a)\frac{\mathrm{Tr}\left[U_{th}|\psi\rangle\langle\psi|_L U_{th}^{\dagger}\mathcal{E}\left(\frac{\mathbb{1}_R}{d_R}\right)\right]}{\sqrt{\mathrm{Tr}\left[(P_L\rho_{in}P_L)^2\right]}} \tag{2.30}$$

Note that in this case $C \neq C'_{LL}$, since the contributions C_{RL} is not taken into account. The measured correlation is thus defined by two terms: the first takes into account the control over the encoded subspace only and the eventual leakage from it, while the second takes into account mixing from the $\mathcal{R}$ subspace to the $\mathcal{L}$ subspace. State tomography of the input state $\mathbb{1}_R$ after the algorithm allows one to calculate the correlation on the logical subspace C_L.

To characterize the control of quantum gate operations most generally, many metrics have been suggested [56, 119, 105]. A good operational metric is for example the average gate fidelity (or fidelity of entanglement), that can be measured as the average of correlations of a complete orthonormal set of input states: $\bar{F} = \sum_j C^j = \sum_j \mathrm{Tr}\left[U_{th}\rho^j U_{th}\mathcal{E}(\rho^j)\right]$. Similarly, the encoded operational fidelity can be defined as the average correlation over an orthonormal set of operators spanning $\mathcal{L}$: $\bar{F}_L = \sum'_j C^j_{LL} = \sum'_j \mathrm{Tr}\left[U_{th}\rho^j_L U_{th}\mathcal{E}(\rho^j_L)\right]$.

The fidelity on the logical subspace focuses on the achieved control in the implementation of the desired transformation on the protected subspace; this new metric is immune to

unitary or decoherent errors within $\mathcal{R}$ alone:

$$\begin{aligned}\bar{F}_L &= \sum_j' C_{LL}^j = \sum_j' \mathrm{Tr}\left[U_{th}\rho_L^j U_{th}(\sum_\mu A_\mu P_L \rho_L^j P_L A_\mu)\right] \\ &= \sum_\mu |U_{th}A_{\mu,L}|^2/N^2\end{aligned} \tag{2.31}$$

The extent to which $U_{L,exp}$ is close to $U_{th,L}$ can be determined from $\bar{F}_L$, while the avoidance of subspace mixing will be specified by the gap between $\bar{F}$ to $\bar{F}_L$.

2.5 Conclusions

As demonstrated by the encoded Bell state experiment, subsystem pseudo-pure states offer not only a greater SNR but also a less complex state preparation. By no means does this logical encoding overcome the exponential loss of signal suffered by pseudo-pure states; however, for the corresponding state in the full Hilbert space, the gain is significant. As we explore larger Hilbert spaces and more complex encodings, these advantages become tantamount.

4 spins	DFS	1 logical qubit. Isotropic noise. What differences with 3-qubit NS?
5 spins	NS	2 logical qubits. Create Bell-State
	QEC	2 errors. 1-logical qubit QEC for σ_x errors.
	QEC	2-logical qubits QEC for σ_x errors
6 spins	DFS	3-logical qubits σ_z noise. Create GHZ state
	GHZ	Create 2 GHZ then encode them. σ_z-noise
	QEC DFS	Concatenate 2-qubit DFS with 3-qubit QEC.
9 spins	Shor's Code	9-qubit QEC to correct all single-qubit errors

Table 2.2: **In the table are shown experiments on 4-9 qubits** that will be achievable with the initialization method proposed

In particular, this method coupled with the experimental control on an Hilbert space of about 10 qubits, would allow for the study of a repeated QEC code, the Shor code for protecting against single qubit errors, or a multi-layered encoding like QEC using three DFS encoded qubits or vice-versa. In addition encoded versions of gates essential to algorithms, like the Quantum Fourier Transform, can be carried out with liquid phase NMR. The

effective noise superoperator on the logical subspace can also be reconstructed, to gain an insight on how encoding schemes modify the noise structure.

By considering metrics of control for only the logical degrees of freedom of our system, we also reduce the number of input states needed to characterize a particular gate sequence, as far as only the behavior of the protected information is of interest.

The state initialization method proposed could also find application in a broader context and in a variety of physical implementations, whenever exact purification of the system is possible, but costly. Quite generally, a qubit need not to be identified with a physical two-level system, but rather with a subsystem whose operator algebra generators satisfy the usual commutation and anti-commutation relationships. State initialization and purification could be performed on these subsystems only, thus allowing experimental advantages similar to the ones shown in the particular case of logical qubits.

Chapter 3

Control of Encoded Qubits

Decoherence-Free Subsystems (DFS) are a powerful mean of protecting quantum information against noise that exhibits symmetry properties. Universal computation within DFS has been shown to be possible from a theoretical point of view [138, 140, 8]. In particular, universal fault-tolerant computation within a DFS is possible if the exchange interaction between qubits can be switched off and on at will [75, 95, 96, 44]. The issue that we address here arises in systems where this Hamiltonian does not occur naturally or other interactions are present as well and need to be actively refocused.

The total Hamiltonian is conveniently divided into a time-independent part, $\mathcal{H}_{int}$, and a part that depends on a set of experimentally controllable, time-dependent parameters, $\mathcal{H}_{ext}(\alpha_i(\mathrm{t}))$. There are many useful DFS encodings for which the generators of logical qubit rotations are not contained in the set of available total Hamiltonians: $\mathcal{H}_{tot} = \mathcal{H}_{int} + \mathcal{H}_{ext}$. Although the total Hamiltonian allows universal control on the whole Hilbert space, implying that also any desired propagator on the logical subsystem can be composed from the evolution under a series of time dependent external Hamiltonians, the instantaneous total Hamiltonian need not preserve the protected subsystem, and the dynamics can temporarily drive the system outside of the protected subspace. In such cases, the extent to which universal fault-tolerant computation is possible depends on the details of the control fields, as well as the *spectral density* of the noise [132]. This chapter will discuss these issues in the context of a specific QIP implementation based on liquid-state NMR.

In Section (3.1) we show that the radio-frequency control fields used in NMR necessarily

[†]This chapter has been adapted from reference [27]

cause the encoded information to "leak" from the protected subsystem into other parts of the total system Hilbert space, where it is subject to decoherence. This is illustrated by numerical simulation of a simple example – the encoding of one logical qubit in a two-spin decoherence-free subspace for collective dephasing [54], which was already introduced in chapter (2). It is further shown that in the case of two DFS qubits, each with the same noise model, the leakage rate is generally nonzero even in the absence of the control Hamiltonian.

In Section (3.2) we study modulation schemes that can reduce the noise effects, in order to keep the leakage from compromising the DFS encoding. First, we briefly review the application of stochastic Liouville theory [62, 30] to understand the effective decoherence in the presence of an external Hamiltonian that modulates the spin dynamics, as is the case for strongly-modulating pulses (SMP) [56, 111] or optimal control theory [79], dynamical decoupling [138] or bang-bang control [141]. We then use these results to quantitatively understand the Carr-Purcell [28] (CP) sequence. CP is perhaps the original dynamical decoupling sequence and the archetype for observing the influence of the noise correlation time on the effective decoherence rate.

We will show that the CP sequence can be effective at suppressing both leakage and decoherence provided that one can modulate the system on a time scale shorter than the correlation time of the noise. Under the assumption of instantaneous and perfectly selective single spin π-pulses, the exact dependence of the overall gate fidelity on the pulse rate and the correlation time of the noise is derived for a single DFS qubit. Finally we apply these ideas to a physical system with realizable models of control fields. This includes limitations on the available RF power and the lack of frequency selectivity among the physical spins. As expected, pulses of finite duration degrade the gate fidelities of these operations. Analytical solutions are generally not feasible, and hence the amount of degradation that can be expected for a range of experimentally realistic parameters is evaluated by means of numerical simulations for simple quantum gates operating upon one or two encoded qubits.

3.1 Leakage from Decoherence-Free Subsystems

In many physical implementations, qubits are not embodied in well isolated two-level states. Rather, they are embedded in larger Hilbert spaces, containing additional states that are in-

tended to not participate in the computation. In addition, when physical two-state systems are combined into logical qubits for noise protection and correction, additional redundant degrees of freedom are introduced. A finite leakage [131, 150] to external degrees of freedom can destroy the coherent dynamics of the qubit. Here we are interested in particular in the leakage of logical qubits to the unprotected subsystems, leakage that could be caused by the internal Hamiltonian itself or by the control fields applied to implement specific logic gates. Many modulation methods have been engineered to refocus the terms in the internal Hamiltonian responsible for leakage [24]. Here we explore in particular the fidelity that can be reasonably expected based on the details of the modulation scheme and the spectral density of the noise.

In this section we use the simple DFS introduced in chapter (2) to motivate our discussion. The two-spin DFS considered, with the encoding: $|0\rangle_L = |01\rangle,\ |1\rangle_L = |10\rangle$, defines a basis set for the operator space on one encoded qubit:

$$\begin{array}{lcllcl} \sigma_z^L & \Leftrightarrow & \frac{\sigma_z^1 - \sigma_z^2}{2} & \sigma_x^L & \Leftrightarrow & \frac{\sigma_x^1\sigma_x^2 + \sigma_y^1\sigma_y^2}{2} \\ \mathbb{1}^L & \Leftrightarrow & \frac{\mathbb{1}^{1,2} - \sigma_z^1\sigma_z^2}{2} & \sigma_y^L & \Leftrightarrow & \frac{\sigma_x^1\sigma_y^2 - \sigma_y^1\sigma_x^2}{2} \end{array} \tag{3.1}$$

This two spin-$\frac{1}{2}$ particle Hilbert space ($\mathcal{H} = \mathbb{C}^4 = \mathbb{C}^2 \otimes \mathbb{C}^2$) can be described as a direct-sum of the total angular momentum subspaces, $Z_0 \oplus Z_{+1} \oplus Z_{-1}$[1], where l is the total angular momentum projected along the quantization axis. The logical basis states $|0\rangle_L$ and $|1\rangle_L$ reside exclusively in Z_0, where $Z_0 \equiv \mathbb{C}^2$. What we mean by leakage is that the instantaneous state in $\mathbb{C}^4$ has elements in $Z_{\pm 1}$. In this case, the information within the state of the system cannot be described completely by the four operators above (Eq. 3.1). Since the total angular momentum with $l = 0$ is a constant of the motion under the system-environment Hamiltonian, a state not completely represented as linear combinations of (Eq. 3.1) is affected by decoherence. We will explore this DFS as implemented in liquid state NMR for both one and two logical qubits.

The internal Hamiltonian (in the rotating frame, see Eq. (1.1)) for two spins in liquid-state NMR already is exclusively in Z_0 and thus can be expressed by the operators in Eq. 3.1; it does not cause mixing of the subspaces Z_l,

$$\mathcal{H}_{int} \ = \ \tfrac{\Delta\omega_{12}}{2}(\sigma_z^1 - \sigma_z^2) + \tfrac{\pi}{2}\, J_{12}\, \vec{\sigma}^1 \cdot \vec{\sigma}^2, \tag{3.2}$$

[1]With the notations of chapter (2) this is $\mathcal{H} = \mathcal{L} \oplus \mathcal{R}$, where $\mathcal{R} = Z_{+1} \oplus Z_{-1}$

where $\Delta\omega_{12}$ is the difference in chemical shift of the two spins and J_{12} the scalar coupling constant. The former coefficient scales the logical σ_z^L operator, while the latter scales the σ_x^L operator. Thus evolution under the internal Hamiltonian alone generates a continuous rotation about an axis in the logical xz-plane making an angle of $\arctan(\pi J_{12}/\Delta\omega_{12})$ with the logical x-axis.

As illustrated below, more general gates can be obtained via the interplay of the internal Hamiltonian and an external time-dependent RF (radiofrequency) field, described by the Hamiltonian H_{ext} in Eq. 1.2. Note that H_{ext} cannot be expressed as a linear combination of the logical Pauli operators. In the presence of RF fields the evolution of a state inside the DFS under the total Hamiltonian necessarily causes the information to "leak" outside of the DFS, where it is no longer immune to collective dephasing. This combination of $\mathcal{H}_{int}$ and $\mathcal{H}_{ext}(t)$ can generate any unitary in the $\mathbb{C}^4$ Hilbert space, guaranteeing universality. In the absence of decoherence and assuming ideal controls, we can reach a unit fidelity for any desired gate [77, 15]. Our interest is assessing the fidelity of control for a finite decoherence, for a finite bandwidth of our control parameters, and for Hamiltonians not respecting the symmetry of the logical subspace.

A measure of the amount of information protected by the encoding is the magnitude square of the system state projection onto the encoded subsystem. Conversely, the coupling of the system to external degrees of freedom can be quantified by the normalized rate of information leakage from the DFS, which is proportional to the projection of the state change per unit time $|\dot{\psi}\rangle$ onto the non-protected subspace:

$$R = \sum_n \frac{|\langle n|\dot{\psi}\rangle|^2}{|\langle\dot{\psi}|\dot{\psi}\rangle|^2}, \tag{3.3}$$

where $|n\rangle$ are basis states of the unprotected subsystems. The leakage rate depends on the initial state of the logical qubit. For example, in the case of the DFS encoding considered, the leakage rate,

$$R = \frac{|\langle 00|\dot{\psi}\rangle|^2 + |\langle 11|\dot{\psi}\rangle|^2}{|\langle\dot{\psi}|\dot{\psi}\rangle|^2}, \tag{3.4}$$

is zero for any value of the total Hamiltonian parameters if the initial state is the singlet state (since collective operators cannot change the total angular momentum of the system,

the singlet state of total spin zero cannot evolve to any other state). We are therefore interested in computing the maximum rate of loss of information, when varying the initial state.

Assuming that the initial state is in the DFS, its most general form is:

$$|\psi(0)\rangle = \cos(\theta/2)|01\rangle + e^{i\phi}\sin(\theta/2)|10\rangle \tag{3.5}$$

the change of the state per unit time under the action of the total Hamiltonian, $\mathcal{H}_{tot} = \mathcal{H}_{int} + \mathcal{H}_{ext}$, is given by the Schrödinger equation:

$$\begin{aligned} |\dot{\psi}\rangle \;&= -i\mathcal{H}_{tot}|\psi\rangle = -i[\Delta\omega(\cos(\theta/2)|01\rangle - e^{i\phi}\sin(\theta/2)|10\rangle) \\ &+J(-\cos(\theta/2) + 2e^{i\phi}\sin(\theta/2))|01\rangle + J(2\cos(\theta/2) - e^{i\phi}\sin(\theta/2))|10\rangle \\ &+\omega_{\mathsf{rf}}(\cos(\theta/2) + e^{i\phi}\sin(\theta/2))(|00\rangle + |11\rangle)] \end{aligned} \tag{3.6}$$

We can simplify this expression by considering only two dimensionless frequencies, since the rate will only depend on the ratios $\Delta\tilde{\omega} = \frac{\Delta\omega}{J}$ and $\tilde{\omega}_{\mathsf{rf}} = \frac{\omega_{\mathsf{rf}}}{J}$. Rearranging the terms, we have:

$$\begin{aligned} |\dot{\psi}\rangle \;&= -i[(\Delta\tilde{\omega} - 1)\cos(\theta/2) + 2e^{i\phi}\sin(\theta/2)]|01\rangle \\ &-i[-(\Delta\tilde{\omega} + 1)e^{i\phi}\sin(\theta/2) + 2\cos(\theta/2)]|10\rangle \\ &-i[\tilde{\omega}_{\mathsf{rf}}(\cos(\theta/2) + e^{i\phi}\sin(\theta/2)(|00\rangle + |11\rangle)] \end{aligned} \tag{3.7}$$

The rate of leakage from of the DFS is then given by inserting equation (3.7) into equation (3.4):

$$R(\theta,\phi) = \frac{2\tilde{\omega}_{\mathsf{rf}}^2|\cos(\theta/2) + e^{i\phi}\sin(\theta/2)|^2}{5 + \Delta\tilde{\omega}^2 + 2\tilde{\omega}_{\mathsf{rf}} - 2\Delta\tilde{\omega}\cos\theta + 2(\tilde{\omega}_{\mathsf{rf}}^2 - 2)\cos\phi\sin\theta} \tag{3.8}$$

The maximum rate can be computed analytically by taking the derivatives of the rate with respect to θ and ϕ:

$$\partial_\phi R = \frac{2\tilde{\omega}_{\mathsf{rf}}^2\sin\phi\sin\theta\,(9 + \Delta\tilde{\omega}^2 - 2\Delta\tilde{\omega}\cos\theta)}{\left[5 + \Delta\tilde{\omega}^2 + 2\tilde{\omega}_{\mathsf{rf}}^2 - 2\Delta\tilde{\omega}\cos\theta + 2(\tilde{\omega}_{\mathsf{rf}}^2 - 2)\cos\phi\sin\theta\right]^2} \tag{3.9}$$

$$\partial_\theta R = \frac{2\tilde{\omega}_{\mathsf{rf}}^2\left[(9 + \Delta\tilde{\omega}^2)\cos\phi\cos\theta - 2\Delta\tilde{\omega}(\cos\phi + \sin\theta)\right]}{\left[5 + \Delta\tilde{\omega}^2 + 2\tilde{\omega}_{\mathsf{rf}}^2 - 2\Delta\tilde{\omega}\cos\theta + 2(\tilde{\omega}_{\mathsf{rf}}^2 - 2)\cos\phi\sin\theta\right]^2} \tag{3.10}$$

The maximum is thus obtained when

$$\begin{cases} \sin\phi \sin\theta \,(9 + \Delta\tilde{\omega}^2 - 2\Delta\tilde{\omega}\cos\theta) = 0 \\ (9 + \Delta\tilde{\omega}^2)\cos\phi\cos\theta - 2\Delta\tilde{\omega}(\cos\phi + \sin\theta) = 0 \end{cases} \tag{3.11}$$

which has two solutions corresponding to global extremes for $\phi = 0$ (and with opposite sign, for $\phi = \pi$):

$$\begin{cases} \theta = -\dfrac{\pi}{2} \pm k\pi, \;\; k \in \mathcal{N} \\ \theta = \arccos\left[\dfrac{4\Delta\tilde{\omega}(9 + \Delta\tilde{\omega}^2)}{81 + 22\Delta\tilde{\omega}^2 + \Delta\tilde{\omega}^4}\right] \pm k\pi \end{cases} \tag{3.12}$$

The first solution corresponds to a minimum in the leakage rate. The maximum rate is obtained for the second solution and it is:

$$R_m = \frac{4\tilde{\omega}_{\mathsf{rf}}^2(9 + \Delta\tilde{\omega})^2}{4\tilde{\omega}_{\mathsf{rf}}^2(9 + \Delta\tilde{\omega})^2 + (3 + \Delta\tilde{\omega}^2)^2}, \tag{3.13}$$

and it is plotted in Fig. (3-1).

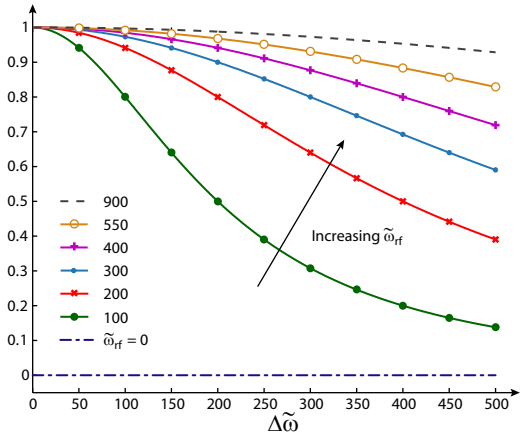

Figure 3-1: **Leakage rate from a two-spin DFS**, maximized with respect to the possible initial states. The leakage rate R is plotted as a function of the dimensionless difference in chemical shifts $\Delta\tilde{\omega} = \Delta\tilde{\omega}/J$, for various values of the normalized RF power $\tilde{\omega}_{\mathsf{rf}} = \omega_{\mathsf{rf}}/J$

Notice that the information is perfectly conserved only in the absence of an external field. This is compatible with an use of the DFS as a quantum memory, but not for computation. A way to decrease the rate at which information leaks from the protected subspace is to increase the difference in frequency ($\Delta\tilde{\omega}$) between the two spins. As long as $\tilde{\omega}_{\mathsf{rf}} \ll \Delta\tilde{\omega}$, the zero-quantum subspace eigenstates $|01\rangle$ and $|10\rangle$ are very close to the

Hamiltonian eigenstates, and therefore close to constants of the motion: The leakage out of the zero-quantum subspace is thus quenched, but as it will be seen in the following, this limit does not allow us to obtain finite rotations of the qubit (see Fig. (3-3)).

The rate of leakage does not give any insight about the fate of the information once it had leaked out to the unprotected part of the Hilbert space. Subsequent evolution could bring back the system to the protected subspace, and in that case the interesting quantity is the extent of the 'damage' caused by decoherence during the permanence outside the DFS. It is thus important to study the integrated effects of leakage over an extended amount of time, motivated by the fact that no transformation of the system can be instantaneous.

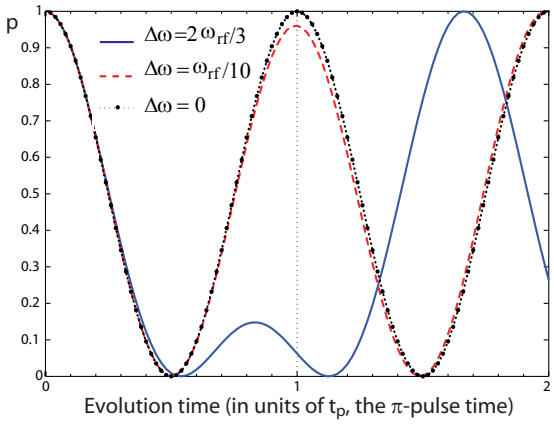

Figure 3-2: **Projection onto the logical subspace** of a state initially inside the DFS, during application of an RF pulse for various ratios of $\frac{\Delta\omega}{\omega_{\text{rf}}}$. Defining the projection operator onto the logical subspace as P_L , we plot $p(t) = \text{Tr}\left[(P_L\rho(t))^2\right] / \text{Tr}\left[\rho(t)^2\right]$, for $t = 0 \rightarrow 2t_p$, where $\rho(t) = e^{-i\omega_{\text{rf}}t(\sigma_x^1+\sigma_x^2)}\sigma_z^L e^{i\omega_{\text{rf}}t(\sigma_x^1+\sigma_x^2)}$ and $\omega_{\text{rf}}t_p = \pi$. The logical state completely returns to the subspace after application of a π-pulse to both spins only when the spins have identical resonance frequencies ($\Delta\omega = 0$). If the ratio $\frac{\Delta\omega}{\omega_{\text{rf}}}$ is non-zero, as required for universality, the return to the logical subspace is imperfect (in particular, it is in general possible to go back to a state very close to the initial state in a time $t > t_p$, but it is much more difficult to implement a π rotation). A logical π-pulse using a single period of RF modulation is not possible, a more complex RF modulation, like composite pulses [93], strongly-modulating pulses [56, 111] or optimal control theory [79], is required. In the above model, $\frac{\omega_{\text{rf}}}{J} = 500$; the initial state of the system is σ_z^L

In the case of ideal control fields, an instantaneous π-pulse ($t_p \rightarrow 0$) corresponds to a logical operation [54], since $P_x(\pi) = e^{-i\pi/2(\sigma_x^1+\sigma_x^2)} = -e^{-i\pi/2(\sigma_x^1\sigma_x^2)}$, which is equivalent to a π pulse around σ_x^L. Figure (3-2) motivates the extent to which universality within the subsystem can be obtained in the finite t_p regime. In this figure, we plot the purity of the projection of $\rho(t) = e^{-i\omega_{\text{rf}}t(\sigma_x^1+\sigma_x^2)}\sigma_z^L e^{i\omega_{\text{rf}}t(\sigma_x^1+\sigma_x^2)}$ on the logical subspace. In the limit

of very high RF power ($\frac{\Delta\omega}{\omega_{\mathsf{rf}}} \to 0$), the system undergoes a π-pulse in a time $t_p = \frac{\pi}{\omega_{\mathsf{rf}}}$ and returns completely to the subspace after this time. It remains outside the subspace only for the duration of the pulse. For ω_{rf} which are physically relevant ($\omega_1 < 2\pi 100$ kHz and $0 < \Delta\omega < 2\pi 20$ kHz), a single RF pulse does not result in a logical π-rotation due to off-resonance effects. Experimentally we are limited to finite t_p and even our simple two logical qubit model system is sufficient to introduce several key challenges in implementing coherent control over logical qubits: (i) decoherence due to leakage outside the subspace during RF modulation periods, (ii) decoherence due to leakage outside the subspace after RF modulation, and (iii) loss of fidelity due to cumulative leakage with respect to the spectral density of the noise.

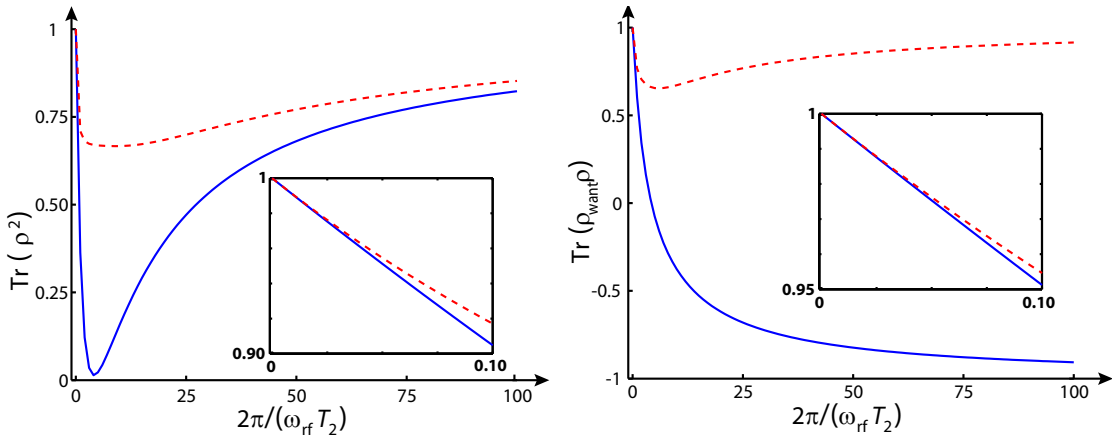

Figure 3-3: **Loss of fidelity due to totally correlated decoherence** during the application of a π-pulse about the x-axis to the two spins of the DFS (see text). The dashed curves (red in the on-line version) are for the initial states $\rho_0 = \mathbb{1}^L$ or $\rho_0 = \sigma_x^L$, while the lower curves (blue in the on-line version) are for $\rho_0 = \sigma_y^L$ or $\rho_0 = \sigma_z^L$. The left-hand plot shows the trace of ρ^2 following the π-pulse as a function of the inverse product of the RF power ω_{rf} and the relaxation time T_2. The right-hand plot shows the correlation with the ideal final state, i.e. the trace of $\rho_f \rho$, following the π-pulse as a function of this same parameter.

Figure (3-3) shows an illustrative example of the integrated effects of a π-pulse applied to the two spins in such a DFS on the purity ($\mathrm{Tr}\left[\rho^2\right]$) and correlation with the ideal final state ($\mathrm{Tr}\left[\rho_{\mathsf{want}}\rho\right]$) as a function of the ratio of the relaxation rate $1/T_2$ to the RF power ω_{rf}. The initial states were chosen from the four logical Pauli operators (3.1), and we made the approximation that the internal Hamiltonian is zero during the application of these π-pulses. As would be expected, the desired result (negating the state in the case of $\rho_0 = \sigma_y^L, \sigma_z^L$, or preserving it for $\rho_0 = \mathbb{1}^L, \sigma_x^L$) is rapidly degraded by the totally correlated decoherence

during the π-pulse, unless the Rabi frequency is considerably faster than the relaxation rate. The increase in both the coherence and the correlation when the relaxation becomes fast compared to the rotation rate is due to a sort of "quantum Zeno" effect [72], so that the RF field itself is unable to rotate the state out of the DFS. In a complete analysis of the 2-spin case the effects shown in Fig. (3-2) must be combined to those in Fig. (3-3).

Manipulating more than one logical qubit introduces further complexities to the control versus leakage problem. For the DFS considered, the extension to 2 logical qubits encoded into 4 physical qubits leads to the following basis states:

$$\begin{aligned} |00\rangle_L &\Leftrightarrow |0101\rangle, \qquad & |10\rangle_L &\Leftrightarrow |1001\rangle, \\ |01\rangle_L &\Leftrightarrow |0110\rangle, \qquad & |11\rangle_L &\Leftrightarrow |1010\rangle \end{aligned} \tag{3.14}$$

As before, we define leakage as any evolution that will cause the state to be not fully described by a linear combination of this four basis vectors. Since we focus on the challenges unique to controlling multiple logical qubits, we assume the internal Hamiltonian to be given by the Hamiltonians of each logical pair (as in eq. (3.2)) and a coupling between two spins pertaining to two distinct logical qubits:

$$\mathcal{H}_{int} = \mathcal{H}_{L1} + \mathcal{H}_{L2} + \tfrac{1}{2}\pi J_{23}\, \vec{\sigma}_2 \cdot \vec{\sigma}_3 \tag{3.15}$$

The interaction term $\mathcal{H}^I_{23} = \vec{\sigma}_2 \cdot \vec{\sigma}_3$ couples the system initially in the subspace defined by the state (3.14) to the subspace defined by the states

$$|0011\rangle \quad \text{and} \quad |1100\rangle, \tag{3.16}$$

for example $e^{-i\pi/4\mathcal{H}^I_{23}}|0101\rangle = \frac{1-i}{\sqrt{2}}|1100\rangle$. If the noise is collective only over each pair of spins that encodes a logical qubits [136], the states (3.16) are not protected against it and will decohere. The internal Hamiltonian will therefore be responsible for leakage and the ultimate decay of the system.

Notice that we would in general expect the noise to be collective over all the physical qubits, and not pairwise collective. In the case of NMR, this corresponds to a fluctuating external magnetic field, which is fully correlated. However, the differences in energies between qubits could be strong enough to effectively add a non-collective component to the

noise. In particular, we can consider in NMR the case in which each pair is formed by spins of a different chemical species. In this case, the difference in gyromagnetic ratio makes the strength of the noise acting on each pair unequal, so that the noise is no longer collective. On the other hand, when the Zeeman energy separation is considerable, the coupling between spins can be very well approximated by the diagonal part of $\mathcal{H}^I_{23}$, i.e. $\sigma^2_z\sigma^3_z$, which does not cause leakage.

When the noise generator is fully collective (as for homonuclear systems in NMR), the internal Hamiltonian still causes leakage, via the coupling to the states in Eq. (3.16). Since these states belong to the zero eigenvalue subspace of the noise generator, they do not decohere. Information could still be lost at the measurement stage, since the states in Eq. (3.16) are not faithfully decoded to a physical state[2]. A unitary operation is enough to correct for this type of leakage, and since decoherence is not an issue here, there are no concerns regarding the time scale over which the correction should be applied; however, amending for this unwanted evolution would in general mean the introduction of an external control, that, as seen, is a source of leakage leading to decoherence.

For logical encodings other than the DFS considered, the natural Hamiltonian may drive the state out of the protected subspace even for single logical qubits; for example, the *noiseless subsystem* considered in Ref. [57] (see also Section (2.2.1))will evolve out of the protected subspace whenever the chemical shifts or scalar couplings among its three constituent spins are not all equal.

If we wish to do something more complicated than merely freeze the evolution of the system, e.g. to rotate the DFS qubits while simultaneously refocusing all the inter-qubit couplings, the complexity of the modulation sequence increases and the various causes of leakage will combine. In attempting to demonstrate a universal set of logic gates on a pair of two-spin DFS qubits by liquid-state NMR, leakage turned out to be an unavoidable problem for all practical intents and purposes. Fortunately, it turns out that in many practical situations other means of inhibiting decoherence are also available, and can allow one to leave the protected subspace if need be in order to simplify the implementation of logic gates on encoded qubits. Dynamical decoupling is a particularly promising class of techniques for these purposes, which are applicable whenever the correlation time of the

[2]Notice the similarity of this issue with the requirements on Logical Pseudo-Pure states discussed in Section (2.1)

noise is long compared to the rate at which the system can be coherently modulated. The next section will analyze the principles involved in this approach, and show how they may be applied to some simple but realistic examples.

3.2 Noise refocusing by strongly modulating fields.

Unavoidable excursions from the protected subspace under a time-dependent Hamiltonian do not preclude high fidelity quantum operations. Decoherence does not act instantaneously and if we limit the duration of these excursions sufficiently, the leakage rate stays small and logical operations largely unaffected by decoherence are still possible. Furthermore, refocusing techniques much like those used for coherent control can reduce the effects of the noise. The earliest example of a pulse sequence that could correct for random field fluctuations with long correlation times was given by Carr and Purcell as early as 1954 [28, 101]. Today this would be regarded as dynamical decoupling or ''bang-bang" control [142] and it has been applied beyond magnetic resonance, for example to the control of decoherence in spin-boson models [133]. We propose to use this same modulation scheme to counteract the noise effects and study its efficiency. In this section we outline a formalism, based on the well-known stochastic Liouville formalism [59, 71, 30] and cumulant expansion, which allows us to analyze the effects of dynamical decoupling on decoherence. We show that if the rate of the modulation is much greater than the rate of variation of the noise, as given by the correlation time τ_c, the effects of the noise can be reduced. In the following section we apply this to the above two-spin DFS.

Stochastic Liouville theory is based on a semiclassical model of decoherence, in which the Hamiltonian at any instant in time consists of a deterministic and a stochastic part. In the simplest case of NMR T_2 relaxation, this typically takes the form

$$\mathcal{H}_{tot}(t) \;=\; \mathcal{H}_{det}(t) + \mathcal{H}_{st}(t) \;=\; \mathcal{H}_{int} + \mathcal{H}_{\mathsf{rf}}(t) + \sum\nolimits_k \omega_k(t) Z_k \;, \tag{3.17}$$

where $\mathcal{H}_{int}$ is the static internal Hamiltonian, $\mathcal{H}_{\mathsf{rf}}(t)$ is the RF Hamiltonian, the $\omega_k(t)$ describe the phase shifts due to stochastic, time-dependent fluctuating fields and Z_k are the generators of each of these noise sources, i.e. operators which describe how these classical fields are coupled to the quantum system. In the two-spin DFS example considered previously, there is only one noise generator $Z = (\sigma_z^1 + \sigma_z^2)/2$ with $\omega(t) = \gamma B(t)$, which describes

collective fluctuations parallel to the applied static magnetic field.

The time evolution of the system density matrix ρ is then describe by the stochastic Liouville equation. We introduce the superoperator $\mathcal{L}(t)$ defined on Liouville (operator) space via

$$\mathcal{L}(t) \;=\; \mathcal{H}^{*}_{tot}(t)\otimes \mathbb{1} - \mathbb{1}\otimes \mathcal{H}_{tot}(t) \;=\; \mathcal{L}_{det}(t) \,+\, \sum\nolimits_{k}\omega_k(t)\mathcal{Z}_k \tag{3.18}$$

where $\mathcal{Z}_k = Z^{*}_k \otimes \mathbb{1} - \mathbb{1}\otimes Z_k$. This superoperator is the (super-)generator of motion for the density operator $\hat{\rho}$ in Liouville space, meaning

$$\hat{\rho}(t) = \mathcal{U}\,\hat{\rho}(0) \;=\; \mathcal{T}\exp\!\Big[-i\int_0^t dt'\,\mathcal{L}(t')\Big]\,\hat{\rho}(0) \tag{3.19}$$

where $\mathcal{T}$ is the usual time ordering operator. Since what is actually observed in an experiment is the statistical average over the microscopic trajectories of the system $\langle\hat{\rho}(t)\rangle$, we have to take the ensemble average superpropagator to obtain $\langle\hat{\rho}(t)\rangle = \big\langle\mathcal{U}\big\rangle\hat{\rho}(0)$. The problem of calculating the average of the exponential of a stochastic operator has been solved by Kubo [86] using the cumulant expansion. In terms of the *cumulant averages* $\langle\cdots\rangle_c$, the superpropagator is given by (see Appendix A.2):

$$\big\langle\mathcal{U}\big\rangle \;=\; \exp\left(-i\int_0^t dt_1\,\langle\mathcal{L}(t_1)\rangle_c - \frac{1}{2}\mathcal{T}\int_0^t dt_1\int_0^t dt_2\,\langle\mathcal{L}(t_1)\mathcal{L}(t_2)\rangle_c + \cdots\right) \tag{3.20}$$

Provided $\|\langle\mathcal{L}(t)^k\rangle_c\| t_c^k \ll 1,\ \forall t,k$ we can safely neglect high order terms in the exponential argument without having to restrict the analysis to short time evolutions.

Similar expressions are obtained in the formalism of average Hamiltonian theory (AHT) [68] for the coherent (instead of stochastic) averaging of the system evolution under control Hamiltonians that are cyclic and periodic in time (see Appendix A.1). We can obtain simplifications analogous to those encountered in AHT if we analyze the evolution in the interaction frame (called "toggling frame" in NMR) defined by the cyclic RF propagator $U_{\mathsf{rf}}(t)$ [69]. In this frame the noise operators acquire a further time-dependency (coherently imposed by the cyclic excitation) in addition to the stochastic time dependency of their coefficients $\omega_k(t)$. The total Hamiltonian in the toggling frame is

$$\tilde{\mathcal{H}}_{tot}(t) \;=\; \tilde{\mathcal{H}}_{det}(t) + \sum\nolimits_{k}\omega_k(t)\tilde{Z}_k(t), \tag{3.21}$$

where the toggling frame equivalent $\tilde{O}$ of any given operator is defined by

$$\tilde{O}(t) = U_{\mathsf{rf}}^{\dagger}(t)\, O\, U_{\mathsf{rf}}(t), \tag{3.22}$$

with :

$$U_{\mathsf{rf}}(t) \;\equiv\; \mathcal{T}\exp\Big(-i\int_0^t dt'\,\mathcal{H}_{\mathsf{rf}}(t')\Big), \tag{3.23}$$

and $U_{\mathsf{rf}}(t_c) = \mathbb{1}$ for cyclic controls, so that the toggling frame and laboratory frame coincide at the end of each cycle.

This time-dependent change of basis in Liouville space induces a change of basis in the space of superoperators acting on Liouville space, as a result of which the noise super-generators $\mathcal{Z}_k$ also become time-dependent, i.e.

$$\tilde{\mathcal{Z}}_k(t) \;=\; \tilde{Z}_k(t)\otimes\mathbb{1} \;-\; \mathbb{1}\otimes\tilde{Z}_k(t)\;. \tag{3.24}$$

Returning now to the problem of interest here, in which there is only one noise generator which describes totally correlated decoherence as above and the corresponding random variable $\omega(t)$ is stationary and zero mean, following the results in Appendix A, we obtain the first two cumulants in the toggling frame:

$$\begin{aligned}
\tilde{\mathcal{K}}_1(t) &= \frac{1}{t}\int_0^t dt'\,\langle \mathcal{L}_{det}(t') + \omega(t')\tilde{\mathcal{Z}(t')}\rangle \;=\; \frac{1}{t}\int_0^t dt'\,\tilde{\mathcal{L}}_{det}(t') \\
\tilde{\mathcal{K}}_2(t) &= \frac{1}{t^2}\int_0^t dt_1\int_0^{t_1} dt_2\,\Big(\big[\tilde{\mathcal{L}}_{det}(t_1),\tilde{\mathcal{L}}_{det}(t_2)\big] \;+\; 2\,G(t_2-t_1)\,\tilde{\mathcal{Z}}(t_1)\,\tilde{\mathcal{Z}}(t_2)\Big)
\end{aligned} \tag{3.25}$$

In the last line we have introduced the autocorrelation function $G(t,\Delta t) = \langle\omega(t+\Delta t)\omega(t)\rangle$ for the stationary random noise variable $\omega(t)$. Because we assume the environment to be at thermal equilibrium, the noise distribution is stationary and the autocorrelation function depends only on the difference between times, $G(t,\Delta t)\equiv G(\Delta t)$.

If we consider the terms in which only the non-stochastic part of the Liouvillian appears, they are equivalent to the expansion of the propagator in the absence of noise:

$$\begin{aligned}
&\mathcal{U}' = \mathcal{T}e^{-i\int_0^t \tilde{\mathcal{L}}_{int}(t')dt'} = e^{-i\bar{\mathcal{L}}_{int}t}, \text{with :} \\
&\bar{\mathcal{L}}_{int} = \tfrac{1}{t}\Big(\int_0^t \tilde{\mathcal{L}}_{int}(t')dt' - \int_0^t dt_1\int_0^{t_1} dt_2[\tilde{\mathcal{L}}_{int}(t_1),\tilde{\mathcal{L}}_{int}(t_2)] + \cdots\Big)
\end{aligned} \tag{3.26}$$

where $\bar{L}_{int}$ is the average Liouville operator as given by the extension of AHT to Liouville operators (that we call Average Liouville Theory or ALT).

Average Hamiltonian theory is a powerful tool to devise multiple pulse sequences that either provide the desired evolution or, in the case of refocusing sequences, suspend any evolution. The pulse sequences found in this way however only assure that the effective propagator at the end of the evolution period is the desired one, while no other restrictions are imposed to the dynamics. This is why AHT of the unitary evolution alone is not enough to give the entire picture of the dynamics in the case of encoded operator and decoherence: For encoded states, as seen in the previous section, it is important to study the entire evolution in time, to look for leakage sources. Using average Liouville theory (ALT) to design not only the unitary part of the evolution, but also modulation schemes for the refocusing of the noise is the natural extension of AHT to the treatment of encoded qubit dynamics.

Consider the problem of rotating a logical qubit encoded in the above DFS around the logical x-axis. To obtain the σ_L^x operator when the two spins are coupled by the weak coupling Hamiltonian, $\frac{\pi}{2}J\sigma_z^1\sigma_z^2$, we can simply rotate this operator to the transverse plane, and wait for a time $t_p = \frac{\phi}{\pi J}$ to get a rotation by an angle ϕ around the logical x-axis[3]. During this process, however, the system leaves the DFS for a non-negligible time, so coherence is lost unless we apply ALT to find a modulation scheme to counteract decoherence. In the following, we will use the tools presented in this section to show that a Carr-Purcell-style sequence applied during the time t_p can be effective when the correlation time of the noise τ_c is long compared to the time constant of the modulation. Other sequences can be used to refocus the effects of different type of couplings to external degrees of freedom (i.e. different noise generators).

3.2.1 Refocusing noise with a Carr-Purcell sequence

The implementation of a σ_x^L rotation on a two-spin DFS qubit is given by a $(\pi/2)$-rotation of both spins in the DFS qubit about the y-axis, followed by a Carr-Purcell-style sequence consisting of an even number $2n$ of π-pulses separated by equal time intervals $\tau = t/2n$,

[3]See also Section (2.3) for more details and an experimental implementation

and finally the inverse $(\pi/2)$-rotation, i.e.

$$\left[\frac{\pi}{2}\right]_y \Big(-\tau - [\pi]_x - \tau - [\pi]_x \Big)^n \left[\frac{\pi}{2}\right]_{\bar{y}} \tag{3.27}$$

This transforms the weak $\sigma_z\sigma_z$ coupling between the two spins of the DFS qubit into $\sigma_x\sigma_x$, which projects to the σ_x^L operator within the DFS (Eq. (3.1)). Setting $\tau = \phi/(2n\pi J)$ thus yields a rotation by an angle ϕ around the logical x-axis. Even though the state of the two spins is outside the DFS throughout the time $2n\tau$, the sequence of π-pulses is able to refocus the effects of the noise provided $\tau \ll \tau_c$.

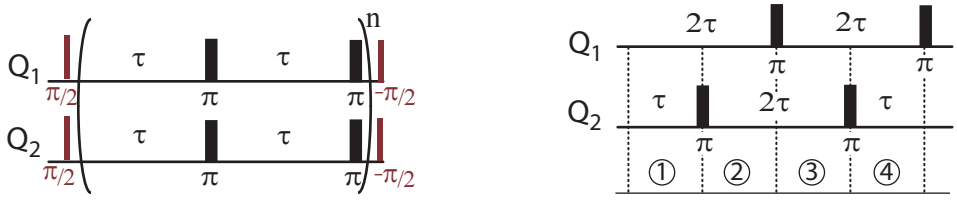

Figure 3-4: **Carr-Purcell sequence** (Left) and **Time-Suspension sequence** (Right). Notice that this sequence has the same number of pulses as 1 cycle of the non selective CP-sequence.

Assuming instantaneous π-pulses, this follows from AHT since during any cycle $(0, 2\tau)$ the internal Hamiltonian in the toggling frame $\tilde{\mathcal{H}}_{int}$ alternates between $+\Delta\omega(\sigma_x^1 - \sigma_x^2) + (\pi/2)J\sigma_x^1\sigma_x^2$ (in the interval $(0,\tau)$) and $-\Delta\omega(\sigma_x^1 - \sigma_x^2) + (\pi/2)J\sigma_x^1\sigma_x^2$ (for $t \in (\tau, 2\tau)$), so that the zeroth-order average Hamiltonian is just $\bar{\mathcal{H}}^{(0)} = (\pi/4)\sigma_x^1\sigma_x^2 = (\pi/4)\sigma_x^L$, which is the desired unitary evolution. This is in fact also the average Hamiltonian to all orders, since the toggling frame Hamiltonian commutes at all time, and the first cumulant is just the corresponding superoperator $\tilde{\mathcal{K}}_1 = \mathcal{K}_1 = (2\tau)^{-1}(\bar{\mathcal{H}}^* \otimes \mathbb{1} - \mathbb{1} \otimes \bar{\mathcal{H}})$.

Again because the toggling frame Hamiltonians commute, the deterministic part of the Liouvillian $\tilde{\mathcal{L}}_{det}(t)$ does not contribute to $\tilde{\mathcal{K}}_2 = \mathcal{K}_2$ at the end of each cycle, nor at the end of the entire sequence. The second cumulant is therefore determined by the stochastic part alone:

$$\mathcal{K}_2 = \frac{2}{(2n\tau)^2} \int_0^{2n\tau} dt_1 \int_0^{t_1} dt_2 \; G(t_1 - t_2)\tilde{\mathcal{Z}}(t_1)\tilde{\mathcal{Z}}(t_2) \tag{3.28}$$

Notice that this is the only contribution for gaussian noise, since the noise operator and the

internal Hamiltonian commute at any time. The total propagator is thus given by:

$$\langle \mathcal{U} \rangle = e^{-i\frac{\pi}{4}\tilde{\sigma}_L^x} e^{-\frac{1}{2}\mathcal{K}_2 t^2} \tag{3.29}$$

where $\tilde{\sigma}_L^x$ is the superoperator form of the logical σ_x operation.

Because each π-pulse simply changes the sign of $\tilde{\mathcal{Z}}(t)$ from the preceding interval, it follows that $\tilde{\mathcal{Z}}(t) = +\mathcal{Z}_x$ if t is in an even interval $\big(2k\tau,\, (2k+1)\tau\big)$, $k = 0, 1, \ldots n-1$, and $\tilde{\mathcal{Z}} = -\mathcal{Z}_x$ if t is in an odd interval $\big((2k-1)\tau,\, 2k\tau\big)$, $k = 1, 2 \ldots n$, where $\mathcal{Z}_x$ is the noise super-generator rotated along the x-axis.

The double integral in Eq. 3.28 can thus be expressed as:

$$\mathcal{K}_2 = \tilde{Z}^2 \zeta = \frac{2\tilde{Z}^2}{(2n\tau)^2}[2nA + \sum_{k=1}^{2n}\sum_{h=1}^{k-1}(-1)^{k+h} B_{k,h}] \tag{3.30}$$

where

$$A = \int_0^\tau dt_1 \int_0^{t_1} dt_2 G(t_1 - t_2) \tag{3.31}$$

and

$$B_{k,h} = \int_{k\tau}^{(k+1)\tau} dt_1 \int_{h\tau}^{(h+1)\tau} dt_2 G(t_1 - t_2) \tag{3.32}$$

for $k = 1, \ldots, 2n$ and $h < k$.

In the case of gaussian noise with correlation function $G(\tau) = \Omega^2 e^{-\tau/\tau_c}$, we obtain

$$A = (\Omega\tau_c)^2(\tau/\tau_c + e^{-\tau/\tau_c} - 1) \tag{3.33}$$

and

$$B_{k,h} = \bar{B} e^{-(k-h)\tau/\tau_c}, \quad \bar{B} = (\Omega\tau_c)^2 e^{-\tau/\tau_c}(e^{\tau/\tau_c} - 1)^2 \tag{3.34}$$

On evaluating the double geometric series in ζ one obtains the closed form:

$$\begin{aligned} \zeta \;=\; & \tfrac{2\,\Omega^2\tau_c^2}{(2n\tau)^2}\Big[2n\Big(\tau/\tau_c + e^{-\tau/\tau_c} - 1\Big) + \\ & \left(\tfrac{1-e^{-\tau/\tau_c}}{1+e^{-\tau/\tau_c}}\right)^2 \Big(1 - 2n\big(1 + e^{-\tau/\tau_c}\big) - e^{-2n\tau/\tau_c}\Big)\Big], \end{aligned} \tag{3.35}$$

which is easily shown to go to zero as $\tau/\tau_c \to 0$. In the limit $\tau/\tau_c \to \infty$ the behavior of ζ depends instead on the noise strength: If a constant noise strength is assumed, $\zeta \to 0$ as

$\frac{\Omega^2}{\tau/\tau_c} \to 0$. If instead we assume $\Omega\tau_c$ =cst, $\zeta \to \infty$, since it is now $\zeta \propto \frac{\tau/\tau_c}{2n\tau^2}$, and the fidelity will go to zero.

We can quantify the protection afforded by the modulation scheme by taking the entanglement fidelity [105, 56] of the superoperator with the ideal propagator for the sequence as a measure of its efficacy, $F \equiv \mathrm{Tr}\left[U_{\mathrm{id}}^{-1} S\right]$. Since the unitary part of the evolution commutes with the noise and gives the ideal propagator, the fidelity is just the trace of the superoperator, which for a single two-spin DFS qubit is

$$F(\zeta) \;=\; \mathrm{Tr}\left[e^{-\mathcal{Z}_x^2 \zeta (2n\tau)^2/2}\right]/2^4 \;=\; \left(3 + 4\, e^{-2\zeta n^2\tau^2} + e^{-8\zeta n^2\tau^2}\right)/8\;. \tag{3.36}$$

The fidelity for cycles of CP-sequences of length 4 and 16 are plotted in Fig. (3-5). As expected, it shows an improvement for an higher number of intervals and shorter time spacings with respect to the correlation time.

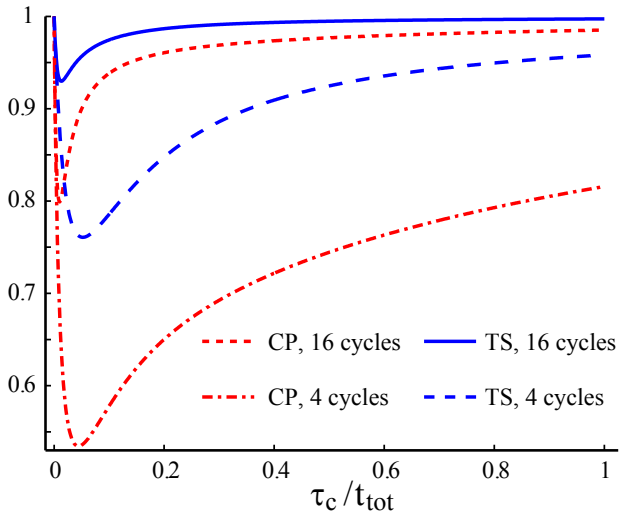

Figure 3-5: **Gate fidelity as a function of the correlation time** for 4 and 16 cycles of the Carr-Purcell (CP) and Time-Suspension sequences (TS). The noise strength Ω was fixed at 1 Hz., while the duration of the entire sequence was fixed at $t_{tot} = 4$ sec (where $t_{tot} = 2n\tau$ for the CP sequence and $t_{tot} = 4n\tau$ for the TS sequence). The increase in fidelity at very short correlation times is due to the phase fluctuations becoming so fast that they produce essentially no effect at the given noise strength Ω (this is a phenomenon known as motional narrowing).

It is interesting to also consider a sequence that completely refocuses the internal Hamiltonian (this will be referred to in the following as the Time-Suspension (TS) sequence [39, 38]). Selective pulses on just one spin are now required and the cycle (repeated n

times) is composed of 4 steps (see Fig. (3-4)).

If we sandwich the TS-sequence between a pair of $(\pi/2)$-pulses as we did for the CP, and again assume a stationary and Markovian Gaussian distribution of totally correlated noise, we find it more effective at protecting the system from decoherence even when the number of π-pulses on each spin and the cycle time is the same, since the effective modulation rate is then faster (if $\tau_{\mathsf{cp}} = t_c/2$ as in the CP sequence, there is a pulse every $\tau_{\mathsf{ts}} = \tau_{\mathsf{cp}}/2$ in the TS sequence).

To derive the fidelity attenuation of the TS sequence let consider first the basic cycle of the sequence, composed of 4 time intervals. The average internal Hamiltonian is now zero, while the noise operator in the toggling frame is $\tilde{Z}_1 = \pm(\sigma_z^1 + \sigma_z^2)/2$ in the intervals 1 and 3 respectively and $\tilde{Z}_2 = \pm(\sigma_z^1 - \sigma_z^2)/2$ in the other two intervals (as defined in figure (3-4)). Contributions to the second order cumulant average from single time intervals can be derived as before using the quantities defined in Eq. (3.33) and (3.34).

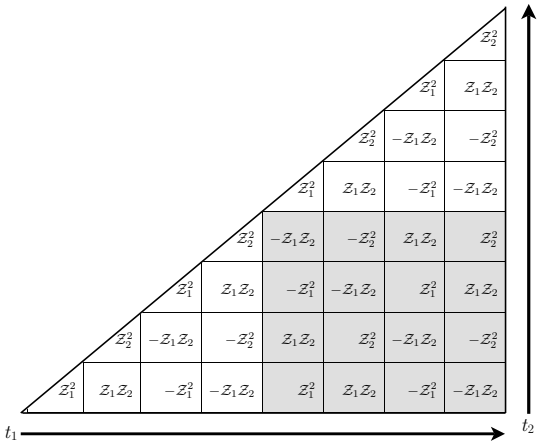

Figure 3-6: **Domain of integration** and toggling frame noise operators for the TS sequence, for the calculation of the second order cumulant.

By inspection of the domain of integration, the second order cumulant, $\mathcal{K}_2^{(t)}$, for the first cycle (corresponding to the first lower-left triangle in Fig. (3-6)) is given by:

$$\begin{aligned}\mathcal{K}_2^{(t)} &= \left(\mathcal{Z}_1^2(2A - B_{3,1}) + \mathcal{Z}_2^2(2A - B_{4,2}) + \mathcal{Z}_1\mathcal{Z}_2(B_{2,1} - B_{4,1} - B_{3,2} + B_{4,3})\right)/(4\tau)^2 \\ &= \left((\mathcal{Z}_1^2 + \mathcal{Z}_2^2)(2A - \bar{B}e^{-2\frac{\tau}{\tau_c}}) + \mathcal{Z}_1\mathcal{Z}_2\bar{B}(e^{-\frac{\tau}{\tau_c}} - e^{-3\frac{\tau}{\tau_c}})\right)/(4\tau)^2\end{aligned} \tag{3.37}$$

If the sequence is repeated n-times, each cycle define a region in the domain of integration. These are either 4 by 4 time step triangles (equivalent to the first cycle) or squares,

like the shaded area in Fig. (3-6), which is the first of the possible squares. Each triangle will give the same contribution calculated above for the first cycle(if there are n cycles, we will have n of them). The second cumulant from the first 4 by 4 square, corresponding to the variable of integrations t_1 in the second cycle and t_2 in the first cycle, is:

$$\begin{aligned}\mathcal{K}_2^{(s)} &= \big(\mathcal{Z}_1^2(B_{5,1}+B_{7,3}-B_{5,3}-B_{7,1})+\mathcal{Z}_2^2(B_{6,2}+B_{8,4}-B_{6,4}-B_{8,2})+\\ &\quad \mathcal{Z}_1\mathcal{Z}_2(B_{6,1}-B_{8,1}+B_{5,2}-B_{7,2}-B_{6,3}+B_{8,3}-B_{5,4}+B_{7,4})\big)/(4\tau)^2\end{aligned} \tag{3.38}$$

which gives:

$$\begin{aligned}\mathcal{K}_2^{(s)} &= (\mathcal{Z}_1^2+\mathcal{Z}_2^2)\bar{B}(2e^{-4\frac{\tau}{\tau_c}}-e^{-2\frac{\tau}{\tau_c}}-e^{-6\frac{\tau}{\tau_c}})/(4\tau)^2+\\ &\quad \mathcal{Z}_1\mathcal{Z}_2\bar{B}(e^{-3\frac{\tau}{\tau_c}}-e^{-\frac{\tau}{\tau_c}}+e^{-5\frac{\tau}{\tau_c}}-e^{-7\frac{\tau}{\tau_c}})/(4\tau)^2\end{aligned} \tag{3.39}$$

To calculate the contributions from t_1 in cycle k and t_2 in cycle h, it is enough to multiply this cumulant $\mathcal{K}_2^{(s)}$ by $e^{-4\frac{\tau}{\tau_c}(k-h)}$ (since the cycle time is 4τ). In general, for n cycles we obtain:

$$\mathcal{K}_2 = \frac{1}{n^2}(n\mathcal{K}_2^{(t)}+\sum_{k=2}^{n}\sum_{h=1}^{k-1}e^{-4\frac{\tau}{\tau_c}(k-h)}\mathcal{K}_2^{(s)}) \tag{3.40}$$

The relaxation superoperator for the TS-sequence is thus given by $\mathcal{K}_2 = \zeta_1(\mathcal{Z}_1^2+\mathcal{Z}_2^2)+\zeta_2\,\mathcal{Z}_1\mathcal{Z}_2$, where $\mathcal{Z}_k = Z_k\otimes\mathbb{1}-\mathbb{1}\otimes Z_k$ $(k=1,2)$ and:

$$\begin{aligned}\zeta_1 = \;& \frac{\omega^2\tau_c^2}{16n^2\tau^2}\left[\left(\frac{1-e^{\tau/\tau_c}}{1+e^{2\tau/\tau_c}}\right)^2\left(e^{-4n\tau/\tau_c}\left(ne^{4\tau/\tau_c}-n+1\right)-1\right)e^{-3\tau/\tau_c}\right.\\ &\left.+2n\frac{\tau}{\tau_c}+n\left(e^{-2\tau/\tau_c}-1\right)\left(2-e^{-\tau/\tau_c}\right)\right]\end{aligned} \tag{3.41}$$

$$\zeta_2 = \frac{\omega^2\tau_c^2}{16n^2\tau^2}\frac{\left(1-e^{\tau/\tau_c}\right)^2e^{-4\tau/\tau_c}}{1+e^{2\tau/\tau_c}}\left[e^{-4n\tau/\tau_c}\left(ne^{4\tau/\tau_c}-n+1\right)+ne^{4\tau/\tau_c}-(n+1)\right] \tag{3.42}$$

The fidelity is again obtained from the trace of the noise superoperator:

$$\begin{aligned}F(\zeta_1,\zeta_2) &= \mathrm{Tr}\left[\exp\left(-\zeta_1(\mathcal{Z}_1^2+\mathcal{Z}_2^2)(4n\tau)^2/2-\zeta_2\mathcal{Z}_1\mathcal{Z}_2(4n\tau)^2/2\right)\right]\\ &= \tfrac{1}{2}\,e^{-\zeta_1(4n\tau)^2}\big(\cosh(-\zeta_1(4n\tau)^2)+\cosh(-\zeta_2(4n\tau)^2/2)\big)\;.\end{aligned} \tag{3.43}$$

Fidelities for 4 and 16 cycles of the TS sequence are plotted in Fig. (3-5), where they are compared to the CP-sequence results.

3.2.2 Simulation of a selective DFS qubit gate

The analytical expressions found above for the attenuation due to totally correlated noise with a stationary Gaussian Markov distribution apply only to the special case of ideal pulses (instantaneous in time), but similar behavior is expected under more realistic assumptions on the control fields. In particular, to act selectively only on some of the spins we would have to use the technique of SMP [56, 111], thereby inducing a much more complex dynamics on the system for which closed form solutions are not available, but which can be studied via numerical simulations.

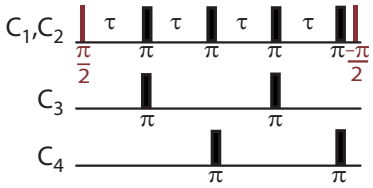

Figure 3-7: **Selective rotation about the logical x-axis** of a two-spin DFS qubit, while the evolution of a second DFS qubit under the internal Hamiltonian of the system is refocused.

We have studied the accuracy with which a rotation about the logical x-axis can be performed by numerical simulations. These simulations included the internal Hamiltonian, the external control Hamiltonian and totally correlated noise $\omega(t)$ with a stationary, Markovian Gaussian distribution. The evolution was discretized into equal time steps, for each of which we calculated the propagator $U(t_k) = \exp(-i(\mathcal{H}_{int} + \mathcal{H}_{\mathsf{rf}}(t_k) + \omega(t_k)Z)\delta t)$. The noise strength $\omega(t_k)$ is extracted from a multivariate gaussian probability distribution[4], with a covariance matrix $C_{j,k} = \Omega^2 e^{-|j-k|\delta t/\tau_c}$, where j and k are integers indicating the time intervals. We then take the average of the superoperators $S_i = \bar{U}_i \otimes U_i$ obtained over a sequence of evolutions differing only by the random number seed.

We have performed one set of simulations using a fictitious two-spin molecule (chemical shift difference: $\Delta\omega = 600$Hz, scalar coupling $J = 50Hz$), and another using the internal Hamiltonian of ^{13}C-labeled crotonic acid, a molecule containing four carbon spins [17]. Both sets of simulations were performed with instantaneous ideal pulses, and again with the strongly-modulating pulses used in actual NMR experiments. SMP are time-depend RF

[4]This distribution was given by $\omega(t_k) = e^{-\delta t/\tau_c}\omega(t_{k-1}) + r_k\sqrt{1 - e^{-2\delta t/\tau_c}}$, where r_k are normal distributed random numbers

fields designed by a numerical search, and perform precise rotations of one or more spins while refocusing the evolution of all other spins in a molecule [56, 111].

In the case of the two-spin molecule, since selective pulses are not required, we compare the results of SMP pulses with the dynamics under short, collective pulses (called "hard pulses", π-pulse time $t_p = 2\mu s$). SMP appear to perform better even if they require longer times. In the crotonic acid simulations, the sequence was designed not only to implement a selective $\pi/2$-rotation about the logical x-axis on the two spins in one DFS qubit, but to also refocus the evolution of the other two spins under the molecule's internal spin Hamiltonian (see Fig. (3-7)).

The fidelities of these simulations are plotted as a function of the correlation time in Fig. (3-8). Compared to simulations with ideal pulses, we observe a drop in the fidelity due to the finite duration of each pulse. This drop is only in part accounted for by the increase in time in the cycle length. Nevertheless, the effectiveness of the CP-sequence in preventing decoherence during the unavoidable excursions from the DFS is evident.

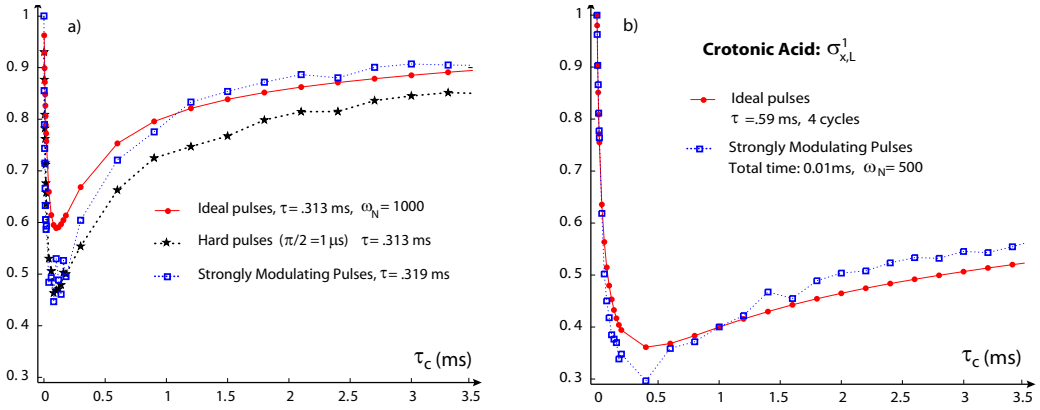

Figure 3-8: **Fidelity for ideal and real pulses.** a) 16-cycles CP sequence implementing a $\pi/2$ rotation about the logical σ_x in a 2-spin DFS. (A fictitious spin system with $\Delta\omega = 600$Hz and J=50Hz was used in the simulation) b) $\pi/2$ rotation about the logical σ_x^1 for Crotonic acid, using Strongly Modulating Pulses and compared to the result for ideal (instantaneous) pulses. The ideal pulses sequence has longer τ intervals, giving the same total time as the SMP one, to account for the finite duration of SMPs.

3.3 Conclusions

In this chapter we have considered the difficulties of operating on quantum information stored in encoded qubits without losing the protection from decoherence offered by the

encoding.

The most significant result is a demonstration that in many realizations, including NMR, the implementation of a universal set of quantum gates may be considerably simplified by briefly leaving the DFS while using dynamical decoupling to inhibit decoherence during these excursions.

We showed how experimental limitations in the control fields available in any real implementation and the natural Hamiltonian itself can cause leakage from the encoded subspace. Although we have focused upon the Hamiltonians and control fields operative in NMR for concreteness, similar difficulties will be encountered in other functional realizations of quantum information processing today, including squids, ion traps and quantum optics.

We found that the effects of this leakage can be greatly reduced by modulating the noise operator, using dynamical decoupling, while implementing the desired gate. This approach depends on the ability to operate on the system on time scales short compared to the correlation time of the noise. In evaluating various possible realizations of quantum information processing, it is important to characterize not only the decoherence rate, but also the spectral density of the underlying noise, to verify that the gate speed is sufficient to allowing the noise to be refocused.

In particular, average Liouvillian theory is a useful tool to calculate the efficacy of control sequences for refocusing the noise, and devise new ones for specific noise generators. These ideas can find wide applications in many of the experimental implementations envisaged for Quantum Information Processing.

Part II

Solid State NMR

Misura ció che é misurabile,
e rendi misurabile ció che non lo é.

Galileo Galilei

Chapter 4

Introduction

Solid state spin systems have been proposed as promising quantum information processing devices [38, 74, 89, 130] based on NMR techniques. Achieving a full scalable quantum information processor is however very challenging, and many technological advances will be required. Nuclear spins are particularly suitable candidates as qubits for their long coherence time, but this come at the expenses of a very weak interaction with the measuring apparatus. Most spin-based QIP proposals require the measurement of single nuclear spins, which is a daunting task on its own, and one that would have an even broader impact.

There are both direct and indirect approaches to single-spin measurement. A direct single-spin detection approach is magnetic resonance force microscopy [83, 117], while some indirect proposals aim at measuring the single spin state via its effect on charge transport [74] or relying on optical detection. The idea behind these last indirect approaches is to transfer the information about the spin state to some other system, which better couples to a measuring device, providing an amplification of the signal. The drawback of most of these proposals is the decoherence that this coupling induces on the system.

In this thesis we propose a new approach to the measurement of a single spin state, based on NMR techniques and inspired by the coherent control over many-body systems envisaged by Quantum Information Processing, to take full advantage of the quantum complexity of the system coherent dynamics. In chapter 5 we present a measurement scheme, in which a single target spin is coupled via the natural magnetic dipolar interaction to a large ensemble of spins. We demonstrate how it is possible to steer the system evolution by applying external radio frequency pulses, so that the spin ensemble reaches one of two orthogonal

states whose collective properties differ depending on the state of the target spin and are easily measured. The key point of the measurement process is the creation of a highly entangled state, which allows amplifying the perturbation created locally in the ensemble by the target spin. The evolution can nonetheless be defined in terms of the Hamiltonian of the spin system, and thus implemented under conditions of real control using well-established NMR techniques. A practical implementation still awaits several experimental building blocks, such as the availability of a very highly polarized state, close to a pure state; even so, this scheme is rich in potential applications and extensions.

An application of quantum information that is particularly promising is simulation of quantum systems [51]. A quantum simulator need not to be a fully-developed quantum computer. Given favorable Hamiltonians and precise (even if not universal) control on the system, it can be possible to simulate interesting physical problems. We have investigate one system that could be used as a quantum simulator and taken the first steps into studying the control, accessible states and physical signatures that would be useful for simulating physical systems of interest in condensed matter theory. In chapter 6 we introduce this system and show the results of an initialization procedure that creates an interesting initial state for simulations and transport of quantum information.

In the rest of this chapter we introduce the nuclear spin systems studied by solid-state NMR and a particular technique, multiple quantum coherence experiments, that allows for a better characterization of the system dynamics.

4.1 Solid State NMR System

The dominant interaction in spin-$\frac{1}{2}$ nuclear systems in a rigid crystalline is the magnetic dipole-dipole interaction. The dipolar Hamiltonian for spins $\mathbf{I} = \sigma/2$ is:

$$\mathcal{H}_{dip} = \sum_{i<j} \frac{\hbar\gamma_i\gamma_j}{|r_{ij}|^3}\left(\mathbf{I}_i \cdot \mathbf{I}_j - \frac{3(\mathbf{I}_i \cdot \mathbf{r}_{ij})(\mathbf{I}_j \cdot \mathbf{r}_{ij})}{|r_{ij}|^2}\right) \tag{4.1}$$

with $\mathbf{r}_{ij}$ is the intra-spin vector.

In a large magnetic field along the z axis, we only consider the energy-conserving *secular* part of the dipolar Hamiltonian, that is, the terms that commute with the stronger Zeeman Hamiltonian (and therefore conserve the total magnetization along the z direction). The dipolar Hamiltonian then takes the form:

$$\mathcal{H}_{dip} = \sum_{ij} b_{ij}[\sigma_z^i\sigma_z^j - \frac{1}{2}(\sigma_x^i\sigma_x^j + \sigma_y^i\sigma_y^j)] \tag{4.2}$$

where the dipolar coupling coefficients are given by:

$$b_{i,j} = \frac{1}{2}\frac{\hbar\gamma_i\gamma_j\left(3\cos\left(\vartheta_{ij}\right)^2 - 1\right)}{|r_{ij}|^3} \tag{4.3}$$

with ϑ_{ij} the angle between intra-spin vector and the external magnetic field direction.

Since experiments are usually conducted at room temperature, the equilibrium state is a highly mixed state, as in the case of liquid state NMR, and it is given by:

$$\rho_{th} = \sum_{i=1}^{N} \sigma_z^i \tag{4.4}$$

where the sum extends to all the spins in the sample. Notice that the argument used in Section (1.1) to find this approximated expression is still valid, even if the internal Hamiltonian comprises now the dipolar Hamiltonian.

The system used in the experiments was a single crystal of fluorapatite ($Ca_5(PO_4)_3F$, see Fig. (4-1)) grown by Prof. Ian Fisher. Apatites, either hydroxyapatites or fluorine containing apatites [49, 42], have been studied in MQC NMR experiments because of their particular geometry [31, 32] and has also been proposed as a system to implement QIP [88]. The fluorapatite crystallizes in the Hexagonal-Dipyramidal crystal system, with cell

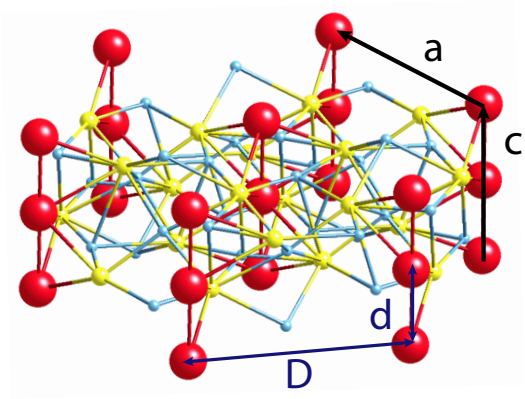

Figure 4-1: **Structure of the crystal fluorapatite.** The large spheres represent the fluorine atoms. Also indicated are the crystal axis a and c and the in-chain distance d between two nearest neighbor fluorine atoms and the cross-chain distance D.

dimensions $a = 9.367$Å and c=6.884Å, and two formula units per cell. The fluorine spins are arranged on linear chains along the c direction, with distance between two atoms $d = 3.442$Å, and 6 adjacent parallel chains at the distance $D = 9.367$Å. Since the dipolar couplings decrease with the cube of the distance between spins, the spin system can be considered a quasi-1D system. In particular, by orienting the c direction of the crystal along the z axis, the ratio of the cross-chain and in-chain dipolar coupling is:

$$\frac{b_\times}{b_{in}} = \frac{1}{2}\frac{d^3}{D^3} \approx 0.0248 \tag{4.5}$$

By changing the orientation of the crystal, it is also possible to explore regimes where the crystal goes from a quasi-1D system to a 2D and 3D system. If for example the crystal is oriented such that the c-axis is at the so-called *magic angle*, $\vartheta_{\text{M}} = \arccos 1/\sqrt{3}$, with the external magnetic field, the in-chain coupling are zero, since the angular coefficient of the dipolar interaction, $(3\cos\vartheta^2 - 1)$, is zero. If we further orient the crystal, such that the B-field is along the direction $[0, \sqrt{2/3}, \sqrt{1/3}]$ in the frame defined by the crystal axis, all the nearest neighbor couplings in the planes perpendicular to the chains are equal (or zero).

4.2 Multiple Quantum Coherences

Quantum coherence refers to a state of a physical system where the phase differences among the various constituent of the system wave function can lead to interferences. In particular, quantum coherences often refer to a many-body system, whose parties have interacted and

therefore show a correlation, a well defined phase relationship. The study and search for macroscopic quantum coherences is a highly exciting area, since it explores the boundary between the classical and quantum world.

In NMR, coherences between two or more spins are usually called *multiple quantum coherences*, to distinguish them from the single quantum coherence operators, which are the usual (direct) observables.. When the system is quantized along the z axis, so that the Zeeman magnetic moment along z is a good quantum number, a quantum coherence of order n is defined as the transition between two states $|m_1\rangle$ and $|m_2\rangle$, such that the difference of the magnetic moment along z of these states $m_1 - m_2 \propto n$. Since the usual NMR experiment is not described in spectroscopic terms of transitions between energy levels, but as a dynamics evolution of the system represented by a density matrix, multiple quantum coherences of order n usually describe states like $|m_2\rangle\langle m_1|$, or elements in the density matrix that correspond to a transition between these two states [134, 104]. The state $|m_2\rangle\langle m_1|$ is also called a coherence of order n.

A particular simple evaluation of the order of a given state is possible when this is expressed in terms of product operators [61] , or in general, of products of the single spin Pauli matrices σ_z, σ_+ and σ_-:

$$\rho_n = \underbrace{\sigma_+^i \dots \sigma_+^h}_{\text{r spins}} \underbrace{\sigma_-^l \dots \sigma_-^m}_{\text{s spins}} \underbrace{\sigma_z^j \dots \sigma_z^k}_{\text{N-r-s spins}} \tag{4.6}$$

Then the coherence order n is just $n = r - s$.

For N spin$\frac{1}{2}$, the 2^N energy levels are partitioned into $N+1$ manifold of equal magnetic moment ($\propto m$), each containing: $\binom{N}{\frac{N}{2}+m}$ states. The number of coherences of a particular order is given by the number of all possible state pairs whose magnetic moments m_1, m_2 differs by n:

$$\begin{array}{c} \sum_{m=0}^{N-n} \binom{N}{\frac{N}{2}+m}\binom{N}{\frac{N}{2}+m+n} = \binom{2N}{N-n}, \quad n \neq 0 \text{ and} \\ \frac{1}{2}\sum_{m=1}^{N-n} \binom{N}{\frac{N}{2}+m}\left[\binom{N}{\frac{N}{2}+m} - 1\right] = \frac{1}{2}\left[\binom{2N}{N} - 2^N\right], \quad n = 0 \end{array} \tag{4.7}$$

Notice that in the case of the zero quantum coherences, we only counted transitions such that $m_1 - m_2 = 0$ but between two different states. Diagonal density matrix terms (representing a 'transition' with the same state) are called populations and do not properly describe a coherence.

Quantum coherences can also be classified based on their response to a rotation around the z axis, as that given by resonance offset or by a phase shift of a pulse. A state of coherence order n will acquire a phase proportional to n under a z-rotation:

$$e^{-i\phi/2\sum\sigma_z}\rho_n e^{i\phi/2\sum\sigma_z} = e^{-in\phi}\rho_n \tag{4.8}$$

We will see in the following that it is possible to use this property to selectively detect a particular quantum coherent order.

The observation of multiple quantum coherence in NMR started in the mid 1970s, as a method for unraveling complex spectra, by filtering transitions based on the coherence order involved [104]. Since higher quantum coherences are sensitive to the number, geometry and interconnectivity among nuclei, they can be used to access information about these properties, that are otherwise masked in a simpler experiment. In particular, since an n quantum coherence can only form in a cluster of n or more spins, it is also possible to estimate the number of spins interacting at a given evolution time; this kind of experiments are called *spin-counting* experiments [11, 103]. More recently, these states have been studied with respect to their decay time [34, 85] and effects of decoherence on them. For a review of applications see [104] and references 27-29 therein.

Coherences can be created by the interplay of rf pulses and free evolution periods, during which interactions among spins occur. We will focus in particular on multiple quantum coherences in solid state NMR, where the interaction is given by the dipolar Hamiltonian Eq. (4.2). The dipolar Hamiltonian conserves the coherence order in the σ_z basis, but it creates correlations among different spins that can be converted to coherences under a similarity transformation, given by rf pulses.

For example, under a $\pi/2$ rotation about the y axis, $R_{\frac{\pi}{2}|_y}$, the dipolar Hamiltonian $\mathcal{H}_{dip}$ (Eq. 4.2) is transformed to:

$$R_{\frac{\pi}{2}|_y}(\mathcal{H}_{dip}) = \textstyle\sum_{ij} b_{ij}\frac{3}{8}(\sigma_+^i\sigma_+^j + \sigma_-^i\sigma_-^j) - \frac{1}{2}\mathcal{H}_{dip}, \tag{4.9}$$

where the first term is responsible for creating even order coherences. With an appropriate sequence of rf pulses and delays we can isolate the first term in Eq. 4.9.

The effects of a series of pulses and delays, organized in a cyclic sequence, can be best evaluated using Average Hamiltonian Theory (AHT) [68, 69], which is an important tool

also in the construction of special purpose pulse sequences (see Appendix A.1). Consider the evolution under the 8-pulse sequence in figure (4-2). Following the rules of AHT it is easy to calculate the zeroth order term in the toggling frame. This is just given by:

$$\mathcal{H}_{DQ} = \sum_{i,j} \frac{1}{2} b_{i,j}(\sigma_i^x \sigma_j^x - \sigma_i^y \sigma_j^y) = \sum_{i,j} b_{i,j}(\sigma_i^+ \sigma_j^+ + \sigma_i^- \sigma_j^-) \tag{4.10}$$

which is usually called a double quantum Hamiltonian, since it can increase the coherences number by steps of two (thus creating even order coherences starting from the population state). In general, pulse sequences can be devised to generate *Grade Raising* Hamiltonians, that is, operators that increase the coherence order of a state.

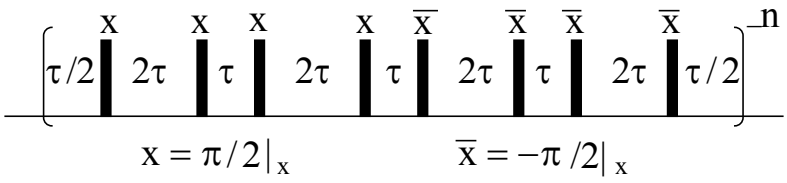

Figure 4-2: **8 pulse Double Quantum sequence.** This sequence of rf pulses and delays creates a Double Quantum Hamiltonian (that is, an Hamiltonian that can excite even order quantum coherences)

By symmetrizing this sequence, that is, going to a sequence with 16 pulses, such that $\tilde{\mathcal{H}}(t_c - t) = \tilde{\mathcal{H}}(t)$, the sequence gives the double-quantum Hamiltonian to first order, with no corrections due to finite width pulses, offset errors or pulse errors. The 16-pulse sequence is the one usually used in the experiments reported in this thesis.

Another approach to describe the dynamics of the creation of MQC is to interpret it with an *hopping model* [103], in which the system is allowed to evolve 'hopping' from one state to another with different coherent number, at a certain rate, dependent on the coherence, and under certain selection rules.

If for example the Hamiltonian under which the MQC are created is the double-quantum Hamiltonian, Eq. (4.10), only even coherence orders can be created and the allowed pathway in Liouville space is as shown in Fig. (4-3), where one has to notices that coherence orders can only vary by step of two, while the effective number of spin increase by one at each step.

MQC intensities cannot be measured directly, since the NMR spectrometer coil is only sensitive to single body, single quantum coherences. MQC created in the system must

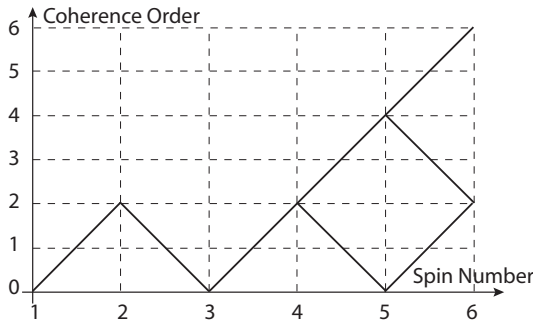

Figure 4-3: **Pathway for the allowed coherence orders** for a given number of spins. By expanding the evolution in a series of commutators, we see that each higher order term in time can only introduce a new spin in the state and modify the coherence order by ± 2. Notice also that 4-quantum coherences can only be created when 5 or more spins are in the cluster, or that it is 4^{th} order process in time.

therefore be tagged before bringing them back to observable operators, in order to separate the contributions of different MQC into the signal. The usual MQC experiment thus involves 4 steps (Fig. (4-4)).

During the preparation time, a pulse sequence creates high coherence orders. The evolution period let the system evolve to better characterize the MQC as required by each particular experiment. The refocusing step brings back the MQC to single spin, single quantum coherence, which is then measured during the detection period. In particular, consider the case where the the refocusing operator is the inverse of the preparation operator up to a phase ϕ, followed by a $\pi/2$-pulse:

$$V = e^{-i\pi/4 \sum \sigma_y^k} V' = e^{-i\pi/4 \sum \sigma_y^k} e^{i\phi/2 \sum \sigma_z^i} U^\dagger e^{-i\phi/2 \sum \sigma_z^i} \tag{4.11}$$

The observed signal is then given by:

$$\begin{aligned} S &= \mathrm{Tr}\left[V' e^{-i\phi/2 \sum \sigma_z^i} U \rho_0 U^\dagger e^{i\phi/2 \sum \sigma_z^i} V'^\dagger \rho_0\right] \\ &= \mathrm{Tr}\left[e^{-i\phi/2 \sum \sigma_z^i} U \rho_0 U^\dagger e^{i\phi/2 \sum \sigma_z^i} U \rho_0 U^\dagger\right] \\ &= \mathrm{Tr}\left[e^{-i\phi/2 \sum \sigma_z^i} \rho_{MQC} e^{i\phi/2 \sum \sigma_z^i} \rho_{MQC}\right] = \textstyle\sum_p \mathrm{Tr}\left[e^{ip\phi} \rho_p^2\right] \end{aligned} \tag{4.12}$$

where ρ_p is the p^{th}-quantum coherence component in the state ρ_{MQC}

By varying the angle ϕ between 0 and 2π in steps of $2\pi/M$, (M being the maximum coherence number created), it is possible to obtain the intensities of the MQC contributions, by fourier-transforming the signal with respect to ϕ. Figure (4-5) shows the MQC spectrum

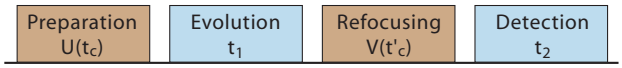

Figure 4-4: **MQC experiment scheme**. The usual multiple quantum experiment is composed of four steps, which are shown in the figure as four blocks, during which a different evolution takes place.

obtained by the double-quantum 16-pulse sequence in CaF_2.

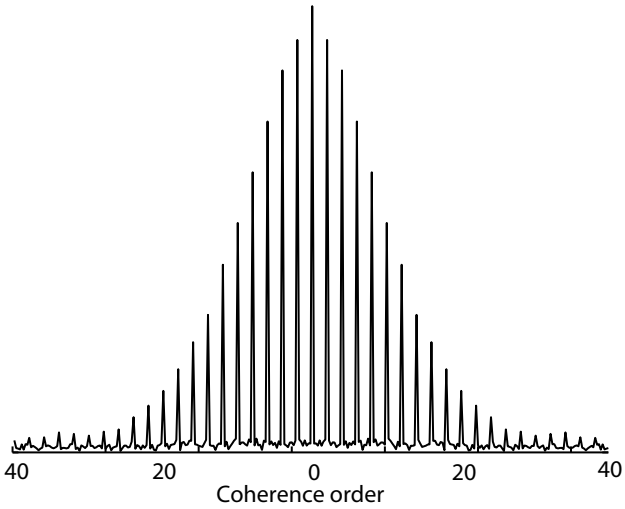

Figure 4-5: **Typical MQC spectrum in CaF_2** showing even quantum coherence intensities [33] (Reproduced with the permission of the author).

The growth and evolution of MQC is a complex many-body dynamics and only approximated models are available to describe it. Besides stochastic models, based on the probability of occupation of different coherent states, and semiclassical models like the hopping model, there is an exact analytical solution of the MQC dynamics under the double-quantum Hamiltonian in 1D systems, in the case of nearest neighbors only [50, 45]. Although this is a very interesting solution for short time, that we will use in chapter (6), it does not explain the creation of higher coherence orders.

Selective MQC

The creation of MQC and the selection rules associated depend on the initial state and pulse sequence used. For example, if the initial state is in the transverse plane, the double-quantum Hamiltonian can create all odd coherences, while a Single Quantum Hamiltonian of the form $\mathcal{H}_{SQ} = \sum_{i,j} b_{i,j}(\sigma_i^z\sigma_j^x + \sigma_i^x\sigma_j^z)$ can create all coherence orders. It is also possible to create a specific coherence order (and all its higher multiple) by selective multiple quantum

coherence experiments [144].

It easier to follow the evolution of the system by focusing on the operator created by a given pulse sequence, which can be ascertained by AHT. The operator obtained should be able to rotate the thermal state to the desired coherence state, so it must be possible to write it as $e^{-i\mathcal{H}_p t}$ where $\mathcal{H}_p$ is an operator composed only by p^{th} coherence order terms. The first step is to create an effective Hamiltonian that *also* contains the coherence order wanted, then a phase cycling scheme can be used to select it.

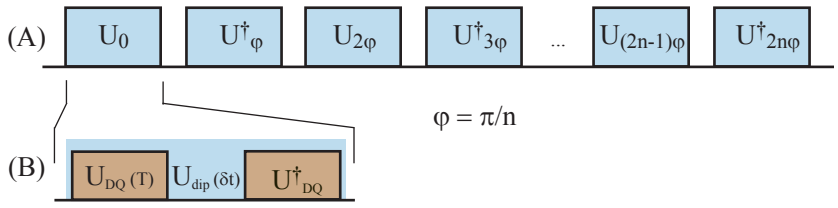

Figure 4-6: **Selective MQC scheme**, for the selection of the n^{th} quantum coherence (with n even). (A) Phase cycling scheme, selecting the wanted coherence, while refocusing the zero quantum terms, too. (B) Basic sub-cycle sequence to create a high coherence order operator. The pulse phases in the DQ pulse sequence are shifted to obtain an effective z-rotation in the super-cycle scheme.

An operator that creates all (all even) coherence orders can be obtained by rotating the free evolution of the system under the action of an Hamiltonian that can create coherences, as the single- (double-)quantum Hamiltonian -see Fig. (4-2). Notice that the effective Hamiltonian of this sub-cycle of the sequence $\mathcal{H}_0 = U_{DQ}\mathcal{H}_{dip}U_{DQ}^{\dagger}$ can contain high order coherences if the time T that we allow the double-quantum Hamiltonian to act for is relatively long ($U_{DQ} = e^{-i\mathcal{H}_{DQ}T}$), but the time of interest of the sub-cycle is only the time δt of free evolution, $U_0 = e^{-i\mathcal{H}_0\delta t}$, which can be kept small, thus ensuring convergence of AHT. To select the desired quantum coherence, this basic sub-cycle is repeated with a shift in the phase of each pulse, which correspond to an effective rotation about z of the Hamiltonian H_0: $U_\phi = e^{-i\phi/2\sum\sigma_z^i}U_0 e^{i\phi/2\sum\sigma_z^i}$. If the coherence to select is the n^{th} order, the cycle is repeated n times with a phase increment of $\phi_0 = 2\pi/n$. To first order, the effective Hamiltonian is given by the sum of Hamiltonians in each cycle:

$$\bar{\mathcal{H}}^{(0)} \propto \sum_k e^{-ik\pi/n\sum\sigma_z^i}\mathcal{H}_0 e^{ik\pi/n\sum\sigma_z^i} \tag{4.13}$$

Rewriting the effective Hamiltonian $\mathcal{H}_0$ in terms of its multiple quantum coherences com-

ponents, $\mathcal{H}_0 = \sum_p \mathcal{H}_p$, we have:

$$\bar{\mathcal{H}}^{(0)} \propto \sum_{k,p} e^{-ipk\pi/n} \mathcal{H}_p = \mathcal{H}_{n\kappa} \tag{4.14}$$

that is, only the n^{th} coherences and its multiple are retained. In order to eliminate also the contribution from zero quantum coherences, the sub-cycle should be repeated $2n$ times, with phase increments of π/n and inverting the time arrow every sub-cycle - see Fig. (4-6).

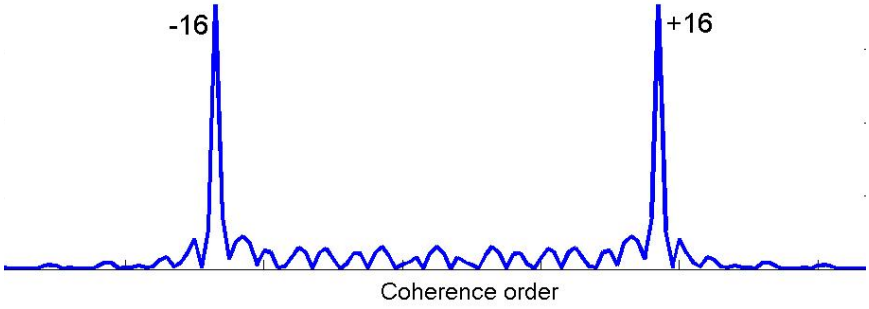

Figure 4-7: **MQC spectrum for a selective MQC experiment in CaF_2**, showing the selection of the 16^{th} quantum coherence order intensities only. (Reproduced with the permission of the author [33])

Chapter 5

Entanglement assisted metrology

The measurement of a single nuclear spin state is an experimentally challenging task, that once solved could yield useful applications as well as valuable physical insights. Potential applications include nuclear spintronics devices [23, 157], biomolecular microscopy [123, 155] and spin based QIP [74]. Spintronics (spin-electronics) studies spin degrees of freedom in solids and aim at building spin-based devices, via the active control of spin dynamics in semiconductor and metals. Although spintronics focuses on electron spins, the interaction with nuclear spins is unavoidable, and leads often to decoherence or undesirable effects. Control and measurement of nuclear spins at the single-spin level would benefit enormously this field.

Directly visualizing molecular structure will have a revolutionary impact upon medical research and structural biology[1]. While electron microscopy (and any other energetic probe, like x-ray) cannot be used to reach this goal, because of the ionization energy lost by electrons traversing a biological molecule, observation of nuclear spin properties of molecules is a promising avenue.

Quantum computation proposals need to prove a scalable mechanism for read-out [43]. Nuclear spins-$\frac{1}{2}$ have been proposed as viable qubits [74, 130, 89, 88], not only because they provide the archetype of a two-level system, but especially because of their long decoherence times. This is due to weak interactions with the environment, but it comes also at the expenses of weak (low-sensitivity) interactions with the measurement apparatus.

[†]This chapter has been adapted from reference [26]

[1]As Richard Feynman said: *"It is very easy to answer many of these fundamental biological questions; you just look at the thing!"* [52]

Many methods have been proposed to increase the sensitivity of nuclear spin measurement beyond the limits of NMR or ESR. The detection of spin resonances is pursued by magnetic force detection [117, 83], by transfer of the spin state to the electron charge [74] and by near field optics [147, 148, 149, 151]. These methods are close to or have reached [47] the limit of single spin detection for electrons, but the measurement of the quantum state of a single nuclear spin has not yet been achieved. Furthermore, these techniques introduce sources of additional decoherence, through quantum measurement back-action (for example, spin relaxation rates in the MRFM environment seem to be faster than in bulk measurements) and sometimes they require special materials to be implemented.

The measurement method that we propose in this thesis uses instead NMR techniques and the dipolar Hamiltonian which couple every nuclear spin system. Since it does not introduce any further decoherence but rather relies on a fully coherent quantum dynamics of the interface with the measuring apparatus, this method is a nondestructive observation process and can thus aim at not only detecting a nuclear spin, but at measuring its state. We rely on entanglement in a nuclear spin ensemble to increase the sensitivity of the measurement: On one side, entanglement has already proved to help reach the quantum measurement limits in spectroscopy [92]; on the other side, nuclear spin ensembles are sensitive probes of single quantum system, as proved by the decoherence they induce on single electrons when not controlled [76], while with good control techniques this decoherence can be reduced [129].

In this chapter, we first describe this measurement process using QIP gates, with ideal algorithms that motivates the use of entanglement to overcome limitations in the control available. We demonstrate this entanglement-based ideal algorithm with a proof of principle experiment in ensemble liquid state NMR. In Section (5.2) we show how equivalent schemes can be defined in terms of the Hamiltonian of the spin system and thus implemented under conditions of real control, using well established NMR techniques. This method requires the ability to control about 10^6 spins (the current low temperature detection limit for NMR) by inducing a coherent dynamics, modulated by the interaction with the target spin. Because of the challenges in creating a macroscopic entangled state, in the short term we expect our method to be used to enhance sensitivity, with a system of about hundred entangled spins (already available experimentally [85]). As no physical limitations prohibit to enlarge the system to the size required for single spin state measurement, this remains however our

ultimate goal.

5.1 Ideal algorithms and the role of entanglement.

The task that we propose to accomplish is the measurement of a single nuclear spin. The single spin, that we will call the *target* spin, is isolated spatially from other similar spins that compose the quantum processor, or more generally the material under study. In order to measure its state, we put it in contact with the measurement device, composed of an ensemble of nuclear spins of a different chemical species. The measurement process amplifies the signal from the single spin by transferring the information about its polarization to a large ensemble of spins. The spin ensemble has therefore the role of a *Spin Amplifier*.

The spins of the ensemble are prepared in a fiducial state before the measurement, the highly polarized ground state where all the spins are aligned with the external magnetic field. This state is in principle achievable by lowering the temperature of the spin ensemble and further using Dynamic Nuclear Polarization to increase the polarization of the nuclear spins by coupling them to electron spins [3, 64, 2]. The polarizations reached in practice are as high as 97% [41].

5.1.1 C-NOT scheme

To amplify the signal from the target spin, the simplest strategy would be to create many copies of its state, by letting the target spin interact with the Amplifier spins. If we could copy the information about the polarization of the target spin onto the Amplifier spins, a weak measurement -as the one implemented in conventional NMR- could extract that information. Unfortunately, the no-cloning [146] theorem forbids such a process for an unknown quantum state. We will therefore restrict the state of the target spin to the two orthogonal eigenstates $|0\rangle$ or $|1\rangle$, as if it had already collapsed to one of these states by a strong measurement. Notice that restricting the measurement to only two orthogonal states is not a limitation in the context of QIP, since it is sufficient for the read-out stage [43], and for imaging as well this restriction is not critical.

To illustrate how a collective measurement can provide knowledge of the single spin state, consider a simple quantum circuit, consisting of a train of Controlled Not (C-NOT) gates between the target spin and each of the Amplifier spins Fig. (5-1). The C-NOT gate

will flip the controlled spin if the target (controlling) spin is in the $|1\rangle$ state and do nothing if it is in the $|0\rangle$ state. Since the C-NOTs act on the fiducial state $|00\ldots0\rangle$, this amounts to effectively copying the target spin state onto the Amplifier spins. The no-cloning theorem does not apply here, since the target spin is already in one of two orthogonal states.

At the end of the circuit, the measurement of the Amplifier magnetization along the z-direction ($M_z \propto \langle\Psi_A|\sum_i^n \sigma_z^i|\Psi_A\rangle$) will indicate the state of the target spin. If the target spin was in the $|0\rangle$ state, the Amplifier spins are still in their initial state, so that $M_z = M_z(0)$. If the Amplifier spins have been rotated because the target spin was in the $|1\rangle$ state, the final state of the amplifier spins is $|11\ldots1\rangle$ and the magnetization has been inverted: $M_z = -M_z(0)$.

Although the measurement involves only collective properties of the Amplifier, this first scheme demands that the ensemble spins are independently addressable and that they all interact with the target spin in order to realize the C-NOT gates.

5.1.2 Entanglement Scheme

Instead of imposing these requirements, we can develop equivalent schemes that connect better to the available control. Relying only on entanglement among the Amplifier spins and on the evolution given by the internal Hamiltonian and collective rotations, these schemes can be realizable in the near term.

Entanglement among particles in an ensemble has been shown to produce changes in macroscopic observables [90] and to enhance the signal-to-noise ratio in spectroscopy [92] up to the Heisenberg limit. In this last experiment, the state of the atoms is prepared in a large *cat-state*, that is, the generalization of the GHZ state $|\psi_{\mathrm{GHZ}}\rangle = (|000\rangle+|111\rangle)/\sqrt{2}$ to n qubits [67]. The cat-state is a maximally entangled state that acquires the phase information with

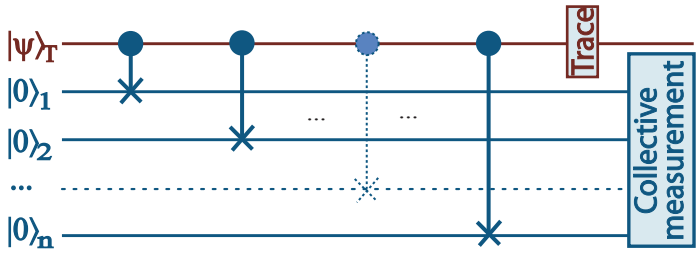

Figure 5-1: **Scheme 1**: Series of C-NOT gates between the target and Amplifier spins. A collective measurement is sufficient to detect the state of the target spin.

optimal sensitivity, since it evolves n times faster under a collective evolution. In a similar way, we want to create an entangled state that is the most sensitive to the action of the target spin.

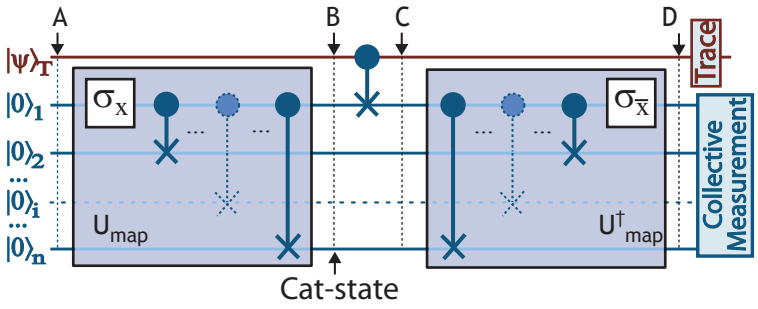

Figure 5-2: **Scheme 2**: Entanglement permits to use only one local action of the target spin. The entangling operator U_{map} can be created with gates on single spins or with a phase modulated sequence, using only the internal dipolar Hamiltonian and collective rf pulses to create the Grade Raising operator as explained in the following Section. The four letters refer to the points where spectra were measured, see Fig. (5-4).

In scheme 1, where the Amplifier spins remain in a factorable state, the interaction with the target spin produces only local changes on individual spin states. On the other hand, with the creation of a macroscopic entangled state [91], the Amplifier is globally affected by a single interaction with the target spin: The propagator creating the cat-state performs an effective change of basis to a reference frame where the local C-NOT gate is a global operator on the Amplifier. We illustrate the role of the entanglement with a second scheme (Fig. (5-2)).

Here the fully polarized state $|00\ldots0\rangle$ is first transformed into the cat-state

$$\frac{1}{\sqrt{2}}(|00\ldots0\rangle \; - \; i|11\ldots1\rangle) \tag{5.1}$$

by a $\pi/2$ rotation about σ_x of the first spin in the amplifier and a series of C-NOTs between this first spin and all the other spins in the amplifier. Then, we invert the state of the first Amplifier spin, conditionally on the state of the target spin. The entanglement is then undone by applying the inverse transformation (that is, a series of C-NOT and the σ_x rotation) in order to bring back the system to a state that gives an observable signal in NMR (see Section (1.1)).

When inverting the evolution to undo the entanglement, the C-NOT and σ_x gates bring the Amplifier back to the initial state if the target spin is in the $|0\rangle$ state. Otherwise

we obtain the state: $|1\rangle_T|111\ldots1\rangle$. As in the previous scheme, measuring the Amplifier magnetization provides information about the target spin state. Notice that we have invoked only one interaction between the target spin and a privileged spin in the Amplifier, a more practical requirement, given the locality of any spin-spin interaction.

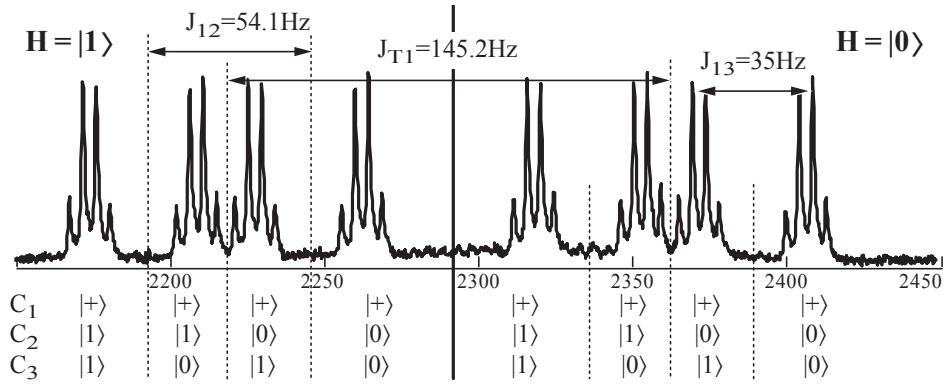

Figure 5-3: **Spectrum of the first carbon at thermal equilibrium in Alanine**, showing the coupling with the proton and the other 2 carbons (The methyl group produces the multiplet splitting). Notice in particular that the couplings with the proton (the target spin) are completely resolved.

Experiment

We have implemented this scheme on a small QIP NMR liquid system, where the target spin is represented experimentally by a macroscopic ensemble of spins. Although their state is detectable, it is measured only indirectly, following the scheme proposed. The single protons of a ^{13}C labeled Alanine molecule ensemble are the target spins, while the 3 carbons compose the Amplifier (see Section (1.1) for the molecule's description).

As it can be seen from the spectrum of the first carbon (Fig. (5-3)), the couplings with the proton are completely resolved, so that we can separate the signal arising from carbons coupled to protons in the $|1\rangle$ state (left) or in the $|0\rangle$ state (right). Before applying the circuit of Fig. (5-2), we put the proton spin into the identity state and prepare the carbons in the pseudo-pure state $|000\rangle$ [38]. The proton state is prepared in a mixture of the two states $|0\rangle\langle 0|$ and $|1\rangle\langle 1|$, thus we can effectively perform two experiments in parallel, and read out the outcomes from just one spectrum.

The gates in Fig. (5-2) are implemented using strongly modulating pulses [112, 56], that allows rotations of individual spins (notice that in liquid state NMR, for a limited number

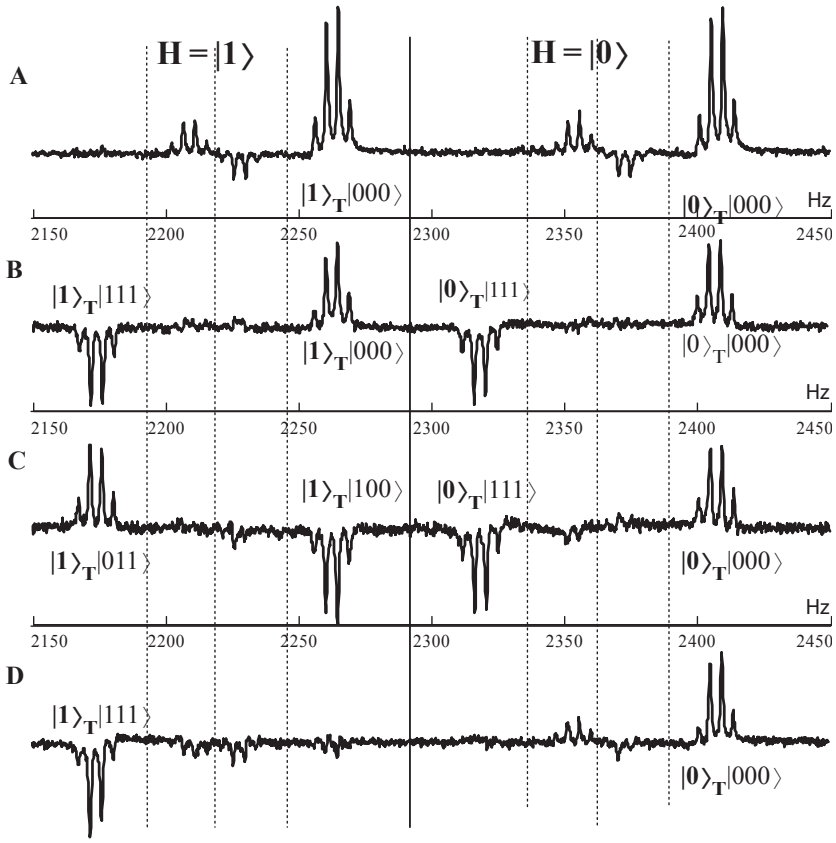

Figure 5-4: **Experimental Results: A**. Initial State: Pseudo-pure state of the 3 carbons, with the target spin in an incoherent superposition of the two possible initial states, $|1\rangle$ (left) and $|0\rangle$ (right). **B**. Cat-state (or GHZ state) for the 3 amplifier spins. **C** After applying a C-NOT on the first Carbon, its magnetization is inverted only on the left hand side of the spectrum (target spin in $|1\rangle$ state), as is the sign of the Cat-state spectrum. **D**.Final state: The polarization of the carbons has been inverted (left) indicating a coupling to the target spin in state $|1\rangle$, while it is unchanged for spins coupled to target spin in the $|0\rangle$ state (right).

of spins that permits frequency resolution, we have universal control on the system). In Fig. (5-4) we show the spectra of Carbon-1 at four steps of the circuit, showing the evolution of the system during the algorithm. The experimental results show that the polarization of the three carbons is inverted conditionally on the state of the proton, giving an indirect measurement of its state.

5.2 Experimentally accessible algorithms

Extending this scheme to larger systems is experimentally challenging, since we need to address individual spins. Yet we can relax some of the requirements on control, thus per-

mitting different implementations, if we allow for more freedom in the final state of the amplifier.

The signature of a successful scheme is that it produces observable contrast,

$$C = \frac{M_z^0 - M_z^1}{M_z(0)}, \tag{5.2}$$

M_z^0 and M_z^1 being respectively the magnetizations obtained when the target spin is in the state $|0\rangle$ or $|1\rangle$ and the initial magnetization is $M_z(0)$. The previous schemes provide the maximum contrast $C = 2$. Even if their characteristics are quite different, they are equivalent since they create the same effective propagator:

$$U_{opt} = E_T^+ \prod_{i=1}^{n} \sigma_x^i + E_T^- \tag{5.3}$$

(where $E_T^+ = |1\rangle\langle 1|$ and $E_T^- = |0\rangle\langle 0|$ are the projectors on the computational basis for the target spin). This is the only operator (up to phase factors or constants of the motion) that results in the maximum contrast.

If we accept a lower, but still observable, contrast ($C \approx 1$) the evolution we should implement,

$$U_{map} U_{cnot} U_{map}^\dagger = E_T^+ \mathcal{A} + E_T^-, \tag{5.4}$$

is such that the operator $\mathcal{A}$ instead of inverting the magnetization should just bring it to zero (we are assuming for simplicity that if the target spin is in the $|0\rangle$ state the amplifier does not undergo any evolution as it was the case in the previous schemes). In this case, $\mathcal{A}$ can have a much more general form than the one seen before ($\mathcal{A} = \prod_{i=1}^{n} \sigma_x$ in the previous schemes), as for example a superposition of $n/2$-quantum operators $\mathcal{A} = \sum_{\{i\}} (\prod_{i=1}^{n/2} \sigma_i^+ + h.c)$. We will present in the following two schemes that follow this insight to relax the conditions on control for the implementation of the measurement algorithm.

5.2.1 MQC scheme

A realizable scheme, taking advantage of this flexibility, is a propagator that still creates a cat-state, but using only collective control and evolution of the Amplifier, such as it is available in a dipolar coupled spin system.

Techniques for generating entanglement have been developed in the context of spin

counting experiments [103, 114]. The aim of these experiments is to estimate the size of a spin cluster by measuring its entanglement (or more precisely the coherence order of the system). Since a cat-state corresponds to an n-spin, n-quantum coherence state, we may use well established techniques [10, 152] to create the n-quantum coherence operator, which rotates the fully polarized state $|00\ldots0\rangle$ into the cat-state.

With the 8-pulse sequence presented in Section (4.2) we create the double quantum operator to zeroth order in AHT:

$$\mathcal{H}_{2Q} = \sum_{ij} b_{ij}(\sigma_+^i\sigma_+^j + \sigma_-^i\sigma_-^j) \tag{5.5}$$

This double quantum operator $\mathcal{H}_{2Q}$ is an example of Grade Raising (GR) Hamiltonians, operators that increase the coherence order of a state. Acting with this Hamiltonian on a 2-body operator such as the dipolar Hamiltonian we can create higher order GR operators. Phase modulated combinations of $\mathcal{H}_{2Q}$ and $\mathcal{H}_{dip}$ have been already shown [144] to permit straightforward synthesis of the pure n-body GR Hamiltonian $\mathcal{H}_{nQ} = \prod_{k=1}^n \sigma_k^+ + \prod_{k=1}^n \sigma_k^{-2}$. The n-quantum propagator $U_{nQ} = e^{-i\frac{\pi}{4}\mathcal{H}_{nQ}}$ rotates the ground state $|00\ldots0\rangle$ into the cat-state, in the same way as a $\pi/2$ rotation about σ_x ($U_{1Q} = e^{-i\frac{\pi}{4}(\sigma^+ + \sigma^-)}$ rotates a single spin to the superposition state $(|0\rangle + |1\rangle)/\sqrt{2}$, since the system behaves as an effective n-spin system [144].

Using the n-quantum propagator U_{nQ} to create and refocus the cat-state instead of the σ_x and C-NOT gates used in scheme 2, we obtain a lower contrast, C=1, but requiring only to manipulate the natural Hamiltonian with the available control via rf pulse sequences. The evolution is given by the propagator $U = U_{nQ}U_{cnot}U_{nQ}^\dagger$; by expanding this expression, we obtain

$$\begin{aligned} U = \quad & E_T^- + E_T^+ \Big(\sigma_x^1 + (\tfrac{\sqrt{2}}{2} - 1)(\textstyle\prod_{i=2}^n E_i^+ + \prod_{i=2}^n E_i^-)\sigma_x^1 \\ & -i\tfrac{\sqrt{2}}{2}(\textstyle\prod_{i=2}^n \sigma_i^+ + \prod_{i=2}^n \sigma_i^-)\sigma_z^1\Big), \end{aligned} \tag{5.6}$$

and this propagator either conserves the magnetization if $|\psi_T\rangle = |0\rangle$ or brings it to zero if $|\psi_T\rangle = |1\rangle$.

Creating the cat-state is experimentally hard, yet we can envisage even simpler schemes. The form of entanglement that influences the contrast is entanglement of the Amplifier spins with the first Amplifier spin (the one which interacts with the target spin), so that

[2]This technique, called Selective Multiple Quantum Coherence is explained in Section (4.2)

a modification in its state will drive a macroscopic change. Hence, it is not necessary to restrict ourselves to the preparation of a cat-state, as a wider class of entangled states is equally useful. To ensure that the first Amplifier spin is entangled with the rest of the spins, we must operate on the system with a GR operator that always contains this first spin. The GR Hamiltonian used previously as a basic tool to create entanglement is now replaced by:

$$\mathcal{H}_{2Q}^{(1)} = \sum_i b_{1i}(\sigma_1^+\sigma_i^+ + \sigma_1^-\sigma_i^-). \tag{5.7}$$

It is easy to create this operator since the coupling between the target and the first spin makes it distinguishable from the other Amplifier spins, so that we can address it individually. To devise a pulse sequence that generates this propagator, we start from the observation that if we repeat the pulse sequence for the $\mathcal{H}_{2Q}$ with a $\pi/2$ phase shift, the overall evolution would be completely refocused. By inverting the closest spin phase in between the two sequences, only the terms containing the first spin will survive, creating the GR1 Hamiltonian:

$$e^{-i\mathcal{H}_{2Q}t}e^{-i\frac{\pi}{2}\sigma_z^1}e^{i\mathcal{H}_{2Q}t} \approx e^{-2i\mathcal{H}_{2Q}^{(1)}t} \tag{5.8}$$

In order to realize a more robust scheme, we can furthermore introduce entanglement only conditionally on the state of the target spin, by applying $\mathcal{H}_{2Q}^{(1)}$ conditionally on the target spin state. This is achieved by making the phase inversion of the first spin conditional on the state of the target spin.

5.2.2 Perturbation Scheme

Even with these generalizations, the experimental task is still demanding: We need to apply the inverse of a rather complex map, but this inversion could dramatically amplify small errors done in its implementation. A metric of the divergence caused by a small perturbation which accumulates over time is the fidelity decay [73, 48]. Let consider a system initially in an arbitrary fiducial state evolving under a given quantum map, given by a sufficiently random unitary operator. After r repetitions of the map, its state is: $|\psi(r)\rangle = U^r|\psi_0\rangle$. If the same system is evolved under a perturbed version of the map, the final state is instead $|\psi_p(r)\rangle = (V_pU)^r|\psi_0\rangle$ and the overlap (or fidelity)

$$F(r) = |\langle\psi_p(r)|\psi(r)\rangle|^2 \tag{5.9}$$

between the two states decays exponentially with the number of repetitions of the map.

We can nonetheless turn these considerations to our advantage by coupling the chaotic dynamics to the single spin. If a perturbation is applied conditionally on the state of the target spin (for example only in the case the target spin is in the $|1\rangle$ state), the resultant states will have an exponentially decreasing fidelity and can be easily distinguished. Since the expectation value of the magnetization is a much weaker measurement than the fidelity, we expect the exponential rate to simply bound the contrast growth rate.

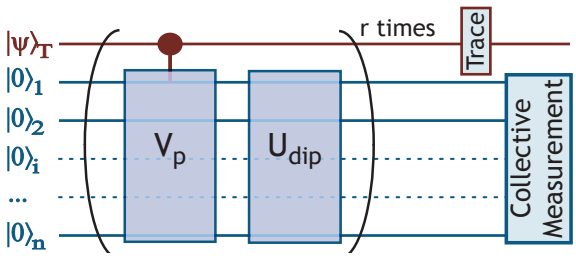

Figure 5-5: **Perturbation Scheme**: By perturbing a pseudo-chaotic propagator with a controlled perturbation, we can amplify the small changes introduced by the target spin up to the point where they are detectable.

Because of the local nature of the spin-spin interactions, the perturbation will be limited to the closest neighbors of the target spin. At a repetition r of the map, the perturbation will have affected only a factor-space of the total Hilbert space of size N_r, giving a completely randomized state and an almost zero polarization for the subsystem considered. If the evolution map is sufficiently random (and thus does not have excessive symmetries), the size N_r can grow to a large fraction of the Hilbert space with the increasing number of repetitions, allowing for a good contrast to be observed. A pseudo-random map possessing these features can be implemented in a solid state NMR system using the dipolar Hamiltonian (Eq. 4.2) propagator as the unperturbed map and as perturbation the $\mathcal{H}_{2Q}^{(1)}$ operator (Eq. 5.7), applied conditionally on the state of the target spin. This many body evolution provides a complex enough dynamics, even in the presence of residual symmetries in the Hamiltonian.

We can explain the effects of this procedure also in terms of creation of entanglement localized around the first neighbor that is then spread out by spin diffusion [13, 154]. These two successive steps, repeated many times, ensure that the change affects all the Hilbert space, creating a global entangled state.

To estimate the entanglement created by this dynamics, we evaluate a global measure

of entanglement for multipartite systems[3] [102]. The average loss of purity upon tracing over one spin:

$$Q = 2 - \frac{2}{n}\sum_i Tr\{\rho_i^2\}, \tag{5.10}$$

where ρ_i is the partial trace over the i^{th} spin is a good measure of global entanglement. For a maximally entangled state $Q = 1$, the polarization is zero. We can always write the state of the system, for any spin i:

$$|\psi\rangle = \alpha_0^i|0\rangle_i|\psi_i^0\rangle + \alpha_1^i e^{i\varphi}|1\rangle_i|\psi_i^1\rangle, \tag{5.11}$$

To obtain the maximum entanglement, we must have $\alpha_0^i = \alpha_1^i = 1/\sqrt{2}$, $\forall i$. This condition in turn implies that:

$$\langle\psi|\sigma_z^i|\psi\rangle = \left(\langle 0|_i\sigma_z^i|0\rangle_i\langle\psi_i^0|\psi_i^0\rangle + \langle 1|_i\sigma_z^i|1\rangle_i\langle\psi_i^1|\psi_i^1\rangle\right)/2 = 0 \tag{5.12}$$

and the polarization is zero.

Simulations

Because of the complexity of the dynamics involved, we found no simple analytic result to predict the contrast growth. We instead simulated the evolution of a limited number of spins in a linear chain, following the polarization and the entanglement as a function of the number of repetitions of the two basic steps ($\mathcal{H}_{2Q}^{(1)}$ and $\mathcal{H}_{Dip}$). The simulations were run using MATLAB ®, evolving the system under the ideal Hamiltonians (that is, we assumed that the grade raising Hamiltonian $\mathcal{H}_{2Q}^{(1)}$ could be implemented perfectly via a pulse sequence). The initial state was the fully polarized ground state and the (perturbed) map applied to the Amplifier when the target spin was in the $|1\rangle$ state was: $U = e^{-it\mathcal{H}_{2Q}^{(1)}}e^{-iT\mathcal{H}_{dip}}$, with: $tb_{1,2} = 1/2$ and $Tb_{1,2} = \pi/\sqrt{2}$[4].

From the simulations we can observe the predicted dynamics: Regions of the physical space farther away from the first spin are excited later in time. When the entanglement reaches $Q \approx 1$ and the polarization goes to ≈ 0, we have a saturation phenomenon, and

[3]Notice that there is no unique measure of entanglement, except for bipartite pure systems [22]

[4]This particular time was chosen since it allows for the perfect transfer of a spin state over 3 spins (the maximum distance allowed for perfect transport), for equal couplings among the spins and an XY Hamiltonian [36].

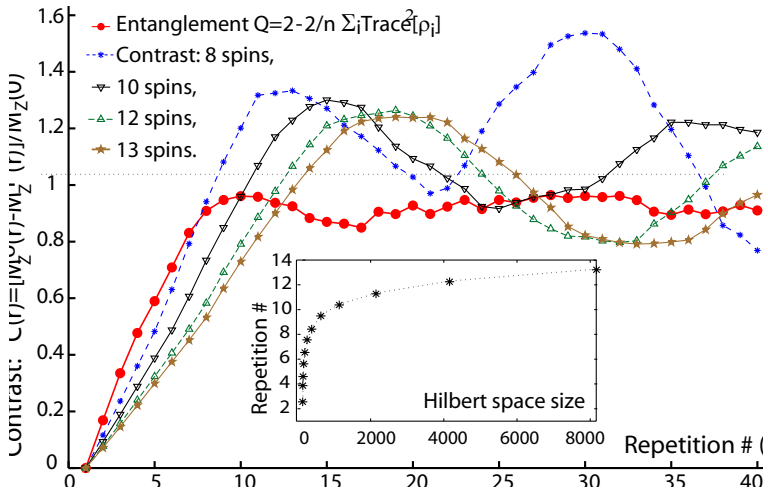

Figure 5-6: **Entanglement (10 spins) and contrast for different number of spins.** In the inset: number of repetitions to reach contrast ≈ 1 as a function of the Hilbert space size, showing a logarithmic dependence.

except for fluctuations, that decrease in amplitude with the number of spins, the macroscopic properties of the state no longer change. This effect, caused by the finite size of the Hilbert space, is also observed in the fidelity decay, that for very strong perturbation saturates at $1/N$, with N the size of the Hilbert space.

Cascade Scheme

Notice that we reach contrast ≈ 1 for a number of repetitions on the order of the spin number, as it was expected since at each cycle only one quantum of polarization can be changed by the action of the GR-Hamiltonian in a 1D chain of spins. We expect a faster rate in 2 and 3 dimensions, due to a higher number of first neighbors. The simulations cannot unfortunately be carried over in these higher dimensions, since the computational resources increase too fast with the number of spins to be considered.

In order to study the scalability of the measurement process in 3D-systems, we have analyzed another scheme which can be reduced more easily to a classical model and therefore simulated [110]. The main conclusions of this study is that not only there is a cubic speedup (only $O(\sqrt[3]{n})$ repetitions of the algorithm basic step are required to reach a contrast $C \approx 1$, instead of $O(n)$ as for the linear scheme), but the larger Hilbert space allows for a larger number of configurations that give the same high contrast, making the algorithm more robust to errors in the initial polarization or in the control.

5.3 Conclusions

In conclusion, we have shown that it is possible to transfer polarization from a target spin to an ensemble of spins, through the creation of a highly entangled state with rf pulses and the coupling between the target spin and its closest neighbors. The characteristics of the different methods discussed range from optimal contrast but with extreme control on the system to a lower contrast and more accessible experimental conditions (as summarized in the table). In particular, the last two methods can find an immediate application to the signal enhancement of rare spins, embedded in a sample containing a more abundant spin species: these schemes require only collective control on the ensemble spins and the number of operations needed is moderate if the ratio of rare to abundant spins is large enough.

The methods and physical systems proposed open the possibility to a new class of devices, where quantum effects, such as entanglement, are used to make a transition from microscopic to macroscopic properties.

	Requisites on Control	**Control Operator**	**Q**	**C**
C-NOT Scheme	Addressability. Non-local interaction with target spin.	$E_T^+ \prod \sigma_x^k + E_T^-$	0	2
Entanglement with C-NOT	Addressability. Local interaction with target spin.	$E_T^+ \prod \sigma_x^k + E_T^-$	1	2
Entanglement with $\mathcal{H}_{GR}^{(n)}$	Collective control. Local interaction. Refocusing the map.	$E_T^+ \mathcal{A} + E_T^-$	1	≈ 1
Pseudo-Random Maps	Collective control. Local interaction.	$E_T^+ \tilde{\mathcal{A}} + E_T^-$	≈ 1	≈ 1

Table 5.1: **Comparison of the different schemes** for the single nuclear spin measurement.

Chapter 6

Simulations and Information Transport in Spin Chains

When a quantum mechanics based computer was first discussed by Feynman [51], its purpose was the simulation of physical problems that are not accessible even to the ever faster classical computers. In particular, physical phenomena that are inherently quantum are in general assumed to be amenable to an easier simulation on quantum computers [98]. Even if quantum simulation protocols are in practice not easy to define [106] and may not be possible for every application, the basic fact that the size of the computational resources in a quantum computer grows at the same pace as the problem to be simulated leaves open the hope for a practical quantum simulator, if one can efficiently use these resources.

Several models of simulations are possible, from a gate-based quantum computer [4, 7] to an adiabatic sweep toward the desired Hamiltonian, for the ground state calculation. A quantum-mechanical system that albeit not universal, could be used to simulate the dynamics under particular Hamiltonians, by tailoring its natural Hamiltonian with external control, would be very useful in condensed matter theory. It is this model that could be successfully implemented in the medium-short time period in solid state NMR-based QIP devices.

In this chapter we present a system, a single crystal of fluorapatite, that can be used to this purpose. We show how we can use the coherent and incoherent control to initialize the system to the desired state. This initial state, where the polarization is concentrated in single spins, instead of being distributed among all the spins in the linear chains that

constitute the crystal, is attractive for studying the transport of polarization and more generally of coherence and information along the chain. Transport of information [36, 78] is not only an important tasks in QIP but also an interesting physical phenomena in its own.

In many solid-state proposals for quantum computers, the transport of information over relatively short distances inside the quantum processor itself is an essential task, and one for which relying on photons, and therefore on a frequent exchanging of information between solid-state and light qubits could be too costly. *Quantum wires* based on spins could be a viable alternative.

Transport in complex many-body spin system has been widely studied as it manifests itself as spin diffusion [19, 66, 154]. This dynamics enhances the differences between classically solvable models (for nearest neighbors couplings in 1D) and the more complex dynamics obtained where all the couplings and higher dimensionality are taken into account [145, 21, 94, 109]. In this chapter we show how we can use the fluorapatite spin system and the signatures given by MQC experiments to explore these questions.

6.1 Selecting the spins at the extremities of the linear chain

An infinite linear chain of dipolarly coupled spin is an highly symmetric system; if the only control available is an external radio-frequency field that acts collectively on all the spins, this symmetry cannot be broken and therefore only a small subspace of the total Hilbert space can be reached by the system during its evolution. In particular, no state that breaks the symmetry of the initial state and of the Hamiltonian is reachable and thus a state with only one spin polarized cannot be reached from the equilibrium state.

If the spin chain is instead of finite length, the symmetry is naturally broken by the boundary conditions. The spins at the extremities of the chain only have one nearest neighbor to which they are strongly coupled. This implies a slight different energy and also a different dynamics under the internal dipolar hamiltonian with respect to the other spins. This evolution and the control Hamiltonians are still not enough for universal control, as it can be verified by calculating the rank of the Lie algebra generated by the internal and control Hamiltonian (this can be done numerically for small systems of 4-5 spins) [118]. Only adding non-unitary control (or more precisely and incoherent control [116]) will allow us to reach the desired state with a high enough fidelity.

The spin system is initially at equilibrium, in the thermal state. As stated in Section (4.1), this can be very well approximated by the state $\rho_0 = \sum_k \sigma_z^k$. Considering all separated chains as individual systems, we can rewrite:

$$\rho_0 = \sum_{m=1}^{M} \sum_{k_m=1}^{N_m} \sigma_z^{k_m}, \tag{6.1}$$

where the index m indicates a particular chain in the crystal. If we consider the short-time evolution only, the spins of different chains do not interact, so that we can consider M independent systems and in a first approximation, we will assume all of them to be equivalent. This can appear to be a system very similar to bulk liquid state NMR. The situation is however very different and the approximation made fails for two reasons. First, the chains do not have all the same length, thus exhibiting different dynamics, depending on the number of spins (moreover, the defects causing the interruption in the fluorine atom chain could be of different types, giving a different magnetic environment). The second important difference from liquid-state bulk NMR is that the couplings between two different chains are not averaged out by relative random motions, they are still present, only they are more than one order of magnitude smaller. Therefore, as soon as we let the system evolve for a time long enough compared to the cross-chain interactions, the approximation of independent systems fails. In order to simplify the analysis and the simulations, we will assume from here on that there is just one chain with a fixed number N of spins, which evolves unitarily under the dipolar hamiltonian and the external control rf field, and decoheres because of its interaction with the environment. The environment therefore includes also the effects of other chains and the distribution in chain composition.

We have studied a pulse sequence, that together with a non-unitary control, given by phase-cycling [29], prepares the initial state $\sigma_z^1 + \sigma_z^N$ starting from the thermal state. This simple pulse sequence (see Fig. (6-1)) relies on the fact that the spins at the chain ends have a different dynamics because of the broken symmetry in the couplings explained above.

The simplest way to observe this difference in the dynamics is to rotate the thermal equilibrium state to the transverse plane $\rho(t = 0^+) = \sum \sigma_x^i$, so that it is no longer an eigenstate of the internal hamiltonian. The following free evolution is the usual free induction decay (FID) measured in a simple $\pi/2-$pulse experiment. The evolution of the system to multi-spin coherences [35] is seen as an apparent decay of the magnetization. When we

look at the polarization of individual spins by numerical simulations of 8-10 spin systems, we notice oscillations in polarization of each one of them (see Fig. (6-2)). In particular the first and last spins have a much slower dynamics (apparent decay) at short time, which is due to the fewer number of couplings. It is thus possible to select a particular time at which while the state of these two spins is still mainly σ_x, all the other spins have evolved to more complex and even multi-body states. A second $\pi/2$ pulse will bring the magnetization of spins 1 and N to the longitudinal (z-)axis, so that the density matrix describing the system can be written as $\rho = \alpha(\sigma_z^1 + \sigma_z^N) + \rho'$ and we would like to select only the first two terms. To do this, we can recur to a phase cycling scheme, which will select only terms that commute with the total magnetization along z: $\sum_i \sigma_z^i$ (like the desired state). Unfortunately, we have not found a solution that also cancels out the zero-quantum terms (that is, components of the density matrix with total magnetic quantum number=0).

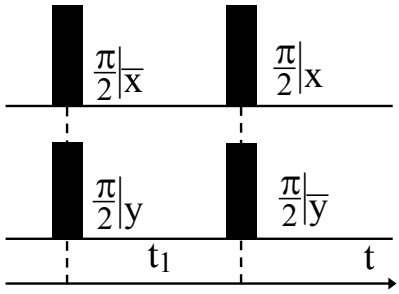

Figure 6-1: **Pulse Sequence** (with phase cycling) to select the two spins at the end of the spin chain

Fig. (6-2) shows the polarization along x of individual spins as a function of the evolution time under the dipolar Hamiltonian. From the commutator expansions of the unitary evolution, we can calculate the approximate coefficients of the polarization (σ_x^i) terms for each spin as a function of time and therefore select the time at which $\sigma_x^i \approx 0$, $\forall i \neq 1$. We found that the optimal time is given by $t_1 = 30.3\mu s$ for the dipolar coupling strength of fluorapatite spin chains. In selecting this time, we have taken into account that for the time considered the polarization of spins $i > 2$ are almost equal and that if the commutator expansion is carried out up to the 8^{th} order, the approximation for the times of interest is excellent.

The free evolution is interrupted at this moment, by a another $\pi/2$ pulse, now about the $-y$ axis. This will bring the remaining magnetization along the x axis back to the longitudinal axis, while the other spin states will mostly stay in the transverse plane or in

multi-spin states.

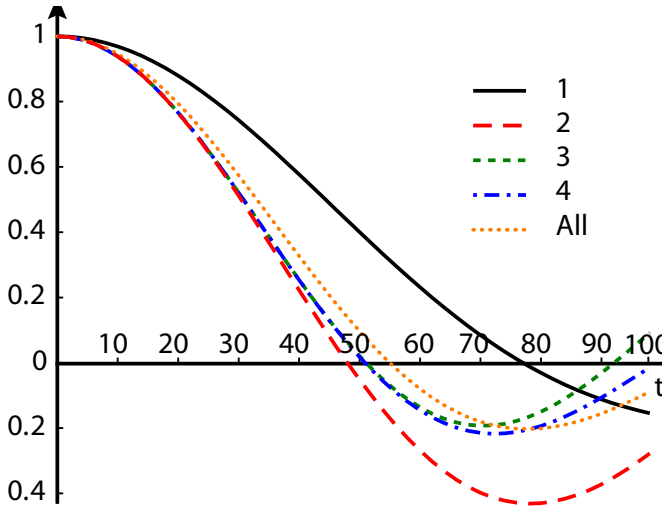

Figure 6-2: **Evolution under the dipolar Hamiltonian** after a one pulse excitation of the thermal equilibrium state to the transverse plane. Plotted are the amplitude of the polarization along the transverse plane for individual spins (8 spins, nearest neighbor dipolar coupling strength b=$\pi/2$). Notice how the evolution (an apparent decay of magnetization) of the first spin is much slower than for the other spins, due to the fact that it is strongly coupled to only another spin.

To select only the wanted terms, we cycle the pulses through different phases, thus averaging to zero all terms which are not either populations or zero quantum terms.

Except for very short chains (3-4 spins), the optimal time is almost independent of the number of spins in the chain, therefore allowing us to choose the time t_1 even not knowing the exact -average- number of spins in a chain. The important difference in the evolution of the very short chains is that the time is long enough for all the spins to start interacting, so that boundaries conditions in the evolution start to have an effect on the dynamics. If the Hilbert space is larger than the subspace that develops correlations during the time t_1 considered, the exact number of spins is instead unimportant.

6.2 Verifying the state preparation

Because of limitations in the detection of magnetic resonance that restrict the observables to the collective transverse magnetization, it is not possible to reconstruct the state of the system. While in liquid state NMR experiments involving a limited number of qubits it is

possible to carry out full state tomography [124] to determine the state of the system, when the Hilbert space is larger this is no longer practical. Notice also that even if we considered a Hilbert space comprised only of the chain of interest, which has a much smaller size than the entire Hilbert space, we do not know exactly its size and therefore it is not possible to devise a tomography procedure. Moreover, since we do not have universal control on the spin systems, we cannot apply the rotations required by tomography. In order to assess the efficiency of the state preparation scheme, we have to observe a subsequent evolution of the system that shows the signature of the particular initial state prepared.

Spectra

A first difference is then expected to be observed in the spectra recorded, since the dynamics under the dipolar Hamiltonian, after a $\pi/2$-pulse, (which is recorded in the FID) is different than for the equilibrium state. In particular, it is important to observe the state at short time, when the effects of the desired initial state should be stronger; the solid echo technique [58] was thus used, to avoid the dead time imposed by the electronics and the pulse ring-down [58]. While this kind of measurement does not give a definite answer to the question whether the polarization has been concentrated on the extremities only, the qualitative differences in the spectra measured are encouraging. In particular, we observe that resolution of the three peaks observed in the thermal state is much better (we obtain narrower lines) as expected from a state in which fewer couplings are available.

A more accurate insight into the state created can be obtained by studying more complex dynamics, depending on the initial state. In particular, a sensitive probe of the dynamics of a correlated many-spin system is the creation and evolution of multiple quantum coherences.

6.2.1 MQC dynamics

As seen in the introduction, grade raising Hamiltonians like the double-quantum Hamiltonian create very complex states of the spin systems, comprising coherent many-spin terms. This evolution is very difficult to analyze and predict, unless we restrict it to one-dimensional systems. In this case, the growth of coherence is slowed down by the fewer number of couplings among spins. If we further assume that only nearest-neighbor couplings are present, this limits the interaction of each spin to only two other spins, and the evolution under the double-quantum Hamiltonian turns out to be exactly solvable [50]. Experimentally, the

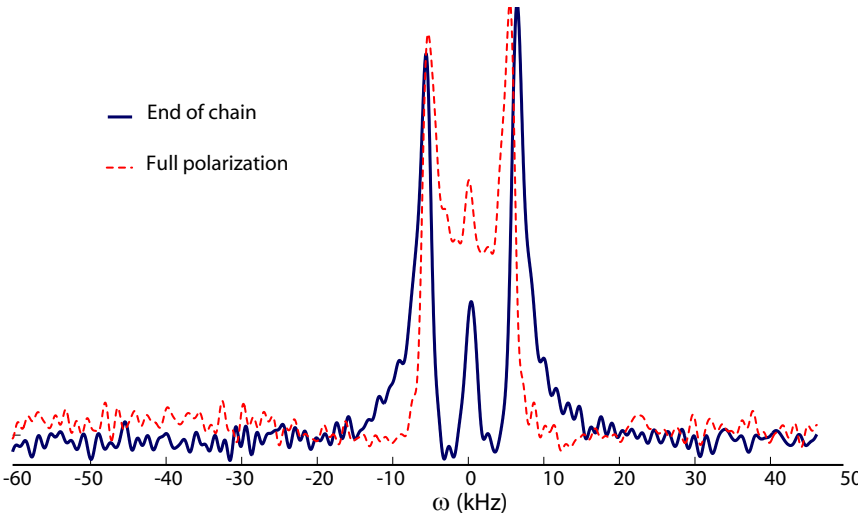

Figure 6-3: **Comparison of the spectra** when the polarization is retained by all spins in the chain (dashed line) and for the excitation of the extremities only (solid line). The FWHM is $\approx 19kHz$ and the distance between peaks $\approx 8kHz$. Experimental data for the sequence in Fig. (6-2) and a Solid Echo read-out, $t_1 = .5\mu s$ for full spin spectrum, $30.3\mu s$ for chain ends excitation.

nearest-neighbor approximation is accurate for short times, while for longer times, weaker couplings start to produce appreciable corrections.

The most important characteristic of 1-D MQC experiments are the oscillations between zero- and double-quantum coherences at short times. It is this restriction of the accessible Hilbert space (that is exact at any time in the nearest-neighbor approximation) that makes the problem tractable analytically. These oscillations are also a signature of the particular initial state chosen, so that we would like to study them to predict the differences in behavior that the initial state we prepare produces.

In the usual MQC experiment (see Section (4.2)), the initial condition is the thermal equilibrium state $\rho(0) = \sum_{j=1}^{N} \sigma_z^j$. We will compare the evolution of this state under the double-quantum Hamiltonian with the dynamics of the state in which only the two spins at the extremity of the chain are initially polarized: $\rho'(0) = \sigma_z^1 + \sigma_z^N$. We will first present an analytical result for the zero- and double-quantum intensities and then compare it to the experimental results. The analytical result is obtained by mapping the spin system to spinless fermion operators (see Appendix B):

$$c_j = -\prod_{k=1}^{j-1} \left(\sigma_z^k\right) \sigma_j^- \tag{6.2}$$

The diagonalization of the double-quantum Hamiltonian [50, 45] is accomplished by using the Fourier transform operators $a_k,\ a_k^\dagger$:

$$a_k = \sqrt{\frac{2}{N+1}} \sum_{j=1}^{N} \sin(kj) c_j \tag{6.3}$$

and the Bogoliubov [99] transformation:

$$\begin{cases} a_k = u_k d_k + v_k^* d_{-k}^\dagger \\ a_{-k} = -u_k d_k + v_{-k}^* d_k^\dagger \end{cases} \tag{6.4}$$

The Hamiltonian $\mathcal{H}_{DQ} = b \sum_{j=1}^{N} \sigma_j^+ \sigma_{j+1}^+ + \sigma_j^- \sigma_{j+1}^-$ is then diagonalized to:

$$\mathcal{H}_{DQ} = 2b \sum_k |\cos k| (d_k^\dagger d_k - \frac{1}{2}), \qquad k = \frac{\pi n}{N+1} \tag{6.5}$$

Initial States

We now express the two initial states considered in terms of Bogoliubov operators d_k. The thermal state has a particularly compact expression. Using the spin to fermion mapping and the Fourier transformed operators, we have

$$\rho(0) = \frac{1}{2} \sum_{j=1}^{N} \sigma_j^z = \sum_{j=1}^{N} \left(\frac{1}{2} - c_j^\dagger c_j \right) \tag{6.6a}$$

$$= \sum_{j=1}^{N} \left[\frac{1}{2} - \frac{2}{N+1} \sum_{k,h} \sin(kj) \sin(hj)\, a_k^\dagger a_h \right] = N \left(\frac{1}{2} - \frac{1}{N} \sum_k a_k^\dagger a_k \right) \tag{6.6b}$$

where we have used the orthogonality relationship (B.13) to simplify the sum.

Using the Bogoliubov transformations (B.22), we have

$$\begin{aligned} \rho(0) &= \tfrac{N}{2} \left[1 - \tfrac{1}{N} \textstyle\sum_k \left(d_k^\dagger d_k + d_{-k} d_{-k}^\dagger + \gamma_k (d_k^\dagger d_{-k}^\dagger + d_{-k} d_k) \right) \right] \\ &= \tfrac{1}{2} \textstyle\sum_k \gamma_k (d_k d_{-k} - d_k^\dagger d_{-k}^\dagger) \end{aligned} \tag{6.7}$$

Consider now the initial state $\rho'(0) = \frac{1}{2}(\sigma_1^z + \sigma_N^z)$. Because we are not summing over all spins, it is no longer possible to use the orthogonality relationships as in (6.6b). This

results in more cumbersome double sums.

$$\begin{aligned}
&\rho'(0) = \tfrac{1}{2}(\sigma_1^z + \sigma_N^z) = 1 - (c_1^\dagger c_1 + c_N^\dagger c_N) \\
&= 1 - \tfrac{2}{N+1} \textstyle\sum_{k,h} a_k^\dagger a_h (\sin(k)\sin(h) + \sin(Nk)\sin(Nh)) \\
&= 1 - \tfrac{2}{N+1} \textstyle\sum_{k,h} a_k^\dagger a_h \sin(k)\sin(h)(1 + \cos[Nk+k]\cos[Nh+h]),
\end{aligned} \tag{6.8}$$

where in the last line we have used the fact that $\sin(Nk) = -\sin k \cos((N+1)k)$. Applying the Bogoliubov transformation we finally obtain:

$$\begin{aligned}
\rho'(0) = 1 - \tfrac{1}{N+1} \textstyle\sum_{k,h} \quad & \sin k \sin h (1 + \cos[Nk+k]\cos[Nh+h]) \\
& \left(\gamma_k d_k^\dagger + d_{-k}\right)\left(\gamma_h d_h + d_{-h}^\dagger\right)
\end{aligned} \tag{6.9}$$

Evolution

The systems evolves under the double quantum hamiltonian with a dynamics described by the propagator $U(t) = \exp(2ib\sum_k |\cos k| d_k^\dagger d_k)$ (the term proportional to identity is dropped since it does not contribute to the evolution of the density matrix). Since the Bogoliubov operators diagonalize the double quantum hamiltonian, their evolution is easily found to be:

$$e^{-i\phi d_k^\dagger d_k} d_k e^{i\phi d_k^\dagger d_k} = e^{i\phi} d_k \tag{6.10}$$

We now define the eigenphases $\varphi_k = 2bt|\cos k|$ and note that $\varphi_k = \varphi_{-k}$ and to introduce a more compact notations we call $\gamma_k \equiv \frac{\cos k}{|\cos k|}$.

The thermal state evolution is easily calculated to be:

$$\rho(t) = \frac{1}{2} \sum_k \gamma_k \left(d_k d_{-k} e^{2i\varphi_k} - d_k^\dagger d_{-k}^\dagger e^{-2i\varphi_k}\right) \tag{6.11}$$

In order to separate contributions from different coherence orders, we must transform back to the fermion operators a_k. With some algebraic manipulations, we have

$$\rho(t) = \underbrace{-\sum_k \cos\varphi_k (a_k^\dagger a_k - \frac{1}{2})}_{\rho^{(0)}} \underbrace{- \frac{i}{2} \sum_k \gamma_k \sin\varphi_k (a_k^\dagger a_{-k}^\dagger + a_k a_{-k})}_{\rho^{(+2)} + \rho^{(-2)}} \tag{6.12}$$

The intensities of the n^{th} quantum coherence as measured in MQC experiment is given by $\mathrm{Tr}\left[\rho^{(n)}\rho(-n)\right]$. We evaluate the trace of the fermion operators a_k, $a_k^\dagger$ in their corre-

sponding occupational number representation, so that only terms like $a_k^\dagger a_k$ are diagonal and contribute to the trace. In particular we have:

$$\begin{aligned}
&\mathrm{Tr}\left[a_k^\dagger a_k^\dagger\right] = 2^{N-1} \\
&\mathrm{Tr}\left[a_h^\dagger a_h a_{k'}^\dagger a_{k'}\right] = \begin{cases} 2^{N-2} & \text{for } k \neq k'; \\ 2^{N-1} & \text{for } k = k'. \end{cases}
\end{aligned} \tag{6.13}$$

The normalized MQC intensities for zero and double quantum are finally given by[1]:

$$J_0 = \frac{1}{N}\sum_k \cos^2\left(4bt\cos k\right) \tag{6.14a}$$

$$J_2 = \frac{1}{2N}\sum_k \sin^2\left(4bt\cos k\right) \tag{6.14b}$$

The evolution of the polarization on the extremity of the chain is calculated from equations (6.9) and (6.10):

$$\begin{aligned}
&\rho'(t) = 1 - \tfrac{1}{N+1}\textstyle\sum_{k,h}\sin k \sin h(1+\cos\left[Nk+k\right]\cos\left[Nh+h\right]) \\
&\times\left(\gamma_k d_k^\dagger e^{-i\varphi_k} + d_{-k}e^{i\varphi_k}\right)\left(\gamma_h d_h e^{i\varphi_h} + d_{-h}^\dagger e^{-i\varphi_h}\right)
\end{aligned} \tag{6.15}$$

Again, we go back to fermion operators to distinguish contributions from different coherence orders:

$$\begin{aligned}
\rho'(t) \quad &= 1 - \tfrac{1/2}{N+1}\textstyle\sum_{k,h}\sin k \sin h(1+\cos\left[Nk+k\right]\cos\left[Nh+h\right]) \\
&\times\left[\gamma_k e^{-i\varphi_k}(\gamma_k a_k^\dagger + a_{-k}) + e^{i\varphi_k}(-\gamma_k a_{-k} + a_k^\dagger)\right] \\
&\times\left[\gamma_h e^{i\varphi_h}(\gamma_h a_h + a_{-h}^\dagger) + e^{-i\varphi_h}(-\gamma_h a_{-h}^\dagger + a_h)\right]
\end{aligned} \tag{6.16a}$$

$$\begin{aligned}
&= 1 - \tfrac{2}{N+1}\textstyle\sum_{k,h}\sin k \sin h(1+\cos\left[Nk+k\right]\cos\left[Nh+h\right]) \\
&\times\Big[(\cos\varphi_k\cos\varphi_h a_k^\dagger a_h + \gamma_k\gamma_h\sin\varphi_k\sin\varphi_h a_h a_k^\dagger) \\
&+i\gamma_k\sin\varphi_k\cos\varphi_h(a_h^\dagger a_{-k}^\dagger - a_{-k}a_h)\Big]
\end{aligned} \tag{6.16b}$$

As it was to be expected, also starting from the non collective initial state, only zero and double quantum coherences are developed, if one only takes into account nearest neighbor couplings. The following identities for the trace of fermion operators are useful to calculate

[1]Notice the discrepancy with the result in [50] which is due to incorrect boundary conditions

the zero- and double-quantum intensities for this initial state:

$$\mathrm{Tr}\left[a_h^\dagger a_{-k}^\dagger a_{-k'} a_{h'}\right] = \begin{cases} 2^{N-2} & \text{for } k = k', h = h'; \\ -2^{N-2} & \text{for } k = -h', h = -k'; \\ 0 & \text{otherwise} \end{cases} \tag{6.17}$$

The zero quantum contribution to the signal is $J_0^{\mathsf{e}} = \mathrm{Tr}\left[\rho_{(0)}^2\right]$, with

$$\begin{aligned} \rho_{(0)} = 1 - \tfrac{2}{N+1} \textstyle\sum_{k,h} \quad & \sin k \sin h (1 + \cos[Nk + k] \cos[Nh + h]) \\ & \times (\cos\varphi_k \cos\varphi_h a_k^\dagger a_h + \gamma_k \gamma_h \sin\varphi_k \sin\varphi_h a_h a_k^\dagger) \end{aligned} \tag{6.18}$$

Using Eq. (6.17), we can evaluate the trace $\mathrm{Tr}\left[\rho_{(0)}^2\right]$:

$$\begin{aligned} J_0^{\mathsf{e}} \quad & = 2^N - \tfrac{4}{(N+1)} \textstyle\sum_{k,h} \sin k \sin h (1 + \cos[Nk + k] \cos[Nh + h]) \\ & \times (\cos\varphi_k \cos\varphi_h \mathrm{Tr}\left[a_k^\dagger a_h\right] + \gamma_k \gamma_h \sin\varphi_k \sin\varphi_h \mathrm{Tr}\left[a_h a_k^\dagger\right]) \\ & + \tfrac{4}{(N+1)^2} \textstyle\sum_{\substack{k,h \\ k',h'}} \sin k \sin h \sin k' \sin h' \\ & \times (1 + \cos[Nk + k] \cos[Nh + h])(1 + \cos[Nk' + k'] \cos[Nh' + h']) \\ & \times \Big(\mathrm{Tr}\left[a_k^\dagger a_h a_{k'}^\dagger a_{h'}\right] \cos\varphi_k \cos\varphi_h \cos\varphi_{k'} \cos\varphi_{h'} + \\ & \mathrm{Tr}\left[a_h a_k^\dagger a_{h'} a_{k'}^\dagger\right] \gamma_k \gamma_h \gamma_{k'} \gamma_{h'} \sin\varphi_k \sin\varphi_h \sin\varphi_{k'} \sin\varphi_{h'} + \\ & \mathrm{Tr}\left[a_h a_k^\dagger a_{k'}^\dagger a_{h'}\right] \gamma_k \gamma_h \sin\varphi_k \sin\varphi_h \cos\varphi_{k'} \cos\varphi_{h'} + \\ & \mathrm{Tr}\left[a_k^\dagger a_h a_{h'} a_{k'}^\dagger\right] \gamma_{k'} \gamma_{h'} \cos\varphi_k \cos\varphi_h \sin\varphi_{k'} \sin\varphi_{h'} \Big) \end{aligned} \tag{6.19}$$

obtaining the following expression:

$$\begin{aligned} & = 2^N - 2^{N-1} \tfrac{4}{(N+1)} \textstyle\sum_{k,h} \sin k^2 (1 + \cos[Nk + k]^2)(\cos{\varphi_k}^2 + \gamma_k^2 \sin{\varphi_k}^2) + \\ & 2^{N-2} \tfrac{4}{(N+1)^2} \textstyle\sum_{k,h} \sin k^2 \sin h^2 (1 + \cos[Nk + k] \cos[Nh + h])^2 \\ & \times \left[\cos{\varphi_k}^2 \cos{\varphi_h}^2 + \sin{\varphi_k}^2 \sin{\varphi_h}^2 - \gamma_k \gamma_h \sin\varphi_k \cos\varphi_k \sin\varphi_h \cos\varphi_h\right] \end{aligned} \tag{6.20}$$

where $\psi_k = 2bt \cos k$, and we note that $\gamma_k \sin\varphi_k = \sin\psi_k$.

Finally, the normalized zero-quantum intensity is given by:

$$J_0^{\mathsf{e}} = \frac{4}{(N+1)^2} \sum_{k,h} \sin k^2 \sin h^2 (1 + \cos[Nk + k] \cos[Nh + h]) \cos(\psi_k + \psi_h)^2 \tag{6.21}$$

The double quantum intensity is given by $J_2^{\mathsf{e}} = \mathrm{Tr}\left[\rho_{(2)} \rho_{(-2)}\right]$, where the $\pm 2-$quantum

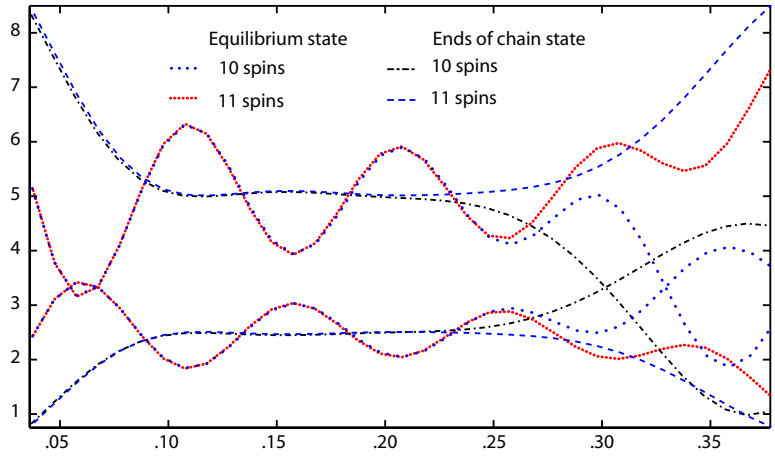

Figure 6-4: **Zero- and double-quantum intensities** as a function of the evolution time under the double-quantum Hamiltonian. Nearest-neighbor couplings only are assumed, with equal strength as given by the fitting to experimental data (see Fig. (6-6)). In particular notice the clear differences in the behavior for the two initial states. Also the even-odd spin number dependence of the MQC intensities is interesting: while this tends to go to zero for large number of spins in the collective initial state case, this difference is observed even for very large number of spins for the other initial state.

coherences are:

$$\rho'_{(2)}(t) = \tfrac{-2i}{N+1} \textstyle\sum_{k,h} \sin k \sin h \quad (1 + \cos[Nk + k] \cos[Nh + h]) \times \gamma_k \sin \varphi_k \cos \varphi_h \, a_h^\dagger a_{-k}^\dagger \tag{6.22a}$$

$$\rho'_{(-2)}(t) = \tfrac{2i}{N+1} \textstyle\sum_{k,h} \sin k \sin h \quad (1 + \cos[Nk + k] \cos[Nh + h]) \times \gamma_k \sin \varphi_k \cos \varphi_h \, a_{-k} a_h \tag{6.22b}$$

Inserting the expression for the trace of fermion operators (6.17) in (6.23),

$$\begin{aligned} J_2^{\mathsf{e}} = & \frac{4}{(N+1)^2} \sum_{\substack{k,h \\ k',h'}} \sin k \sin h \sin k' \sin h' \\ & \times (1 + \cos[Nk + k] \cos[Nh + h])(1 + \cos[Nk' + k'] \cos[Nh' + h']) \\ & \times \sin \psi_k \cos \psi_h \sin \psi_{k'} \cos \psi_{h'} \mathrm{Tr}\left[a_h^\dagger a_{-k}^\dagger a_{-k'} a_{h'}\right], \end{aligned} \tag{6.23}$$

we obtain the final expression for the double quantum intensity evolution:

$$J_2^{\mathsf{e}} = \tfrac{2}{(N+1)^2} \textstyle\sum_{k,h} \sin k^2 \sin h^2 (1 + \cos[Nk + k] \cos[Nh + h])^2 \sin(\psi_k + \psi_h)^2 \tag{6.24}$$

This more complex expression leads to a very different behavior of the coherence inten-

sities as shown in Fig. (6-4), so that it is possible to distinguish even experimentally what was the initial condition of the system.

6.3 Experiment

We performed the experiment on a 300MHz Bruker Avance Spectrometer, with an home built probe tuned to 282.4MHz for the observation of Fluorine. The sample was a single crystal of fluorapatite (Section (4.2)) provided by Prof. Ian Fisher, with a measured $T_1 \approx 200s$ (this is a sign of low impurity concentrations).

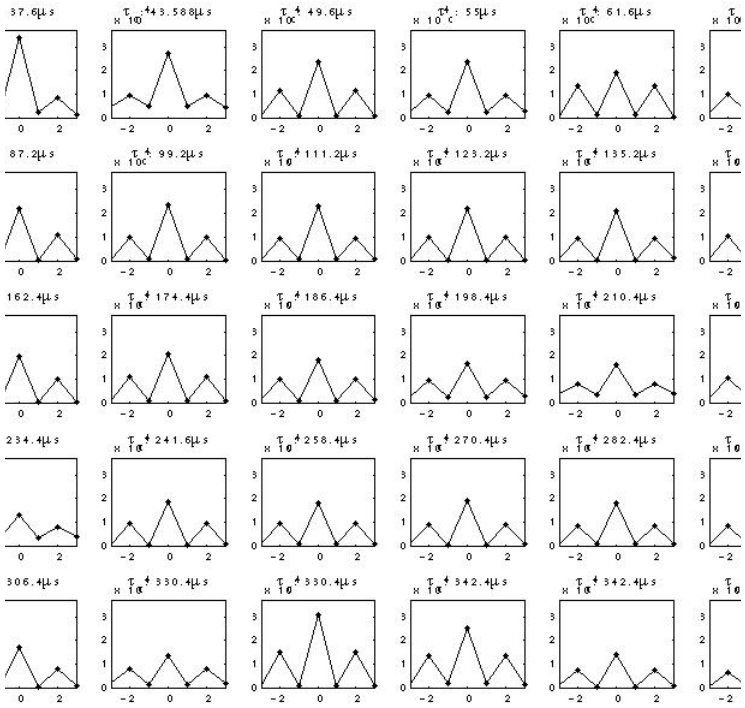

Figure 6-5: **MQC intensities spectra**, for the initial state $\rho_0 = \sigma_z^1 + \sigma_z^N$ and varying evolution time under the 8- and 16-pulse sequence for the creation of the double-quantum Hamiltonian.

We applied the pulse sequence as in Fig. (6-1) followed by a MQC-experiment sequence. In particular, we used the 16-pulse sequence (except for the 3 shorter time-values, where

the 8-pulse sequence was used) to excite the spins, and a phase cycling with increments of $\varphi = 2\pi/8$ to select up to the 4^{th} coherence order, by repeating the experiment 16 times. The time delay between pulses in the MQC sequence was varied from $2\mu s$ to $6.5\mu s$, to increase the excitation time, as well as the number of repetition of the sequence itself (1 or 2 loops). The evolution of the quantum coherences were studied between the times of $37.6\mu s$ to $354.4\mu s$. We compare the results obtained with the evolution for the thermal equilibrium as initial state. In order to take into account the effects of imperfections in the pulse sequence, we applied the pulse sequence as in Fig. (6-1) also to obtain the thermal state, with a very short t_1 time ($t_1 = 0.5\mu s$). The spectra of the MQC intensities are shown in Fig. (6-5) while in figure (6-6) we show the dynamics of the zero and double quantum intensities, normalized to have sum = 1 to take into account the signal decay for longer excitation times. We notice that the four-quantum coherence intensity is as low as the baseline, indicating that the time scale is short enough for the nearest-neighbor approximation to be valid (remember that the nearest-neighbor approximation predicts that only zero- and double-quantum coherences are created).

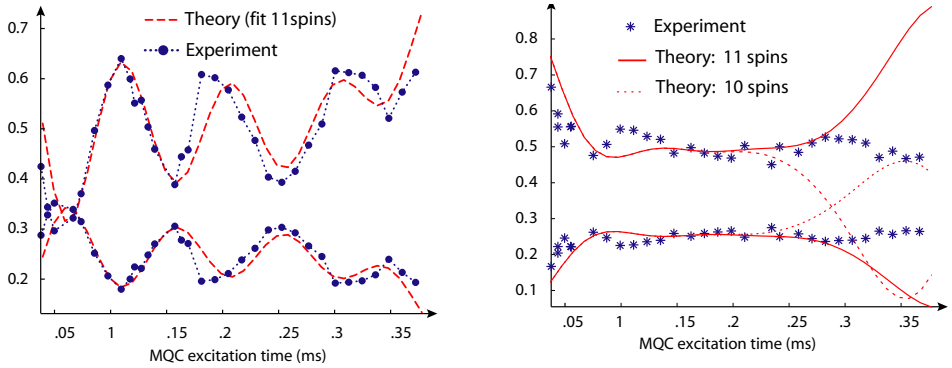

Figure 6-6: **Experimental results.** Left: the initial state is the collective thermal state $\sum_k \sigma_z^k$. The experimental points have been fitted (dashed line) to the theoretical curves for nearest neighbor coupling only, with the dipolar coupling as fitting parameter. The number of spins was varied to find the best fit, which results to be $N = 11$ spins. Right: MQC intensities for the initial state $\rho_0 = \sigma_z^1 + \sigma_z^N$. Also plotted are the theory predictions for the same dipolar coupling and 11 spins (solid line) or 10 spins (dashed line). A mixture of chain lengths, with odd and even number of spins can justify the experimental behavior observed (a constant behavior also for longer time) This behavior is also compatible with the presence of longer chains.

The experimental results for the MQC oscillations starting from the thermal state have been fitted to the theoretical curve, with the dipolar strength and the number of spin as fitting parameters. An average number of a 11-12 spins is predicted. The concordance

with the theoretical predictions is very good, even if the state created contains residual zero-quantum terms. The behavior at longer times for the end of chain state indicates that a distribution of chains of different lengths is present.

6.4 Applications

Transport of Zeeman and dipolar energy in spin systems, caused by energy conserving spin flips, has been the object of much interest, both in the past [13] and in more recent years [154, 19]. The free-evolution transport appears as a gaussian decay, signature of a diffusive behavior, even if it is driven by a unitary evolution that can be experimentally refocused by acting on the system with specific rf pulse sequences [143, 18], which enable the observation of polarization echoes [94, 53]. Experiments using pulse-gradient NMR techniques have been conducted on time scales shorter than the spin-lattice relaxation time, T_1, to measure the diffusion constants. Even if these experiments explore the coherent regime of the spin-dynamics, they still show that the non-conservation of the spatial degrees of freedom of individual spins leads to a phenomenological diffusive behavior. The contradiction between the unitary evolution and the observed irreversible dynamics can be qualitatively explained only by the complexity of the quantum evolution: The many-body dynamics cannot be fully captured by the simple measurements performed on the spin system that trace over much of the information contained in the many-body system.

Various models have been proposed to describe the so-called *spin diffusion*, from classical simulations [126] and hydrodynamics approach [66] to exact solutions taking into account only the part of the dipolar Hamiltonian responsible for the spin flips [65]. This last approach provides an analytical solution in 1D, which however does not agree with the long time behavior of spin diffusion. It is anyway interesting to compare diffusion constants given by experiments of spin diffusion and the time-scale of the transport given by this analytical solution. Transport given by spin-flips only is interesting in its own, since, contrary to spin diffusion, where even for small number of spins the polarization is never transfered to the last spin in an appreciable amount [145, 21], spin-flips allow the transport of information along a 1D chain. Even if this transfer is perfect only for 3 spins [36], a considerable amount of polarization is still transported over longer distances, and the simple free transport can be taken as a zeroth order approximation to more complex schemes for better transport

[78], involving external manipulation of the spin system.

Unfortunately, given the dipolar Hamiltonian (4.2) it is impossible with collective control to break its symmetry and obtain only the spin-flip part of it (the so-called *flip-flop* Hamiltonian). When one restricts the interaction to nearest-neighbor couplings only, this dynamics can however be simulated by the double-quantum Hamiltonian, which behaves in the same way up to a similarity transformation given by the Bogoliubov transformation .

Consider the flip-flop Hamiltonian :

$$\mathcal{H}_{\mathsf{ff}} = \sum_{ij} b_{ij}(\sigma_x^i\sigma_x^j + \sigma_y^i\sigma_y^j) = \sum_{ij} b_{ij}(\sigma_+^i\sigma_-^j + \sigma_-^i\sigma_+^j) \tag{6.25}$$

In the limit of nearest-neighbor couplings only this can be expressed in terms of fermion operators and diagonalized easily:

$$\mathcal{H}_{\mathsf{ff}} = b\sum_j (c_j^\dagger c_{j+1} + c_j c_{j+1}^\dagger) = 2b\sum_k \cos(k)\, a_k^\dagger a_k \tag{6.26}$$

This expression is similar to the double-quantum Hamiltonian (6.5) seen previously, except that there we had to perform a further transformation to Bogoliubov operators to diagonalize the Hamiltonian. This similarity in turn is reflected in the polarization dynamics, even if it is important to mention that the dynamics is quite different with respect to coherences, since the flip-flop Hamiltonian conserves the coherence order (so that the state is always in the zero-quantum coherence manifold) while the double-quantum Hamiltonian can create the double-quantum coherence order (and for couplings among all the spins it creates all the even coherences, while the flip-flop Hamiltonian is still restricted to the zero-quantum subspace only). Assuming that the polarization resides initially on just one spin, spin a, the initial state is:

$$\rho_a(0) = \frac{\mathbb{1}}{2} - \frac{2}{N+1}\sum_{k,h} \sin(ka)\sin(ha)\, a_k^\dagger a_h \tag{6.27}$$

which evolves under (6.26) as:

$$\rho_a^{\mathsf{ff}}(t) = \frac{\mathbb{1}}{2} - \frac{2}{N+1}\sum_{k,h} \sin(ka)\sin(ha)\, e^{-2ib(\cos k - \cos h)t} a_k^\dagger a_h \tag{6.28}$$

At a time t, the polarization transfered to another spin b is given by $\mathrm{Tr}\left[\rho_a^{\mathsf{ff}}(t)\sigma_z^b\right]$, that is:

$$P_{ab}^{\mathsf{ff}}(t) = \frac{4}{(N+1)^2}\Big|\sum_k \sin(ka)\sin(kb)e^{-2ibt\cos k}\Big|^2 \tag{6.29}$$

With calculations similar to the one performed in Section (6.2.1), we can also compute $\rho_a^{\mathsf{dq}}(t)$, that is, the state evolution under the double-quantum Hamiltonian, starting with the polarization on just the spin a:

$$\begin{aligned}\rho_a^{\mathsf{dq}}(t) = \tfrac{\mathbb{1}}{2} - \tfrac{2}{N+1}\textstyle\sum_{k,h} \quad & \Big[(\cos\psi_k\cos\psi_h\, a_k^\dagger a_h + \sin\psi_k\sin\psi_h\, a_h a_k^\dagger) \\ & +i\sin\psi_k\cos\psi_h(a_h^\dagger a_{-k}^\dagger - a_{-k}a_h)\Big]\sin(ka)\sin(ha)\end{aligned} \tag{6.30}$$

and thus the polarization that is transfered to the b spin at the time t by $\mathcal{H}_{DQ}$:

$$P_{ab}^{\mathsf{dq}}(t) = \frac{4}{(N+1)^2}\mathrm{Re}\left[\left(\sum_k \sin(ka)\sin(kb)e^{-2ibt\cos k}\right)^2\right], \tag{6.31}$$

where Re[.] is the real part of a complex number. Notice that these two very similar expressions for the polarization transfer driven by the flip-flop and double-quantum Hamiltonian yield the same result if the number of spins in the chain is odd, while the double quantum Hamiltonian can transfer negative polarization (since it does not conserve the total polarization along the z direction) to spins b, see Fig. (6-7). If we take the absolute value of the polarization, the two Hamiltonians produce the same transport of polarization and therefore the double-quantum Hamiltonian can be used to simulate the flip-flop Hamiltonian that is not available in the system.

The transport of polarization cannot be detected directly (unless one introduces very strong magnetic field gradients, able to produce an appreciable change of frequency over distances of some tens of angstroms). It is however possible to monitor the MQC intensities to detect the occurred transfer of polarization.

The zero- and double-quantum (normalized) intensities for an initial state with only

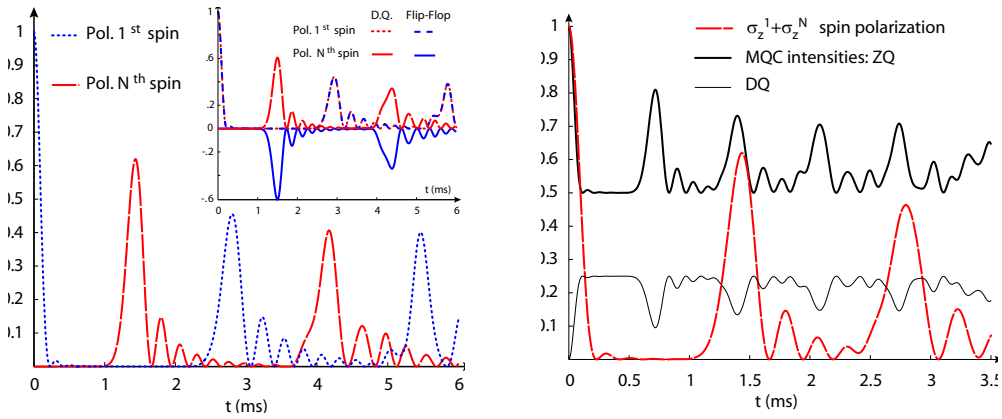

Figure 6-7: Left: **Polarization transfer** from spin one to spin N for a chain of 21 spins with nearest-neighbor coupling only, dipolar coupling strength as in the FAP chain. Right: here we compare MQC intensities and polarization transfer in a 21-spin chain. The initial state was the one we can prepare experimentally, $\rho_0 = \sigma_z^1 + \sigma_z^N$.

spin a polarized are given by:

$$J_0^a = \frac{2}{(N+1)^2} \sum_{k,h} \sin(ka)^2 \sin(ah)^2 \cos(\psi_k + \psi_h)^2 \tag{6.32a}$$

$$J_2^a = \frac{4}{(N+1)^2} \sum_{k,h} \sin(ka)^2 \sin(ha)^2 \sin(\psi_k + \psi_h)^2 \tag{6.32b}$$

as obtained with calculations similar to the ones shown in Section (6.2.1).

These intensities present a beating every time the polarization reaches spin $(\{N, a\} \oplus N)$. These beatings are particularly clear for the transfer from spin 1 to spin N, although they would exist for the magnetization starting at any spin in the chain. If one is therefore interested in the transfer of polarization from one end of the chain to the other it is possible to follow this transfer driven by the double-quantum Hamiltonian by measuring the MQC intensities, which, contrary to the polarization of a single spin, are detectable.

In Fig. (6-7) we show how this transport and detection method would look like in our experimental set-up, where the initial state is $\rho_0 = \sigma_z^1 + \sigma_z^N$. The beatings of the MQC intensities is now faster than the transfer of polarization, since the polarization starts spreading out from the two opposite ends of the chain and creates an extremum in the MQC intensity also when the two waves meet at the center of the chain. This interference can happen with a positive or negative phase, depending on the number (odd or even respectively) of spins in the chain. Every two beatings, however, the maximum of the zero-quantum intensity correspond to the transport of polarization from one end to the other

one.

It will be interesting to investigate the differences between the predicted rate of transport and the experimental one, to observe the effects of the real couplings on the spin dynamics. Next-nearest neighbor couplings and cross-chain couplings offer additional pathways that can result in an acceleration of information transport, which has no classical counterpart. This transition from a behavior that can be simulated classically to the more complex quantum behavior is of tantamount importance in the context of QIP, where the efficiency of a quantum computation is brought by the coherence and interference effects proper of quantum mechanics.

6.4.1 Estimate of the chain length

When the evolution of the system is restricted to the zero- and double-quantum manifolds because of the dimensionality of the system and the restriction to nearest-neighbor couplings only, the double-quantum Hamiltonian, that in 3D systems soon creates high coherence states, mainly acts to transfer polarization and coherence along the chain. The observed MQC intensity evolution thus depends critically on the chain length, even if the initial state is the thermal state. In this case, the oscillations of the MQC intensities tend toward a common behavior as $N \to \infty$, described by Bessel functions [50]):

$$\begin{aligned} J_0(t) &= \tfrac{1}{2}(1 + \mathcal{J}_0(8bt)) \\ J_2(t) &= \tfrac{1}{4}(1 - \mathcal{J}_0(8bt)) \end{aligned} \tag{6.33}$$

where $\mathcal{J}_0(x)$ is the Bessel function of the first kind of order 0.

On the other side, for shorter chains, when the perturbation created by the double-quantum Hamiltonian involves all the Hilbert space, the well-behaved oscillation break down, and a more erratic behavior is observed, given by interferences among different parts of the Hilbert space.

If only one spin is initially polarized, as explained previously, beatings are observed each time the polarization is transported from one extremity of the chain to the other. These features would be more clearly observable than the behavior of the thermal state (this remains true even if there are two spins initially polarized at the opposite ends of the chain as in our experimental situation). The time at which the MQC intensities present an

extremum is directly proportional to the number of spins in the chain[2] (for chain lengths $N \geq 5-6$), and it is found numerically to be given by: $t^* = 0.3956 + 0.266N$.

The state created by the sequence in Section (6.1) is therefore a useful tool to estimate the average chain length in the crystal of fluorapatite. Since the first extremum of the zero-quantum intensity is positive (negative) for odd (even) number of spins, if there is a distribution of chain lengths as expected in practice, the extremum would not be visible, since it would be averaged out. We have thus to detect the second extremum which is always a maximum. Experimentally, this poses a challenge since the evolution time under the double-quantum Hamiltonian could be quite long and effects of non-nearest neighbor couplings and, even worse, cross-chain couplings become important. Further studies on how to reduce these problems are thus necessary.

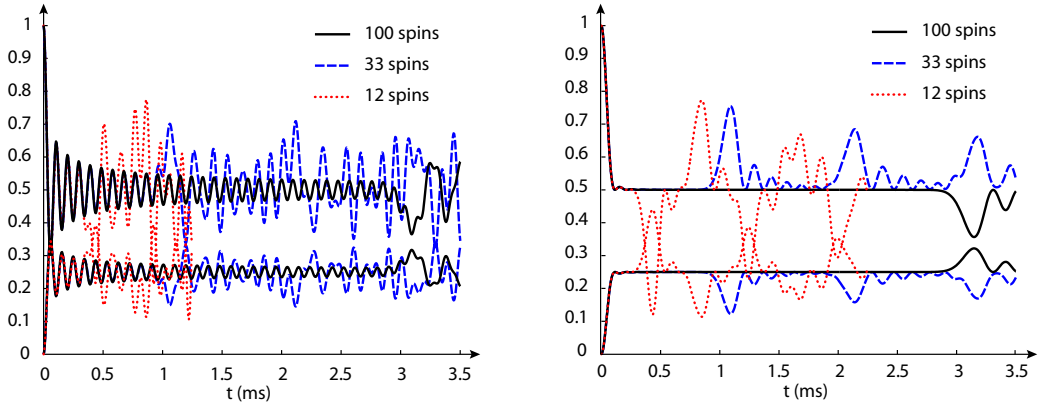

Figure 6-8: **MQC intensities for increasing number of spins in the chain**, with initial state in the thermal state (left) and with only the two spin at the extremity of the chain polarized (right). Notice how in this last case the extrema of the MQC intensities are pushed out in time with increasing number of spins. Also notice the different behavior for even and odd number of spins.

6.5 Conclusions

In this chapter we have studied a physical system, linear chains of spins in a single crystal of FAP, that can be used for quantum information processing tasks. Since the physical characteristics of the system and the experimental apparatus do not provide universal control on the quantum spin system, we propose to use this system not as a candidate quantum

[2]Notice that there is a small difference in the time of polarization transfer and MQC beating, but they are both directly proportional to the number of spins in the chain.

computer, but as a specific task-oriented QIP device. In particular, we have proposed a scheme, combining unitary and non-unitary control, for creating a particular state that breaks the natural symmetry of the system. The preparation of this state is the first step toward universal control on the system, since if we could add the control over one single spin to the collective control over all the other spins, universality could be obtained.

We have furthermore investigated a tool for acquiring a deeper knowledge of the state and dynamics of the system, given the limitations in the read-out procedures. Multiple quantum coherences allow us to gather more information on the multi-body aspects of the system than simple direct observation of the collective polarization. In particular, we used analytical solutions in the limit of nearest-neighbor couplings to interpret the experimental results which confirm the preparation of the desired state.

Finally, we proposed two applications of the state initialization and the MQC tools we developed. We showed the transport of polarization along the chain given by the flip-flop Hamiltonian and we proposed to study this transport experimentally by simulating it via the double-quantum Hamiltonian with the detection made possible thanks to the relation between the transfer to the opposite end of the chain and beatings (given by interferences) of the MQC intensities. These beatings could also in principle allow one to estimate the chain length, since they occur at a rate which is proportional to the chain length.

In conclusion, we have shown how even a quantum system without universal control can be used to study many physical problems of interest in condensed matter theory and quantum information science.

Appendix A

A.1 Average Hamiltonian Theory

The time evolution of the density matrix is expressed by the Liouville equation:

$$i\hbar\dot{\rho} = [\rho, \mathcal{H}] \tag{A.1}$$

which can be easily derived from the evolution of vector states described by Schrödinger equation. If the Hamiltonian $\mathcal{H}$ were time-independent, the solution of this equation would simply be:

$$\rho(t) = U\rho(0)U^{\dagger} \tag{A.2}$$

where the propagator U is given by

$$U = e^{-i\mathcal{H}t} \tag{A.3}$$

(we set $\hbar = 1$). When $\mathcal{H}$ is time dependent and $\mathcal{H}(t)$ does not commute at different time, it is no longer possible to find an explicit expression in this way, since in general:

$$e^A e^B \neq e^{A+B} \quad if \quad [A, B] \neq 0 \tag{A.4}$$

The propagator U, even for a time dependent Hamiltonian, satisfies the equation:

$$i\frac{dU}{dt} = \mathcal{H}U \tag{A.5}$$

Formal solutions [61] can be obtained in terms of the Dyson time-ordering operator:

$$U = Te^{\int_0^t -iH(t')dt'} \tag{A.6}$$

or using the Magnus expansion:

$$U = \exp\{-it[\bar{\mathcal{H}}^{(0)} + \bar{\mathcal{H}}^{(1)} + \bar{\mathcal{H}}^{(2)} + \ldots]\} \tag{A.7}$$

where the lowest order terms are:

$$\begin{aligned}
&\bar{\mathcal{H}}^{(0)} = \tfrac{1}{t}\int_0^t \mathcal{H}(t_1)dt_1 \\
&\bar{\mathcal{H}}^{(1)} = -\tfrac{i}{2t}\int_0^t dt_1[\mathcal{H}(t_1), \int_0^{t_1} dt_2\mathcal{H}(t_2)] \\
&\bar{\mathcal{H}}^{(2)} = \tfrac{1}{6t}\int_0^t dt_1 \int_0^{t_1} dt_2 \int_0^{t_2} dt_3 \times \\
&\{[[\mathcal{H}(t_1), \mathcal{H}(t_2)], \mathcal{H}(t_3)] + [[\mathcal{H}(t_3), \mathcal{H}(t_2)], \mathcal{H}(t_1)]\}
\end{aligned} \tag{A.8}$$

Usually the Hamiltonian of the system is composed by different terms, some of which do not contribute to the interesting dynamics of the system. To remove them, we can make a transformation to an interaction frame. For example in NMR, it is usual to remove the large contribution given by the Zeeman Hamiltonian (which is time independent), since experiments are also normally observed in what is called the rotating frame, given by the Larmor frequency of the spins. If the overall Hamiltonian of the system can be written as $\mathcal{H} = \mathcal{H}_0 + \mathcal{H}_{int} + \mathcal{H}_{\mathsf{rf}}$ (where we separated the Zeeman Hamiltonian $\mathcal{H}_0 = \omega_L \sum_k \sigma_z^k$ from the remaining internal Hamiltonian (1.1)), the transformation to the rotating frame is operated by the propagator $U = e^{-i\mathcal{H}_0 t}$.

The evolution of the density matrix in the rotating frame $\tilde{\rho} = U^\dagger \rho U$, is then:

$$\begin{aligned}
&i\dot{\tilde{\rho}} = i\dot{U^\dagger}\rho U + iU^\dagger\dot{\rho}U + iU^\dagger\rho\dot{U} = \\
&-\mathcal{H}_0 U^\dagger\rho U + U^\dagger[\mathcal{H},\rho]U + U^\dagger\rho U\mathcal{H}_0 = -[\mathcal{H}_0,\tilde{\rho}] + [U^\dagger H U,\tilde{\rho}] \\
&= [\tilde{\mathcal{H}},\tilde{\rho}]
\end{aligned} \tag{A.9}$$

where $\tilde{\mathcal{H}} = U^\dagger(\mathcal{H}_{int} + \mathcal{H}_{\mathsf{rf}})U$. In the same way, we can "jump" to another interaction frame defined by the rf Hamiltonian, and follow only the evolution of the system under its own internal Hamiltonian. This frame is called *toggling frame*. In this case, since $\mathcal{H}_{\mathsf{rf}}$ is not time-independent, the frame transformation is given by the operator U_{rf} satisfying:

$$i\frac{dU_{\mathsf{rf}}}{dt} = \mathcal{H}_{\mathsf{rf}}U_{\mathsf{rf}} \tag{A.10}$$

(where from now on we do not explicitly use any notation for the rotating frame).

The Liouville equation for the density matrix in the toggling frame is given by an equation similar to A.9:

$$i\frac{d\tilde{\rho}}{dt} = [\tilde{\mathcal{H}_{int}}, \tilde{\rho}], \tag{A.11}$$

with $\tilde{\mathcal{H}_{int}} = U_{\mathsf{rf}}^{\dagger}\mathcal{H}_{int}U_{\mathsf{rf}}$, and the time evolution is given by:

$$\tilde{\rho}(t) = U_{int}\rho(0)U_{int}^{\dagger}, \tag{A.12}$$

where U_{int} is given by the Dyson expression: $U_{int} = Te^{-i\int_0^t \tilde{\mathcal{H}}_{int}(t')dt'}$ or the Magnus expression: $U_{int} = e^{-it[\tilde{\mathcal{H}}_{int}^{(0)}+\tilde{\mathcal{H}}_{int}^{(1)}+\ldots]}$.

Average Hamiltonian Theory (AHT) is the theory that studies the simplifications produced on these last equation by using a cyclic and periodic rf-Hamiltonian. If these conditions are met, the expansion giving the propagator converges fast and one needs to evaluate only the lower terms [68],[115].

The requirements for the application of Average Hamiltonian Theory are that the sequence should be:

- **periodic**: $\mathcal{H}_{\mathsf{rf}}(t+Nt_c) = \mathcal{H}_{\mathsf{rf}}(t)$ (for a cycle time t_c, the sequence is repeated N times)
- **cyclic**: $U_{\mathsf{rf}}(t_c) = \pm 1$ (i.e. after a cycle the system is brought back to its initial state)

When both the two conditions are met we have $U_{\mathsf{rf}}(Nt_c) = 1$. In this case, the internal Hamiltonian propagator in the toggling frame has the nice property:

$$U_{int}(nt_c, 0) = U_{int}(nt_c, (n-1)t_c)\cdots U_{int}(2t_c, t_c)U_{int}(t_c, 0) = U_{int}^{n}(t_c, 0) \tag{A.13}$$

(where the notation $U(t_2, t_1)$ means the propagator from time t_1 to time t_2). This equivalence holds because $\tilde{\mathcal{H}}_{int}$ has acquired the same periodicity as U_{rf}.

We define $\bar{\mathcal{H}} = \sum_k \tilde{\mathcal{H}}_{int}^{(k)}$, the effective Hamiltonian given by the Magnus expansion in the time interval $0 - t_c$. If now we only look at the density matrix in observation windows given by $t = Nt_c$, the evolution is given by:

$$\tilde{\rho}(Nt_c) = e^{-iNt_c\bar{\mathcal{H}}}\rho(0)e^{iNt_c\bar{\mathcal{H}}} \tag{A.14}$$

which is equivalent to the evolution under an effective time-independent Hamiltonian. If furthermore $t_c|\tilde{\mathcal{H}}_{int}| \approx t_c\omega_{int} \ll 1$, the Magnus expansion will converge fast, even if the

actual experiment is "long" (i.e. is repeated many time) in order to obtain an overall appreciable dynamics.

Multiple pulse sequences [100] are normally designed in order to obtain some effective Hamiltonian that modulates the wanted dynamics. An example is the 8-pulse sequence Fig. (4-2), designed to create the Double-Quantum Hamiltonian. Since the design of a sequence is not simple, one normally tries to obtain the wanted operator as the zeroth order term in the Average Hamiltonian expansion for ideal pulses. Then all the pulse imperfections and higher orders are considered as errors, and one should try to eliminate them.

For example, to eliminate the effects of finite pulse widths, one can try to adjust the times of the pulses with respect to the delays, in order that they compensate each other. To refocus higher order term, instead, one recurs to *symmetry* properties of the sequence.

It can be shown that if the Hamiltonian in the toggling frame is symmetric: $\tilde{\mathcal{H}}(t_c - t) = \tilde{\mathcal{H}}(t)$, then all the odd order terms are zero. Neglecting pulse errors, to eliminate all the odd orders is just enough to repeat twice the given sequence, back to back.

In general, one could in principle obtain a sequence which produces the wanted propagator to an arbitrary order in the Magnus expansion [144].

A.2 Cumulant expansion solution

Consider a Closed System (CS), composed by the system of interest (from now on called 'the System') and another part that will be called 'the Environment'. The Hamiltonian describing the overall CS is given by:

$$\mathcal{H}_{CS} = \mathcal{H}_S + \mathcal{H}_E + \mathcal{H}_{ES} \tag{A.15}$$

where $\mathcal{H}_S$ is the Hamiltonian acting on the System only, $\mathcal{H}_E$ acts on the Environment only and $\mathcal{H}_{ES}$ describes the coupling between the System and the Environment. If we transform to the interaction frame defined by the Environment Hamiltonian, with the transformation $U_E = e^{-i\mathcal{H}_E t}$, the coupling Hamiltonian will acquire a time dependence:

$$\tilde{\mathcal{H}}_{CS} = U_E \mathcal{H}_{CS} (U_E)^\dagger = \mathcal{H}_S + \tilde{\mathcal{H}}(t)_{ES} \tag{A.16}$$

The reduced (open-system) Hamiltonian that predicts the evolution of the System will be given by:

$$\mathcal{H} = \mathcal{H}_{Det}(t) + \mathcal{H}(t)_{Stoch} = \mathcal{H}(t) + \omega(t)J \tag{A.17}$$

i.e. by the sum of the System Hamiltonian and a stochastic, time dependent part, that is obtained from the coupling Hamiltonian by tracing over the Environment degrees of freedom. In our specific case of an NMR application, the operators acting on the spins (the System) are defined in the rotating frame; the Environment is normally called the *lattice* and its interaction with the spins is considered as the effect of noise on the system. $\mathcal{H}(t)$ is then the sum of the secular internal Hamiltonian and time-dependent RF Hamiltonian in the rotating frame, while $\omega(t)$ is the stochastic, time-dependent fluctuating field and J is the spin part of the noise operator. The time evolution of the (reduced) density matrix ρ is then:

$$\rho(t) = Te^{-i\int_0^t \mathcal{H}(t')dt'}\rho(0)Te^{i\int_0^t \mathcal{H}(t')dt'} \tag{A.18}$$

or in superoperator form:

$$\rho(t) = Te^{-i\int_0^t \mathcal{L}(t')dt'}\rho(0) \tag{A.19}$$

where $\mathcal{L}(t)$ is

$$\mathcal{L}(t) = \mathcal{H}\otimes\mathbf{1} - \mathbf{1}\otimes\mathcal{H} \tag{A.20}$$

Since the total Hamiltonian $\mathcal{H}$ is a stochastic operator, we have to take the ensemble average of the propagator to obtain $\langle\rho(t)\rangle$. The problem of calculating the average of the exponential of a stochastic operator has been solved by Kubo [86, 87] in terms of the cumulant function. First, expand the time-ordered exponential $U = \langle Te^{-i\int_0^t(t')dt'}\rangle$:

$$\begin{aligned} U \quad &= \mathbf{1} - i\int_0^t\langle H(t')\rangle dt' + \tfrac{(-i)^2}{2!}T\int_0^t dt_1\int_0^t dt_2\langle H(t_1)H(t_2)\rangle + \cdots \\ &+\tfrac{(-i)^n}{n!}T\int_0^t dt_1\cdots\int_0^t dt_n\langle H(t_1)\cdots H(t_n)\rangle + \cdots \end{aligned} \tag{A.21}$$

where the term $\langle H(t_1)\cdots H(t_n)\rangle$ is called the n^{th} moment of the distribution. We want now express this same propagator in terms of the cumulant operator $K(t)$, which is defined such that

$$U = e^{K(t)} \tag{A.22}$$

The cumulant function itself can most generally be expressed as a series of term of increasing order in time:

$$K(t) = \sum_{n=1}^{\infty} \frac{(-it)^n}{n!} K_n = -itK_1 + \frac{(-it)^2}{2!} K_2 + \cdots \tag{A.23}$$

Expanding now the exponential A.22 using the expression in equation A.23 we have:

$$\begin{aligned} U &= \mathbf{1} + K(t) + \tfrac{1}{2!}\left(K(t)\right)^2 + \cdots \\ &= \mathbf{1} - itK_1 + \tfrac{(-it)^2}{2!}(K_2 + K_1^2) + \cdots \end{aligned} \tag{A.24}$$

where in the second line we have separated terms of the same order in time. Comparing expression A.24 with equation A.21, we see that by equating terms of the same order we can obtain a set of equations, which will give us the expression for the cumulants K_n in terms of the moments of order $\leq n$. For example:

$$\begin{aligned} K_1 &= \tfrac{1}{t}\int_0^t \langle \mathcal{L}(t')\rangle dt' \\ K_2 &= \tfrac{1}{t^2}\left[T\int_0^t dt_1 \int_0^t dt_2 \langle \mathcal{L}(t_1)\mathcal{L}(t_2)\rangle - K_1^2\right] \end{aligned} \tag{A.25}$$

The propagator can therefore be expressed in terms of the cumulant averages:

$$\begin{aligned} \langle \mathcal{L}(t')\rangle_c &= \langle \mathcal{L}(t')\rangle \\ \langle \mathcal{L}(t_1)\mathcal{L}(t_2)\rangle_c &= T\langle \mathcal{L}(t_1)\mathcal{L}(t_2)\rangle - \langle \mathcal{L}(t_1)\rangle\langle \mathcal{L}(t_2)\rangle \end{aligned} \tag{A.26}$$

Therefore the propagator is given by:

$$U = \exp\left(-i\int_0^t \langle \mathcal{L}(t')\rangle_c dt' - \frac{1}{2}\int_0^t dt_1 \int_0^t dt_2 \langle \mathcal{L}(t_1)\mathcal{L}(t_2)\rangle_c + \cdots\right) \tag{A.27}$$

Appendix B

Fermion Operators

Spin operators of the Pauli group can be mapped to fermion operators, obeying the well-known anticommutation relationships. This mapping is useful in describing the dynamics of various 1D models, since some Hamiltonians can then be diagonalized analytically.

In the following we describe a particular mapping that is suited for describing the creation of Multiple Quantum Coherences.

A mapping from spin to fermion operators goes back to Jordan and Wigner [108], who first transformed quantum spin S = 1/2 operators, which commute at different lattice sites, into operators obeying a Clifford algebra (fermions). This transformation was used to map the one-dimensional Ising model into a spinless fermion model, which is exactly solvable. The JordanWigner transformation (JWT) has been recently generalized to the cases of arbitrary spin S [9, 6] and to 2D spin systems [135].

Given a set of spin-$\frac{1}{2}$ operators S_j^α, each defined at a lattice site j, they obey the commutation relationship:

$$[S_j^\alpha, S_l^\beta] = \delta_{j,l} i S_j^\gamma, \tag{B.1}$$

where $\{\alpha, \beta, \gamma\} = \{x, y, z\}$ and cyclic permutations of these indexes.

We can also introduce the operator $S_j^\pm$:

$$S_j^\pm = (S_j^x \pm i S_j^y)/2 \tag{B.2}$$

which obey the commutation relationships:

$$[S_j^+, S_l^-] = \delta_{j,l} 2 S_j^z, \qquad [S_j^z, S_l^\pm] = \pm \delta_{j,l} 2 S_j^\pm \tag{B.3}$$

The Jordan-Wigner transformations map these operators to fermion operators $c_j,\ c_j^\dagger$, obeying the canonical anticommutation relationships:

$$\{c_j^\dagger, c_l\} = \delta_{j,l}, \qquad \{c_j, c_l\} = \{c_j^\dagger, c_l^\dagger\} = 0, \tag{B.4}$$

where we adopted the notation $\{\ ,\ \}$ for anticommutators. A basis for the Hilbert space on which these operators act is given by the occupation number representation $|n\rangle = |n_1, n_2, ..., n_N\rangle$, where $n_j = \{0, 1\}$ is the occupation number at site j. The state $|n\rangle$ can be obtained from the vacuum state by:

$$|n\rangle \equiv \prod_j (c_j^\dagger)^{n_j} |vac\rangle. \tag{B.5}$$

Then, the action of the fermion operators on such states is given by:

$$c_j|n\rangle = \begin{cases} 0, & \text{if } n_j = 0 \\ -(-1)^{s_j^n}|n'\rangle, & \text{otherwise} \end{cases} \tag{B.6}$$

where $|n'\rangle$ is the vector resulting when the j^{th} entry of $|n\rangle$ is changed to 0 and $s_j^n = \sum_{k=1}^{j-1} n_k$. Analogously:

$$c_j^\dagger|n\rangle = \begin{cases} 1, & \text{if } n_j = 1 \\ -(-1)^{s_j^n}|n'\rangle, & \text{otherwise} \end{cases} \tag{B.7}$$

where $|n'\rangle$ is the vector resulting when the j^{th} entry of $|n\rangle$ is changed to 1.

The mapping from spin to fermion operators can be expressed in several ways, the most intuitive being based on identifying every basis vector $|n\rangle$ in the occupation number representation basis to the corresponding $|n\rangle$ basis vector in the computational basis for the spin operator Hilbert space. Imposing this one by one correspondence on basis states and taking into account the respective actions of spin and fermion operators on their basis vectors, one obtains the mapping:

$$\begin{array}{cc} c_j = -\prod_{k=1}^{j-1}(S_k^z)\, S_j^-, & c_j^\dagger = -\left(\prod_{k=1}^{j-1} S_k^z\right) S_j^+ \\ S_j^- = -\prod_{k=1}^{j-1}\left(1 - 2c_k^\dagger c_k\right) c_j, & S_j^+ = -\prod_{k=1}^{j-1}\left(1 - 2c_k^\dagger c_k\right) c_j^\dagger \end{array} \tag{B.8}$$

Notice also that $S_j^z = 1 - 2c_j^\dagger c_j$.

Consider now the double quantum Hamiltonian:

$$\mathcal{H}_{DQ} = b\sum_{j=1}^{N} \sigma_j^+\sigma_{j+1}^+ + \sigma_j^-\sigma_{j+1}^-, \tag{B.9}$$

where the couplings are restricted to the nearest neighbor spins only. (As explained in Section (4.2), this can be obtained to 2nd order by acting on the dipolar Hamiltonian with a sequence of rf pulses and delays).

We can express it in terms of the fermion operators as:

$$\begin{array}{l} \mathcal{H}_{DQ} = b\sum_{j=1}^{N}\left(\prod_{k=1}^{j}(1-2c_k^\dagger c_k)c_{j+1}^\dagger \prod_{k=1}^{j-1}(1-2c_k^\dagger c_k)c_j^\dagger + h.c.\right) \\ = b\sum_{j=1}^{N}\left((1-2c_j^\dagger c_j)c_{j+1}^\dagger c_j^\dagger + h.c.\right) = -b\sum_{j=1}^{N} c_{j+1}^\dagger c_j^\dagger + c_j c_{j+1}, \end{array} \tag{B.10}$$

Notice that even if the mapping to fermion operators is non local, this quadratic Hamiltonian is mapped to a local Hamiltonian, when one considers only nearest neighbor couplings. The Hamiltonian can then be diagonalized, by using the Fourier transform operators $a_k,\ a_k^\dagger$:

$$\begin{array}{l} a_k = \sqrt{\frac{2}{N+1}}\sum_{j=1}^{N}\sin(kj)\,c_j, \qquad k = \frac{\pi n}{N+1} \\ c_j = \sqrt{\frac{2}{N+1}}\sum_{n=1}^{N}\sin(kj)\,a_k \end{array} \tag{B.11}$$

followed by a Bogoliubov [99] transformation.

Substituting expression (B.11) in equation (B.10) we have[1]:

$$\begin{array}{l} \mathcal{H}_{DQ} = -b\sum_{k,h}\sum_{j=1}^{N}\frac{2}{N+1}\sin(kj)\sin(h(j+1))(a_k a_h + a_h^\dagger a_k^\dagger) \\ = -\frac{2b}{N+1}\sum_{k,h}(a_k a_h + a_h^\dagger a_k^\dagger)\sum_{j=1}^{N}[\sin(kj)\sin(hj)\cos(h) + \sin(kj)\cos(hj)\sin(h)] \\ = -b\sum_{k,h}(a_k a_h + a_h^\dagger a_k^\dagger)\cos(h)(\delta_{k,h} - \delta_{k,-h}) = -b\sum_k \cos(k)(a_k a_{-k} + a_{-k}^\dagger a_k^\dagger) \end{array} \tag{B.12}$$

In the previous derivation we have used the following orthogonality relationships to simplify the sums:

$$\frac{2}{N+1}\sum_{j=1}^{N}\sin(kj)\sin(hj) = \begin{cases} 1, & \text{if } k = h \\ -1, & \text{if } k = -h \\ 0, & \text{otherwise} \end{cases} \tag{B.13}$$

[1]Sums labeled by k are meant to be for $n = 1, .., N$

and[2] :

$$\sum_{j=-N/2}^{N/2} \sin(kj)\cos(hj) = 0 \tag{B.14}$$

The Bogoliubov transformation is a canonical unitary transformation (or change of basis) to a diagonal basis satisfying the same (anti-)commutation relationships as the initial one. [3]

In our case, we want to find a set of operators $\{d_k, d_{-k}\}$ that diagonalize the double quantum Hamiltonian (B.12). We thus first express the evolution of the a_k operators (in the Heisenberg representation) under $\mathcal{H}_{DQ}$:

$$\frac{d\,a_k}{dt} = i[\mathcal{H}_{DQ}, a_k] = -ib\cos(k)a^\dagger_{-k} \tag{B.15a}$$

$$\frac{d\,a^\dagger_k}{dt} = ib\cos(k)a_{-k} \tag{B.15b}$$

The Bogoliubov transformation is given by the linear transformation:

$$\begin{cases} a_k = u_k d_k + v^*_k d^\dagger_{-k} \\ a_{-k} = -u_k d_k + v^*_{-k} d^\dagger_k \end{cases} \tag{B.16}$$

which ensures the $\{d_k\}$ obey the canonical anticommutation rules. Since these operators diagonalize the double quantum Hamiltonian, their evolution is simply given by:

$$\begin{array}{l} \frac{d\,d_k}{dt} = -i\epsilon_k\, d_k \\ \frac{d\,d_{-k}}{dt} = -i\epsilon_k\, d_{-k} \end{array} \tag{B.17}$$

where ϵ_k are the eigenenergies and we have assumed $\epsilon_k = \epsilon_{-k}$. Substituting equations (B.16) and (B.17) into (B.15) we obtain

$$\begin{array}{l} \epsilon_k(-u_k d_k + v^*_k d^\dagger_{-k}) = b\cos k(u^*_k d^\dagger_{-k} - v_k d_k) \\ \epsilon_k(u^*_k d^\dagger_k - v_k d_{-k}) = b\cos k(-u^*_k d_{-k} + v^*_k d^\dagger_k) \end{array} \tag{B.18}$$

[2]Notice that it is always possible to relabel the spin sites such that spins $1 \to N/2$ are mapped to spins $-N/2 \to -1$ and spins $N/2+1 \to N$ are mapped to spins $1 \to N/2$

which, since the d_k are diagonal, define a set of equations in the coefficients $\{u_k, v_k\}$:

$$\begin{cases} u_k \epsilon_k = b\, v_k \cos k \\ v_k \epsilon_k = b\, u_k \cos k \end{cases} \tag{B.19}$$

For this system to have a non-trivial solution, the corresponding determinant must be zero:

$$\begin{vmatrix} \epsilon_k & -b\cos k \\ b\cos k & -\epsilon_k \end{vmatrix} = 0 \tag{B.20}$$

with solution $\epsilon_k = b|\cos k|$. This in turns defines the coefficients $\{u_k, v_k\}$ (given the normalization condition $|u_k|^2 + |v_k|^2 = 1$):

$$u_k = \frac{1}{\sqrt{2}} \frac{\cos k}{|\cos k|}, \qquad v_k = \frac{1}{\sqrt{2}} \tag{B.21}$$

For sake of compactness, we will write $\gamma_k \equiv \frac{\cos k}{|\cos k|}$

The Bogoliubov transformation in matrix form is then:

$$\begin{bmatrix} a_k \\ a_{-k} \\ a_k^\dagger \\ a_{-k}^\dagger \end{bmatrix} = \frac{1}{\sqrt{2}} \begin{bmatrix} \gamma_k & 0 & 0 & 1 \\ 0 & -\gamma_k & 1 & 0 \\ 0 & 1 & \gamma_k & 0 \\ 1 & 0 & 0 & -\gamma_k \end{bmatrix} \begin{bmatrix} d_k \\ d_{-k} \\ d_k^\dagger \\ d_{-k}^\dagger \end{bmatrix} \tag{B.22}$$

Notice that the matrix is real, orthogonal (i.e. $A^{-1} = A$).

Using these transformations, the double quantum Hamiltonian is diagonalized to:

$$\begin{aligned} \mathcal{H}_{DQ} &= -b \textstyle\sum_{n=1}^{N} \cos\left(\frac{n\pi}{N+1}\right) \frac{\cos\left(\frac{n\pi}{N+1}\right)}{|\cos\left(\frac{n\pi}{N+1}\right)|} \left(d_k d_k^\dagger - d_{-k}^\dagger d_{-k}\right) \\ &= 2b \textstyle\sum_k |\cos k| (d_k^\dagger d_k - \frac{1}{2}) \end{aligned} \tag{B.23}$$

Here and in the following we use the fact that $\sum_{k,h} d_{-k} d_{-h} = \sum_{k,h} d_k d_h$ as it follows retracing back the transformation to spin operators.

Bibliography

[1] A. Abragam. *Principles of Nuclear Magnetism.* Oxford Univ. Press, 1961.

[2] A. Abragam and M. Goldman. Principles of Dynamic Nuclear Polarization. *Reports on Progress in Physics*, 41(3):395–467, 1978.

[3] A. Abragam and M. Goldman. *Nuclear Magnetism : Order and Disorder.* Clarendon Press, Oxford, 1982.

[4] D. S. Abrams and S. Lloyd. Simulation of Many-Body Fermi Systems on a Universal Quantum Computer. *Physical Review Letters*, 79:2586–2589, Sept. 1997.

[5] P. Aliferis, D. Gottesman, and J. Preskill. Quantum accuracy threshold for concatenated distance-3 codes. *Quant. Inf. Comput.*, 6:97, 2006.

[6] A. Anfossi and A. Montorsi. Spin-fermion mappings for even hamiltonian operators. *J. Phys. A: Math. Gen.*, 38:4519–4527, 2005.

[7] A. Aspuru-Guzik, A. D. Dutoi, P. J. Love, and M. Head-Gordon. Simulated Quantum Computation of Molecular Energies. *Science*, 309(5741):1704–1707, 2005.

[8] D. Bacon, J. Kempe, D. A. Lidar, and K. B. Whaley. Universal fault-tolerant quantum computation on decoherence-free subspaces. *Physical Review Letters*, 85(8):1758–1761, 2000.

[9] C. D. Batista and G. Ortiz. Generalized jordan-wigner transformations. *Physical Review Letters*, 86:1082, 2001.

[10] J. Baum, M. Munowitz, A. N. Garroway, and A. Pines. Multiple-quantum dynamics in solid state NMR. *The Journal of Chemical Physics*, 83(5):2015–2025, 1985.

[11] J. Baum and A. Pines. NMR Studies of Clustering in Solids. *J. Am. Chem. Soc.*, 108:7447, 1986.

[12] F. Bloch, W. W. Hansen, and M. Packard. Nuclear induction. *Physical Review*, 69:127–127, 1946.

[13] N. Bloembergen. The interaction of nuclear spins in a crystalline lattice. *Physica*, 15:386–426, 1949.

[14] N. Bloembergen and R. V. Pound. Radiation damping in magnetic resonance experiments. *Physical Review*, 95:8–12, 1954.

[15] J. Botina, H. Rabitz, and N. Rahman. A simplified approach to optimally controlled quantum dynamics. *The Journal of Chemical Physics*, 104(11):4031–4040, 1996.

[16] N. Boulant. *Control of open quantum systems*. PhD dissertation, Massachusetts Institute of Technology, Department of Nuclear Engineering, 2004.

[17] N. Boulant, E. M. Fortunato, M. A. Pravia, G. Teklemariam, D. G. Cory, and T. F. Havel. Entanglement transfer experiment in NMR quantum information processing. *Physical Review A*, 65:024302, 2002.

[18] G. S. Boutis, P. Cappellaro, H. Cho, C. Ramanathan, and D. G. Cory. Pulse error compensating symmetric magic-echo trains. *Journal of Magnetic Resonance*, 161:132–137, 2003.

[19] G. S. Boutis, D. Greenbaum, H. Cho, D. G. Cory, and C. Ramanathan. Spin diffusion of correlated two-spin states in a dielectric crystal. *Physical Review Letters*, 92(13):137201, 2004.

[20] H. Breuer and F. Petruccione. *The Theory of Open Quantum Systems*. Oxford Univ. Press, 2002.

[21] R. Brueschweiler and R. R. Ernst. Non-ergodic quasi-equilibria in short linear spin 1/2 chains. *Chemical Physics Letters*, 264:393–397, 1997.

[22] D. Bruss. Characterizing entanglement. *Journal of Mathematical Physics*, 43:4237, 2002.

[23] G. Burkard, H.-A. Engel, and D. Loss. Spintronics and quantum dots for quantum computing and quantum communication. *Fortschr. Phys.*, 48:965–986, 2000.

[24] M. S. Byrd, D. A. Lidar, L.-A. Wu, and P. Zanardi. Universal leakage elimination. *Physical Review A*, 71:052301, 2005.

[25] P. T. Callaghan. *Principles of Nuclear Magnetic Resonance Microscopy*. Oxford Science Publications, 1991.

[26] P. Cappellaro, J. Emerson, N. Boulant, C. Ramanathan, S. Lloyd, and D. G. Cory. Entanglement assisted metrology. *Physical Review Letters*, 94:020502, 2005.

[27] P. Cappellaro, J. S. Hodges, T. F. Havel, and D. G. Cory. Principles of control for decoherence-free subsystems, 2006. quant-ph/0604203.

[28] H. Y. Carr and E. M. Purcell. Effects of diffusion on free precession in nuclear magnetic resonance experiments. *Physical Review*, 94:630–638, 1954.

[29] J. Cavanagh, W. J. Fairbrother, A. G. P. III, and N. J. Skelton. *Protein NMR Spectroscopy*. Elsevier, 1995.

[30] Y. C. Cheng and R. J. Silbey. Stochastic liouville equation approach for the effect of noise in quantum computations. *Physical Review A*, 69:052325, 2004.

[31] G. Cho and J. P. Yesinowski. Multiple-quantum nmr dynamics in the quasi-one-dimensional distribution of protons in hydroxyapatite. *Chemical Physics Letters*, 205:1–5, 1993.

[32] G. Cho and J. P. Yesinowski. 1-H and 19-F Multiple-Quantum NMR Dynamics in Quasi-One-Dimensional Spin Clusters in Apatites. *Journal of Physical Chemistry*, 100(39):15716–15725, 1996.

[33] H. Cho. *Exploring Large Coherent Spin Systems with Solid State NMR*. PhD dissertation, Massachusetts Institute of Technology, Department of Nuclear Engineering, 2005.

[34] H. Cho, P. Cappellaro, C. Ramanathan, and D. G. Cory. Experimental investigation on decay and control of multiple spin correlations. *47 Experimental Nuclear Magnetic Resonance Conference*, 2006.

[35] H. Cho, T. D. Ladd, J. Baugh, D. G. Cory, and C. Ramanathan. Multi-spin dynamics of the solid-state NMR Free Induction Decay. *Physical Review B*, 82:054427, 2005.

[36] M. Christandl, N. Datta, A. Ekert, and A. J. Landahl. Perfect state transfer in quantum spin networks. *Physical Review Letters*, 92:187902, 2004.

[37] D. G. Cory, A. F. Fahmy, and T. F. Havel. Ensemble quantum computing by NMR spectroscopy. *PNAS*, 94(5):1634–1639, 1997.

[38] D. G. Cory, R. Laflamme, E. Knill, L. Viola, T. Havel, N. Boulant, G. Boutis, E. Fortunato, S. Lloyd, R. Martinez, C. Negrevergne, M. Pravia, Y. Sharf, G. Teklemariam, Y. Weinstein, and W. Zureck. NMR based quantum information processing: Achievements and prospects. *Fortschr. Phys.*, 48:875, 2000.

[39] D. G. Cory, J. B. Miller, and A. N. Garroway. Time-suspension multiple-pulse sequences : Applications to solid-state imaging. *J. Mag. Res.*, 90:205–123, 1990.

[40] D. G. Cory, M. D. Price, and T. F. Havel. Nuclear magnetic resonance spectroscopy: an experimentally accessible paradigm for quantum computing. *Phys. D*, 120(1-2):82–101, 1998.

[41] D. G. Crabb, C. B. Higley, A. D. Krisch, R. S. Raymond, T. Roser, J. A. Stewart, and G. R. Court. Observation of a 96% proton polarization in irradiated ammonia. *Physical Review Letters*, 64:2627–2629, 1990.

[42] W. V. der Lugt and J. Caspers. Nuclear magnetic resonance line shape of fluorine in apatite. *Physica*, 30:1658–1666, 1964.

[43] D. P. DiVincenzo. The physical implementation of quantum computation. *Fortschr. Phys.*, 48:771–793, 2000.

[44] D. P. DiVincenzo, D. Bacon, J. Kempe, G. Burkard, and K. B. Whaley. Universal quantum computation with the exchange interaction. *Nature*, 408:339, 2000.

[45] S. I. Doronin, I. I. Maksimov, and E. B. Fel'dman. Multiple-quantum dynamics of one-dimensional nuclear spin systems in solids. *JETP*, 92:597, 2000.

[46] L.-M. Duan and G.-C. Guo. Preserving coherence in quantum computation by pairing quantum bits. *Physical Review Letters*, 79:1953–1956, 1997.

[47] J. M. Elzerman, R. Hanson, L. H. W. van Beveren, B. Witkamp, L. M. K. Vandersypen, and L. P. Kouwenhoven. Single-shot read-out of an individual electron spin in a quantum dot. *Nature*, 430:431, 2004.

[48] J. Emerson, Y. S. Weinstein, S. Lloyd, and D. G. Cory. Fidelity decay as an efficient indicator of quantum chaos. *Physical Review Letters*, 89(28):284102, 2002.

[49] M. Engelsberg, I. J. Lowe, and J. L. Carolan. Nuclear-magnetic-resonance line shape of a linear chain of spins. *Physical Review B*, 7:924929, 1973.

[50] E. B. Fel'dman and S. Lacelle. Multiple quantum nuclear magnetic resonance in one-dimensional quantum spin chains. *The Journal of Chemical Physics*, 107(18):7067–7084, 1997.

[51] R. P. Feynman. Simulating physics with computers. *Internat. J. Theoret. Phys.*, 21(6-7):467–488, 1981/82.

[52] R. P. Feynman. There's plenty of room at the bottom. *Journal of Microelectromechanical Systems*, 1:60–66, 1992.

[53] E. R. Fiori and H. M. Pastawski. Non-markovian decay beyond the fermi golden rule: Survival collapse of the polarization in spin chains. *Chemical Physics Letters*, 420:35–41, 2006.

[54] E. Fortunato, L. Viola, J. Hodges, G. Teklemariam, and D. G. Cory. Implementation of universal control on a decoherence-free qubit. *New J. Phys*, 4:5, 2002.

[55] E. M. Fortunato. *Controlling open quantum systems*. PhD dissertation, Massachusetts Institute of Technology, Department of Nuclear Engineering, 2002.

[56] E. M. Fortunato, M. A. Pravia, N. Boulant, G. Teklemariam, T. F. Havel, and D. G. Cory. Design of strongly modulating pulses to implement precise effective hamiltonians for quantum information processing. *Journal of Chemical Physics*, 116:7599, 2002.

[57] E. M. Fortunato, L. Viola, M. A. Pravia, E. Knill, R. Laflamme, T. F. Havel, and D. G. Cory. Exploring noiseless subsystems via nuclear magnetic resonance. *Physical Review A*, 67(6):062303, 2003.

[58] E. Fukushima and S. B. W. Roeder. *Experimental pulse NMR : a nuts and bolts approach*. Addison-Wesley Pub. Co., 1981.

[59] D. Gamliel and H. Levanon. *Stochastic Processes in Magnetic Resonance*. World Scientific Publishing Company, 1995.

[60] N. A. Gershenfeld and I. L. Chuang. Bulk Spin-Resonance Quantum Computation. *Science*, 275(5298):350–356, 1997.

[61] B. C. Gerstein and C. R. Dybowski. *Transient techniques in NMR of solids, an introduction to theory and practice*. Academic, Orlando, Fla., 1985.

[62] R. Ghose. Average liouvillian theory in nuclear magnetic resonance - principles, properties, and applications. *Conc. Magn. Res.*, 12(3):152–172, March 2000.

[63] D. Giulini, E. Joos, C. Kiefer, J. Kupsch, I. Stamatescu, and H. D. Zeh. *Decoherence and the Appearance of a Classical World in Quantum Theory.* Springer-Verlag, Berlin, FRG, 1996.

[64] M. Goldman. *Spin Temperature and NMR in Solids.* Clarendon Press, Oxford, 1970.

[65] D. Greenbaum. Magnetization and spin-spin energy diffusion in the XY model: A diagrammatic approach. *Journal of Magnetic Resonance*, 179:11–19, Mar. 2006.

[66] D. Greenbaum, M. Kindermann, C. Ramanathan, and D. G. Cory. Hydrodynamic approach to coherent nuclear spin transport. *Physical Review B*, 71:054403, 2005.

[67] D. M. Greenberger, A. Horne, and A. Zeilinger. Going beyond bell's theorem. In M. Kafatos, editor, *Bell's theorem, Quantum Theory, and Conceptions of the Universe*, pages 69–73, Dordrecht, 1989. Kluwer.

[68] U. Haeberlen. *High Resolution NMR in Solids: Selective Averaging.* Academic Press Inc., 1976.

[69] U. Haeberlen and J. S. Waugh. Coherent averaging effects in magnetic resonance. *Physical Review*, 175(2):453–467, 1968.

[70] S. R. Hartman and E. L. Hahn. Nuclear double resonance in the rotating frame. *Physical Review*, 128:2042–2053, 1962.

[71] T. F. Havel, Y. Sharf, L. Viola, and D. G. Cory. Hadamard products of product operators and the design of gradient-diffusion experiments for simulating decoherence by nmr spectroscopy. *Physical Letters A*, 280(5-6):282–288, 2001.

[72] W. M. Itano, D. J. Heinzen, J. J. Bollinger, and D. J. Wineland. Quantum zeno effect. *Physical Review A*, 41(5):2295–2300, 1990.

[73] P. Jacquod, P. Silvestrov, and C. Beenakker. Golden rule decay versus lyapunov decay of the quantum loschmidt echo. *Physical Review E*, 64(5):055203, 2001.

[74] B. E. Kane. A silicon-based nuclear spin quantum computer. *Nature*, 393:133–137, 1998.

[75] J. Kempe, D. Bacon, D. A. Lidar, and K. B. Whaley. Theory of decoherence-free fault-tolerant universal quantum computation. *Physical Review A*, 63(4):042307, 2001.

[76] A. Khaetskii, D. Loss, and L. Glazman. Electron spin evolution induced by interaction with nuclei in a quantum dot. *Physical Review B*, 67(19):195329, May 2003.

[77] N. Khaneja, R. Brockett, and S. J. Glaser. Time optimal control in spin systems. *Physical Review A*, 63(3):032308, 2001.

[78] N. Khaneja and S. J. Glaser. Efficient transfer of coherence through ising spin chains. *Physical Review A*, 66(6):060301, 2002.

[79] N. Khaneja, T. Reiss, C. Kehlet, T. Schulte-Herbuggen, and S. Glaser. Optimal control of coupled spin dynamics: design of nmr pulse sequences by gradient ascent algorithms. *J. Magn. Res.*, 172:296–305, 2005.

[80] E. Knill, I. Chuang, and R. Laflamme. Effective pure states for bulk quantum computation. *Physical Review A*, 57(5):3348–3363, 1998.

[81] E. Knill, R. Laflamme, and L. Viola. Theory of quantum error correction for general noise. *Physical Review Letters*, 84(11):2525–2528, 2000.

[82] E. Knill, R. Laflamme, and W. H. Zurek. Resilient Quantum Computation. *Science*, 279(5349):342–345, 1998.

[83] J. Kohler, J. A. J. M. Disselhorst, M. C. J. M. Donckers, E. J. J. Groenen, J. Schmidt, and W. E. Moerner. Magnetic resonance of a single molecular spin. *Nature*, 363:242–244, 1993.

[84] K. Kraus. General state changes in quantum theory. *Annals of Physics*, 64:311–335, 1971.

[85] H. G. Krojanski and D. Suter. Scaling of decoherence in wide nmr quantum registers. *Physical Review Letters*, 93(9):090501, 2004.

[86] R. Kubo. *Fluctuation relaxation and resonance in magnetic system.* Oliver and Boyd Edinburgh, 1961.

[87] R. Kubo. Stochastic liouville equations. *Journal of Mathematical Physics*, 4(2):174–183, 1963.

[88] T. D. Ladd, J. R. Goldman, A. Dana, F. Yamaguchi, and Y. Yamamoto. Quantum computation in a one-dimensional crystal lattice with nmr force microscopy, 2000.

[89] T. D. Ladd, J. R. Goldman, F. Yamaguchi, Y. Yamamoto, E. Abe, and K. M. Itoh. All-silicon quantum computer. *Physical Review Letters*, 89(1):017901, 2002.

[90] J.-S. Lee and A. K. Khitrin. Quantum amplifier: Measurement with entangled spins. *The Journal of Chemical Physics*, 121(9):3949–3951, 2004.

[91] A. J. Leggett and A. Garg. Quantum mechanics versus macroscopic realism: Is the flux there when nobody looks? *Physical Review Letters*, 54(9):857–860, 1985.

[92] D. Leibfried, M. D. Barrett, T. Schaetz, J. Britton, J. Chiaverini, W. M. Itano, J. D. Jost, C. Langer, and D. J. Wineland. Toward Heisenberg-Limited Spectroscopy with Multiparticle Entangled States. *Science*, 304(5676):1476–1478, 2004.

[93] M. Levitt. Composite pulses. *Prog. Nucl. Magn. Reson. Spectrosc.*, 18:61, 1986.

[94] P. R. Levstein, G. Usaj, and H. M. Pastawski. Attenuation of polarization echoes in nmr: A study of the emergence of dynamical irreversibility in many-body quantum systems. *Journal Chemical Physics*, 108:2718, 1998.

[95] D. A. Lidar, D. Bacon, J. Kempe, and K. B. Whaley. Decoherence-free subspaces for multiple-qubit errors. i. characterization. *Physical Review A*, 63(2):022306, 2001.

[96] D. A. Lidar, D. Bacon, J. Kempe, and K. B. Whaley. Decoherence-free subspaces for multiple-qubit errors. ii. universal, fault-tolerant quantum computation. *Physical Review A*, 63(2):022307, 2001.

[97] D. A. Lidar, I. L. Chuang, and K. B. Whaley. Decoherence-free subspaces for quantum computation. *Physical Review Letters*, 81(12):2594–2597, 1998.

[98] S. Lloyd. Universal Quantum Simulators. *Science*, 273(5278):1073–1078, 1996.

[99] D. C. Mattis. *The theory of magnetism. 1, Statics and dynamics*. Springer Verlag, 1985.

[100] M. Mehring. *Principle of High Resolution NMR in Solids*. Springer-Verlag, 1983.

[101] S. Meiboom and D. Gill. Modified spin-echo method for measuring nuclear relaxation times. *Review of Scientific Instruments*, 29(8):688–691, 1958.

[102] D. A. Meyer and N. R. Wallach. Global entanglement in multiparticle systems. *J. Math. Phys.*, 43:9, 2002.

[103] M. Munowitz, A. Pines, and M. Mehring. Multiple-quantum dynamics in nmr: A directed walk through liouville space. *The Journal of Chemical Physics*, 86(6):3172–3182, 1987.

[104] A. Munowitz M, Pines. Principles and application of multiple-quantum nmr. *Advances in Chemical Physics*, 66:1–152, 1987.

[105] M. A. Nielsen. A simple formula for the average gate fidelity of a quantum dynamical operation. *Physics Letters A*, 303:249, 2002.

[106] G. Ortiz, J. E. Gubernatis, E. Knill, and R. Laflamme. Quantum algorithms for fermionic simulations. *Physical Review A*, 64(2):022319, 2001.

[107] A. W. Overhauser. Polarization of Nuclei in Metals. *Physical Review*, 92:411–415, 1953.

[108] J. P and W. E. About the pauli exclusion principle. *Zeitschrift fur Physik. B*, 47:631, 1928.

[109] H. M. Pastawski and G. Usaj. Dimensional crossover in spin diffusion: A manifestation of the quantum zeno effect. *Physical Review B (Condensed Matter and Materials Physics)*, 57(9):5017–5020, 1998.

[110] C. A. Perez-Delgado, M. Mosca, P. Cappellaro, and D. G. Cory. Single spin measurement using cellular automata techniques, 2006. quant-ph/0601054.

[111] M. A. Pravia, N. Boulant, J. Emerson, A. Farid, E. M. Fortunato, T. F. Havel, R. Martinez, and D. G. Cory. Robust control of quantum information. *J. Chem. Phys.*, 119:9993–10001, 2003.

[112] M. Price, S. Somaroo, A. E. Dunlop, T. F. Havel, and D. G. Cory. Generalized methods for the development of quantum logic gates for an nmr quantum information processor. *Physical Review A*, 60:27772780, 1999.

[113] E. M. Purcell, H. C. Torrey, and R. V. Pound. Resonance Absorption by Nuclear Magnetic Moments in a Solid. *Physical Review*, 69:37–38, 1946.

[114] C. Ramanathan, H. Cho, P. Cappellaro, G. S. Boutis, and D. G. Cory. Encoding multiple quantum coherences in non-commuting bases. *Chemical Physics Letters*, 369:311, 2003.

[115] W. Rhim and D. Elleman. a. *J. Chem. Phys.*, 60:11, 1974.

[116] R. Romano and D. D'Alessandro. Incoherent control and entanglement for two-dimensional coupled systems. *Physical Review A*, 73(2):022323, 2006.

[117] D. Rugar, R. Budakian, H. J. Mamin, and B. W. Chui. Single spin detection by magnetic resonance force microscopy. *Nature*, 430(6997):329–332, 2004.

[118] S. G. Schirmer, H. Fu, and A. I. Solomon. Complete controllability of quantum systems. *Physical Review A*, 63:063410, 2001.

[119] B. Schumacher. Sending entanglement through noisy quantum channels. *Physical Review A*, 54:2614, 1996.

[120] A. Shaka, J. Keeler, T. Frenkiel, and R. Freeman. Improved sequence for broadband decoupling: Waltz-16. *J. Magn. Res.*, 52:335, 1983.

[121] P. W. Shor. Scheme for reducing decoherence in quantum computer memory. *Physical Review A*, 52:2493–2496, 1995.

[122] P. W. Shor. Fault-tolerant quantum computation. In *37th Annual Symposium on Foundations of Computer Science*, pages 56–65. IEEE Comput. Soc. Press, Los Alamitos, CA, 1996.

[123] J. A. Sidles, J. L. Garbini, and G. P. Drobny. The theory of oscillator-coupled magnetic resonance with potential applications to molecular imaging. *Review of Scientific Instruments*, 63(8):3881–3899, 1992.

[124] D. T. Smithey, M. Beck, M. G. Raymer, and A. Faridani. Measurement of the wigner distribution and the density matrix of a light mode using optical homodyne tomography: Application to squeezed states and the vacuum. *Physical Review Letters*, 70(9):1244–1247, 1993.

[125] A. Sodickson and D. G. Cory. A generalized k-space formalism for treating the spatial aspects of a variety of nmr experiments. *Prog. Nucl. Magn. Res. Spectrosc.*, 33(77), 1998.

[126] D. K. Sodickson and J. S. Waugh. Spin diffusion on a lattice: Classical simulations and spin coherent states. *Physical Review B*, 52:6467–6479, Sept. 1995.

[127] I. Solomon. Relaxation processes in a system of two spins. *Physical Review*, 99:559, 1955.

[128] A. Steane. Multiple particle interference and quantum error correction. *Proceedings Royal Society.London A*, 452:2551, 1996.

[129] D. Stepanenko, G. Burkard, G. Giedke, and A. Imamoglu. Enhancement of electron spin coherence by optical preparation of nuclear spins. *Physical Review Letters*, 96(13):136401, 2006.

[130] D. Suter and K. Lim. Scalable architecture for spin-based quantum computers with a single type of gate. *Physical Review A*, 65(5):052309, 2002.

[131] L. Tian and S. Lloyd. Resonant cancellation of off-resonant effects in a multilevel qubit. *Physical Review A*, 62:050301, 2000.

[132] C. Uchiyama and M. Aihara. Multipulse control of decoherence. *Physical Review A*, 66:032313, 2002.

[133] C. Uchiyama and M. Aihara. Synchronized pulse control of decoherence. *Physical Review A*, 68:052302, 2003.

[134] S. Vega and A. Pines. Operator formalism for double quantum nmr. *The Journal of Chemical Physics*, 66(12):5624–5644, 1977.

[135] F. Verstraete and J. I. Cirac. Mapping local hamiltonians of fermions to local hamiltonians of spins. *Journal of Statistical Mechanics: Theory and Experiment*, 2005(09):P09012, 2005.

[136] L. Viola. Quantum control via encoded dynamical decoupling. *Physical Review A*, 66:12307, 2002.

[137] L. Viola, E. M. Fortunato, M. A. Pravia, E. Knill, R. Laflamme, and D. G. Cory. Experimental Realization of Noiseless Subsystems for Quantum Information Processing. *Science*, 293(5537):2059–2063, 2001.

[138] L. Viola and E. Knill. Robust dynamical decoupling of quantum systems with bounded controls. *Physical Review Letters*, 90:037901, 2003.

[139] L. Viola and E. Knill. Verification procedures for quantum noiseless subsystems. *Physical Review A*, 68(3):032311, 2003.

[140] L. Viola, E. Knill, and R. Laflamme. Constructing qubits in physical systems. *J. Phys. A*, 34:7076, 2001.

[141] L. Viola and S. Lloyd. Dynamical suppression of decoherence in two-state quantum systems. *Physical Review A*, 58:2733, 1998.

[142] L. Viola, S. Lloyd, and E. Knill. Universal control of decoupled quantum systems. *Physical Review Letters*, 83:4888, 1999.

[143] W-K. Rhim and A. Pines and J. S. Waugh. Time-Reversal Experiments in Dipolar-Coupled Spin Systems. *Physical Review B*, 3(3):684–696, 1971.

[144] W. S. Warren, D. P. Weitekamp, and A. Pines. Theory of selective excitation of multiple-quantum transitions. *The Journal of Chemical Physics*, 73(5):2084–2099, 1980.

[145] J. S. Waugh. Equilibrium and ergodicity in small spin systems. *Molecular Physics*, 95(5):731–735, 1998.

[146] W. Wootters and W. Zurek. A single quantum cannot be cloned. *Nature*, 299:802–803, 1982.

[147] J. Wrachtrup, A. Gruber, L. Fleury, and C. von Borczyskowski. Magnetic resonance on single nuclei. *Chemical Physics Letters*, 267:179–185, 1997.

[148] J. Wrachtrup, C. von Borczyskowski, J. Bernard, M. Orrit, and R. Brown. Optical detection of magnetic resonance in a single molecule. *Nature*, 363:244–245, 1993.

[149] J. Wrachtrup, C. von Borczyskowski, J. Bernard, M. Orrit, and R. Brown. Optically detected spin coherence of single molecules. *Physical Review Letters*, 71(21):3565–3568, 1993.

[150] L.-A. Wu, M. S. Byrd, and D. A. Lidar. Efficient universal leakage elimination for physical and encoded qubits. *Physical Review Letters*, 89:127901, 2002.

[151] M. Xiao, I. Martin, E. Yablonovitch, and H. W. Jiang. Electrical detection of the spin resonance of a single electron in a silicon field-effect transistor. *Nature*, 430:435–439, 2004.

[152] Y.-S. Yen and A. Pines. Multiple-quantum nmr in solids. *The Journal of Chemical Physics*, 78(6):3579–3582, 1983.

[153] P. Zanardi and M. Rasetti. Noiseless quantum codes. *Physical Review Letters*, 79(17):3306–3309, 1997.

[154] W. Zhang and D. G. Cory. First Direct Measurement of the Spin Diffusion Rate in a Homogenous Solid. *Physical Review Letters*, 80:1324–1327, 1998.

[155] O. Zuger, S. T. Hoen, C. S. Yannoni, and D. Rugar. Three-dimensional imaging with a nuclear magnetic resonance force microscope. *Journal of Applied Physics*, 79(4):1881–1884, 1996.

[156] W. H. Zurek. Decoherence and the transition from quantum to classical. *Physics Today*, October:36–44, 1991.

[157] I. Zutic, J. Fabian, and S. D. Sarma. Spintronics: Fundamentals and applications. *Reviews of Modern Physics*, 76(2):323, 2004.